CHARACTERIZATION OF THE TOMATO SNRK1 COMPLEX ACTIVITY AND ITS ROLE IN BACTERIAL INFECTION

A Dissertation

by

DONGYIN SU

Submitted to the Office of Graduate and Professional Studies of
Texas A&M University
in partial fulfillment of the requirements for the degree of

DOCTOR OF PHILOSOPHY

Chair of Committee,	Timothy Devarenne
Committee Members,	Thomas Meek
	Libo Shan
	Xiuren Zhang
Head of Department,	Gregory Reinhart

August 2018

Major Subject: Biochemistry

ABSTRACT

The Sucrose non-fermenting related kinase 1 (SnRK1) complex is a hetero trimer found in plants consisting of a catalytic α-subunit and regulatory β and γ subunits. The SnRK1 complex can regulate a variety of metabolic pathways in response to changes of energy status in the cell. Furthermore, the SnRK1 complex was proposed to play a role in bacterial resistance due to its interaction with the programmed cell death (PCD) inhibitor Adi3 (AvrPto-dependent Pto-interacting protein 3). In the presence of bacteria expressing the effector protein AvrPto, Adi3 will not be phosphorylated, thus releasing its cell death suppression activity and PCD occurs. PCD signaling components may regulate SnRK1 complex activity, the SnRK1 complex in turn can regulate downstream metabolic pathways through phosphorylation of key enzymes in the metabolic pathways or transcription reprogramming.

In order to better understand the function and regulation of the tomato SnRK1 complex, the activity and regulation of the α-subunit was studied. A previous study identified the SnRK1.1 α-subunit. A search of the tomato genome database resulted in the identification a second SnRK1 α-subunit, SnRK1.2, and the upstream activation kinase SnAK. In the phylogenetic analysis of SnRK1 sequences from monocots and dicots *Sl*SnRK1.2 clusters only with other Solanaceae SnRK1.2 sequences, suggesting possible functional divergence of these kinases from other SnRK1 kinases. Tomato SnRK1.2 exhibits lower kinase activity compared to SnRK1.1 even after SnAK activation. Moreover, in vitro reconstitution of the SnRK1 complex revealed that SnRK1.2 complexes could have higher activity if Sip1 or Tau2 was used as the β-subunit. On the other hand, SnRK1.1 have higher activity when Gal83 or Tau2 was used as the β-subunit. These

studies suggest the SnRK1.2 phylogenetic divergence and lower SnRK1.2 kinase activity compared to SnRK1.1 may be indicative of different *in vivo* roles for each kinase.

One substrate of SnRK1, nitrate reductase (NR), was used to study the effect of Adi3 phosphorylation status on NR activity through the regulation of SnRK1 complex. Contrary to previous observations that Adi3 inhibits SnRK1 activity, our result shows that a phosphomimetic version of Adi3 caused an increase in NR phosphorylation by SnRK1.1. While there is previous contradicting evidence for both promotional and inhibitory effects of the β-subunit on NR, the results here show that addition of the Gal83 β-subunit had no effect on NR activity.

Finally, we studied the effect of effector proteins, AvrPto and AvrPtoB, on SnRK1 complex activities. Our results show that AvrPto inhibits SnRK1 activity in resistant plants, while it had no effect on susceptible plants.

ACKNOWLEDGEMENTS

I would like to thank my advisor Dr. Timothy Devarenne for giving me the opportunity to learn and grown as a researcher with him. I want to especially thank for his patience and the freedom he gave me to explore new things in my research.

I would also like to thank my committee members, Dr. Shan, Dr. Meek, and Dr. Zhang, as well as my previous committee member Dr. Holzenburg, for their guidance and support for my research, and their insight on science in general.

I would like to thank the past and current Devarenne lab members, Anna, Julian, Joel, Hem, Mehmet, Dan, and Incheol for all the good discussion about science and research or life in general. I would like to thank them for making my every day in the lab so enjoyable.

I would like to thank the faculty and staff in the Department of Biochemistry and Biophysics for their help and encouragement throughout the years. I would like to thank Dr. Mary Bryk for her kind encouragement, Rafael Almanzar for helping me with academic processes, and Terry Lovingshimer for patiently working with me to adjust the growth chamber.

Finally, thanks to my mother and father for their encouragement and to my husband for his patience and love.

CONTRIBUTORS AND FUNDING SOURCES

This work was supervised by a dissertation committee consisting of Dr. Timothy Devarenne and Drs. Thomas Meek, and Xiuren Zhang of the Department of Biochemistry and Biophysics, and Dr. Libo Shan of Department of Plant Pathology and Microbiology.

The mass spectrometry analysis of Tau2 phosphorylation sites in Chapter III was performed by Dr. Sixue Chen of the Biology Department, University of Florida. All other work conducted for the dissertation was completed by the student independently.

The work conducted for the dissertation was supported by Agriculture and Food Research Initiative Competitive Grants Program Grant no. 2010-65108-20526 and no. 2014-67013-21560 from the USDA National Institute of Food and Agriculture, Agriculture and Food Research Initiative.

NOMENCLATURE

SNF1	Sucrose non-fermenting 1
SnRK	Sucrose non-fermenting related kinase
AMPK	AMP-regulated protein kinase
NR	Nitrate Reductase
Adi3	AvrPto-dependent Pto-interacting protein 3
PCD	Programmed cell death
HR	Hypersensitive response
PTI	Pathogen-triggered immunity
PAMPs	Pathogen associated molecular patterns
ETS	Effector-triggered susceptibility
ETI	Effector-triggered immunity
NLS	Nuclear localization signal
Pst	*Pseudomonas syringae* pv *tomato*
At	*Arabidopsis thaliana*
Sl	*Solanum lycopersicum*

TABLE OF CONTENTS

Page

Page

LIST OF FIGURES

Page

CHAPTER I

INTRODUCTION AND LITERATURE REVIEW

1.1. Plant Pathogen Interactions[1]

1.1.1. Defense—Pathogen-Triggered Immunity (PTI)

Like mammalian systems, plants also have a non-specific mechanism to recognize highly conserved pathogen associated molecular patterns (PAMPs)[1]. Pattern recognition receptors (PRRs), a group of plant transmembrane proteins (or protein complexes), can recognize and bind to PAMPs and trigger a defense response[2]. A well-studied PRR is Flagellin-sensing 2 (FLS2). FLS2 can recognize flg22, a 22 amino acids fragment of bacterial flagellin component [3]. Upon binding with flg22, FLS2 can then form a complex with Brassinosteroid Associated Kinase 1 (BAK1) and Botrytis-induce Kinase 1 (BIK1) [4]. The FLS2/BAK1/BIK1 complex transduces the signal of flg22 recognition through a series of phosphorylation events[5]. As a result, the plant will elicit a plethora of responses to fight off the pathogen including MAPK cascade activation, Ca^{2+} influx into the cytosol, ROS production, cell wall thickening, stomata closure, WRKY gene transcription , and systemic responses mediated by hormone signals [6,7].

1.1.2. Counter defense—Effector-Triggered Susceptibility (ETS)

In order to effectively infect plant hosts, pathogens also developed mechanisms that counteract plant immunity. Some pathogens produce effector proteins and secret them into host cells. Unlike the PAMPs that usually come from an essential process or physical structure of the

---

[1] Part of the data reported in this chapter is reprinted with permission from S. Dongyin, T.P. Devarenne, *In vitro* activity characterization of the tomato SnRK1 complex proteins, BBA-Proteins and Proteomics (2018), DOI.10.1016/j.bbapap.2018.05.010, © 2018 Elsevier B.V.

pathogen, effector proteins are specifically evolved to facilitate the infection of plants, so the effectors can be quite diverse and evolve relatively fast [8]. Effector proteins can promote nutrient leakage[9] and bind, modify, or target proteins involved in PTI for degradation, thus suppress host immune responses [10,11].

1.1.3. Counter-counter defense—Effector-Triggered Immunity (ETI)

During the long co-evolution between plant and pathogen, plants also developed mechanism to fight back by producing resistance (R) proteins that recognize effector proteins or self proteins that have been modified by effector proteins [1]. Upon recognition, R proteins can either directly transduce signals that trigger defense responses or protect PRRs from being suppressed by PAMPs [12]. ETI usually results in an influx of Ca^{2+}, increase of ROS and NO production, expression of defense related proteins and a hypersensitive response (HR) of the infected cell and systemic acquired resistance through hormone regulation [13,14].

1.2. Programmed Cell Death (PCD) and the Hypersensitive Response (HR)

1.2.1. Different types of PCD

PCD is defined by the genetically controlled destruction of cells that play an important role in development and defense [15]. In animals, the term apoptosis is usually used in place of PCD to describe the process that involves the phagocytosis of the cell remnants by macrophages, which does not happen in plants [16]. In plants, there are three distinct types of PCD: 1) vacuole-mediated PCD, which is characterized by the swelling then collapse of the vacuole [17]; 2) senescence, which has a longer process than other PCD and usually involves the salvation of

nutrients from sensing tissues [18]; 3) hypersensitive response, which occurs rapidly to restrict the spread of a pathogen [19].

1.2.2. Hypersensitive response (HR)

The HR is a special form of PCD. Unlike senescence which may take several months or even years to happen, HR can happen in several hours in response to pathogen attack [20]. The rapid response enables plants to limit nutrient supply to the pathogen, thus inhibiting the spread of the pathogen [15]. Although HR is often compared with mammalian apoptosis, the appearance of DNA laddering and apoptotic bodies during the HR is still under debate, while mitochondrial swelling and vacuolization of the cell caused by HR are not seen in apoptosis [20].

1.3. *Pseudomonas syringae* pv. *tomato* (*Pst*) and the AvrPto-Pto Model.

Pst is a gram-negative bacterium that can infect tomato and *Arabidopsis thaliana*, causing bacterial spec disease that is characterized by small necrotic lesions over the whole plant [21]. The lesions can also be found on both ripe and unripe tomato fruit, making the tomatoes unmarketable [22]. *Pst* spreads under wet conditions through rain or aerosols and enter leaf apoplastic space through stomata or wounds [22]. *Pst* then infects tomato by injecting effector proteins into the cell through its type III secretion system [23]. These effector proteins suppress PTI and hijack cellular mechanisms, leading to cell death that results in the speck phenotype [24]. The full 6,397,126 bp genome of *Pst* DC3000 has been sequenced, so it serves a good model organism for the study of plant-bacterium interaction. In *Pst* DC3000, more than 28 type III effectors have been confirmed to be active and sufficiently expressed [25].

1.3.1. Pst effector proteins AvrPto and AvrPtoB induced virulence in susceptible plants

Among the over 28 effector proteins in *Pst* DC3000, AvrPto and AvrPtoB are best studied due to the naturally occurring R protein Pto in tomato that can interact with AvrPto and AvrPtoB and confer resistance to *Pst* [26]. AvrPto and AvrPtoB expression are regulated by the hypersensitive-response and pathogenicity (hrp) box and is induced by plant apoplastic space conditions [27].

AvrPto is a 18.3 kDa protein that localizes to the plant membrane by myristoylation at the Gly2 position, the myristoylation and membrane localization is important for its virulent activities [28]. AvrPtoB is a 59 kDa protein, although it has no sequence similarity and very little structural similarity to AvrPto, AvrPtoB can bind to similar proteins as AvrPto does [29]. AvrPto and AvrPtoB disrupt PTI in susceptible plants by binding to FLS2 and BAK1 and disrupting the flg22 induced formation of the FLS2-BAK1 signaling complex, resulting in the suppression of PTI responses [30–32]. Besides disruption of the FLS2-BAK1 complex by competitive binding, AvrPtoB can also inhibit PTI by ubiquitination of FLS2, which leads to FLS2 degradation [33]. In addition to inhibiting the PTI response, AvrPto and AvrPtoB can also inhibit miRNA maturation, causing a decrease of the PTI related miR171, miR173 and miR393 levels [34]. AvrPto and AvrPtoB also change plant hormone levels, increasing the production of ethylene and ABA, while causing brassinosteroid insensitivity, promoting disease-associated cell death [31,35,36].

1.3.2. Pto and Prf confer resistance to Pst

The tomato cultivar ‘Farthest North’, a cross between a tomato(*S. Lycopersicum*) cultivar ‘Bison” and an unknown wild tomato (*S. pimpinellifolium*), was believed to be the first

commercially available *Pst* resistant tomato cultivar[37]. Later studies revealed that the resistance is due to the Pto protein, which confers resistance to *Pst* through interaction with AvrPto and AvrPtoB [38]. Unlike other R proteins, Pto does not have leucine-rich repeats (LRR) [27]. So, Pto requires another protein, Prf, which contains an LRR domain and nucleotide binding (NB) domain, to function together to trigger ETI (Figure 1) [39,40].

Pto is a Ser/Thr protein kinase that can autophosphorylate on the Thr-199 residue [41]. This autophosphorylation stabilizes its P+1 loop, which can in turn interacts with the GINP (Gly-Ile-Asn-Pro) motif of AvrPto [42]. Pto also interacts with AvrPto through a loop preceding the β1 loop [42]. Binding of AvrPto to Pto releases Pto inhibition of Prf activity, which triggers the HR response and programmed cell death [43]. AvrPtoB is a much larger protein than AvrPto but only the first 307 amino acids are required for interacting with Pto to trigger the HR response [44]. Similar to the interaction with AvrPto, Pto also interacts with AvrPtoB through its P+1 loop in a similar conformation [42]. Additionally, Pto interacts with AvrPtoB through the L1 loop of Pto [45]. For both interaction with AvrPto and AvrPtoB, Pto needs to be in its active conformation [42,45].

Interestingly, both AvrPto and AvrPtoB inhibit Pto kinase activity, which is hard to explain for the activation of the HR response [42,45]. Later studies showed that to trigger the HR response, at least two pairs of Pto-Prf complexes are required, one pair acts as a "sensor" while the other pair acts as a "helper" [43]. It has been proposed that binding of AvrPto or AvrPtoB to the sensor Pto disrupts its P+1 loop leading to the release of Prf inhibition. The derepressed sensor Pto activates the helper Pto through the Prf NB domain [43]. The helper Pto in turn phosphorylates the sensor Pto, resulting in full activation of the whole complex and eventually leading to the HR response in a process that is still not well studied [43].

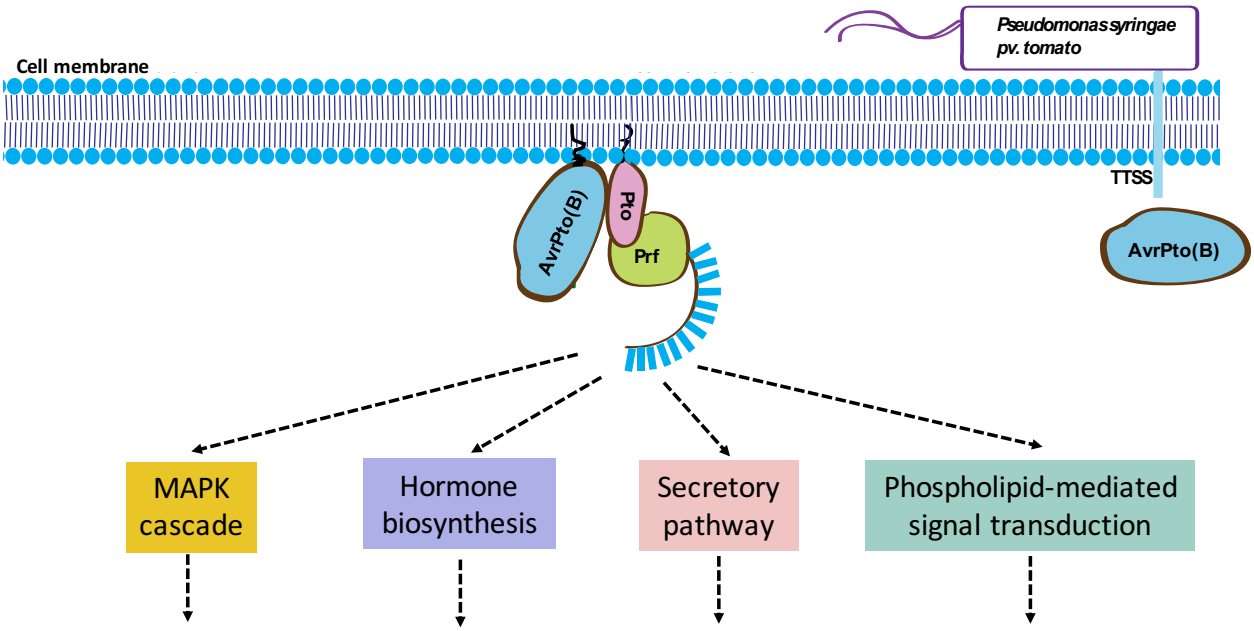

Figure 1. Pto and Prf mediated ETI response to AvrPto/AvrPtoB. *Pst* injects AvrPto/AvrPtoB into tomato through the type III secretion system (TTSS). AvrPto/AvrPtoB binding to Pto releases Pto's inhibition on Prf, activating MAPK cascade, hormone biosynthesis, secretory pathways, and phospholipid-mediated signal transduction, which lead to ETI responses characterized by Ca2+ influx, ROS and NO production, HR, and expression of defense related genes.

1.3.3. AvrPto-dependent Pto-interacting proteins (Adi)

In an effort to understand how Pto triggers the HR response in the presence of AvrPto, a yeast three-hybrid screen for proteins that interact with Pto in a AvrPto dependent manner (Adi) was performed [46]. Among the five Adi proteins discovered, Adi3 was further studied due to the possibility that it is involved in the activation of Pto [46]. Adi3 is a group VIII AGC protein kinase whose activity is regulated by Pdk1. Adi3 is a negative regulator of PCD in the absence of pathogen [47]. Virus-induced silencing of Adi3 causes spontaneous cell death in tomato plants, on the other hand, overexpression of Adi3 decreases PCD in the presence of cell death inducers such as AvrPto and autoactive forms of Pto [41, 42]. In an unchallenged cell, Adi3 interacts with Pdk1 through the Adi3 PIF motif and is phosphorylated by Pdk1 at Ser539 in the kinase domain [48]. The phosphorylated Adi3 localizes to the nucleus, guided by the nuclear localization signal (NLS) in its T-loop in an endosome dependent manner [42]. Once in the nucleus Adi3 functions as a PCD suppressor (Figure 2)[47,49]. In the presence of AvrPto, Adi3 will bind to Pto in an AvrPto dependent manner, preventing phosphorylation by Pdk1 [41,44]. As a result, Adi3 will not be able to localize to the nucleus but accumulate in endosome systems [49]. The loss of Adi3 nuclear localization disrupts its function as a cell death suppressor and PCD will occur (Figure 3) [50].

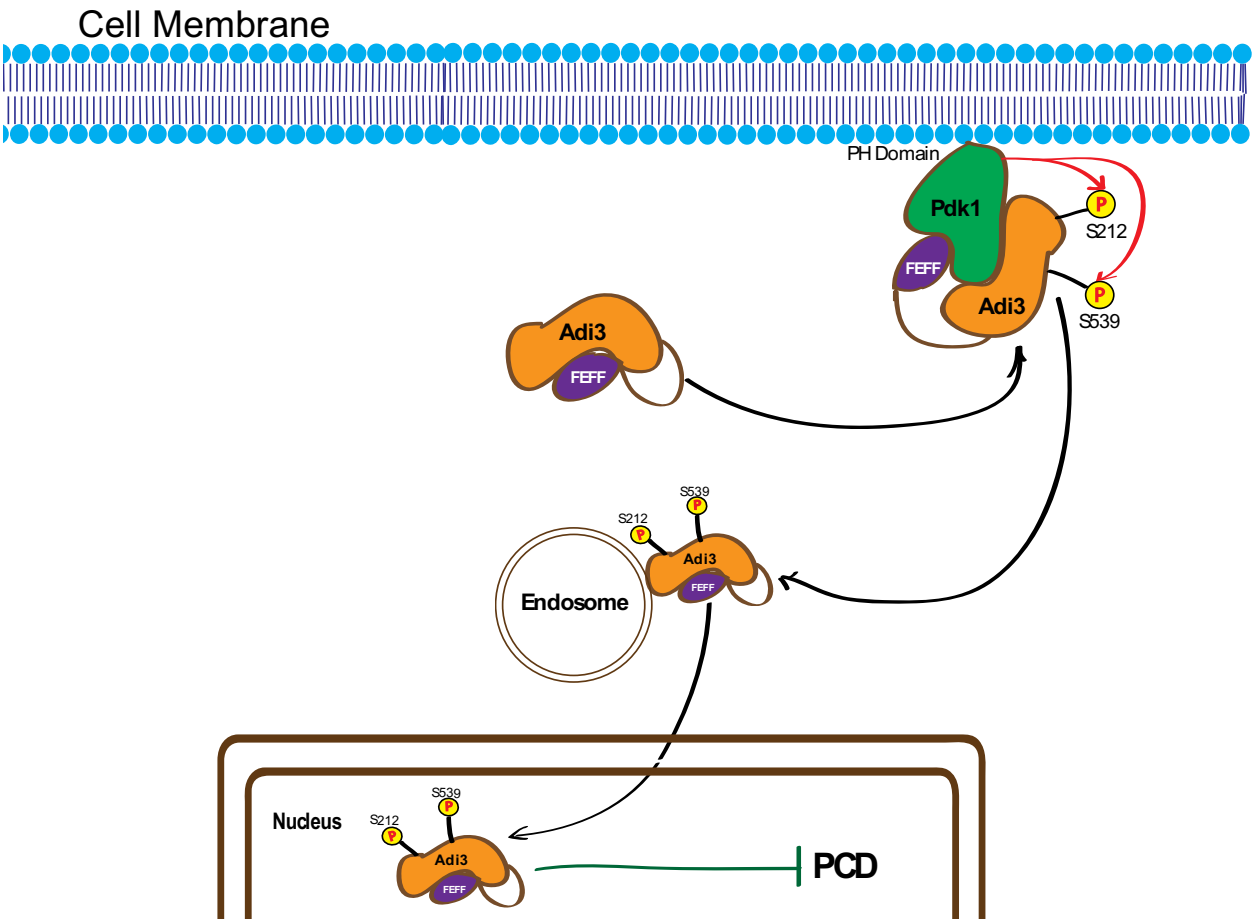

Figure 2. Adi3 inhibits PCD in healthy tomato cells. In the absence of AvrPto, Pdk1 can bind and phosphorylate Adi3 at Ser539. Adi3 then localized to the nucleus guided by NLS signals in its T-loop region in an endosome dependent manner. In the nucleus, Adi3 function as a cell death suppressor.

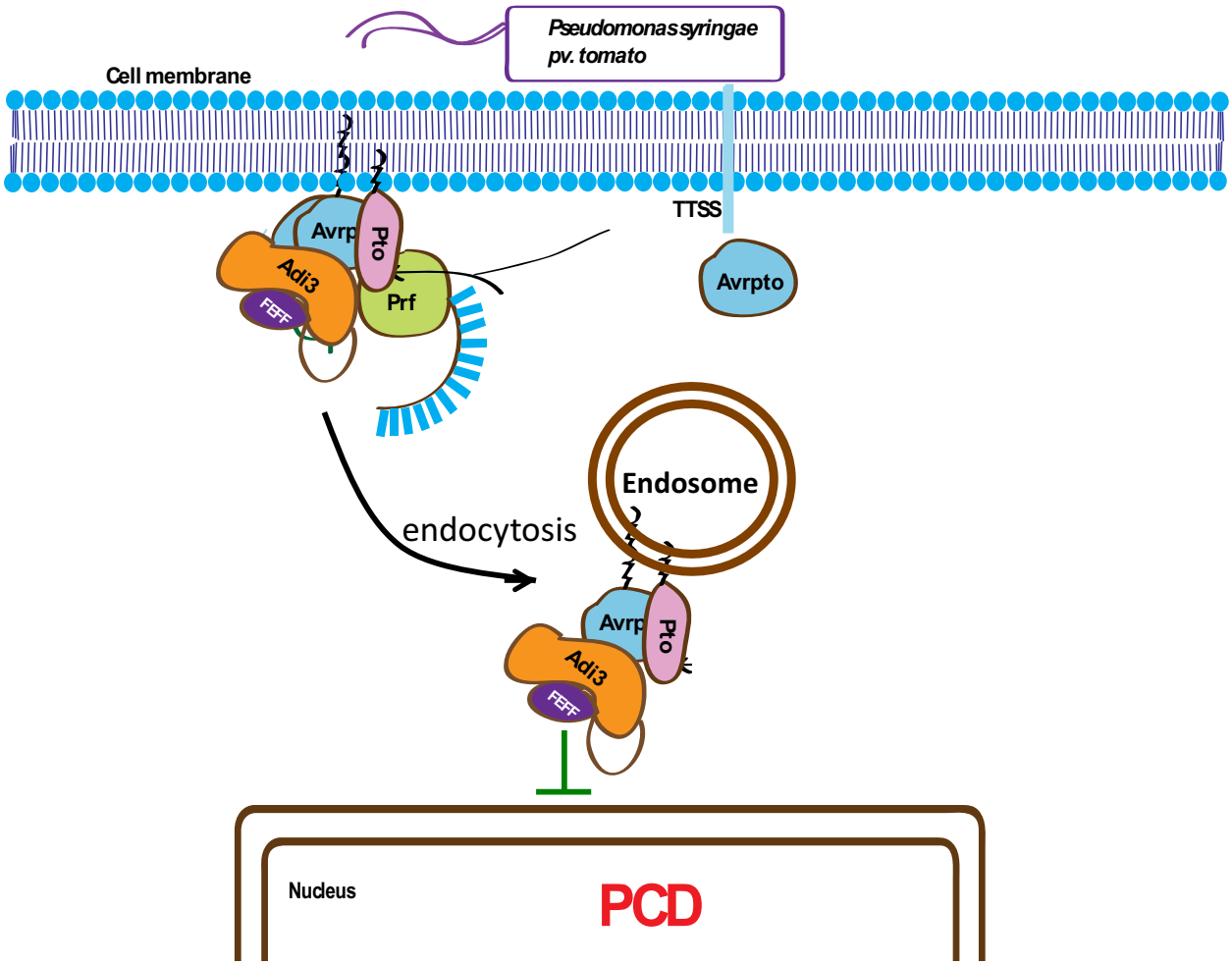

Figure 3. Adi3 regulation in response to *Pseudomonas syringae* pv. *tomato(Pst)*. When infected by Pst that can secret AvrPto into tomato cells through type III secret system, Adi3 can bind to Pto in an AvrPto dependent manner. Adi3 binding to AvrPto and Pto disrupts Adi3 phosphorylation by Pdk1. As a result, Adi3 cannot localize to the nucleus and accumulates in endosome system. Disruption of Adi3 nucleus localization inhibits its cell death suppression function, leading to programmed cell death in the presence of AvrPto.

1.4. The SnRK1 Complex

1.4.1. SnRK1 is a conserved complex in yeast, mammals and plants

To better understand the mechanism of Adi3 regulated PCD, a yeast two-hybrid assay was carried out using a *Pst* challenged library to identify proteins that interact with Adi3 during *Pst* infection. One of the proteins that was found to interact with Adi3 is the Sucrose non-Fermenting Related Kinase1.1 (SnRK1.1) protein, which is the α-subunit of the SnRK1 protein complex [19]. SnRK1 is a plant serine/threonine protein complex that has homolog in both yeast Sucrose Non-fermenting 1 (Snf1) and mammalian AMP-activated protein kinase (AMPK).

First discovered in yeast, the Snf1 complex plays a central role in energy expenditure and metabolism [51,52]. The Snf1 complex and its homologs are well conserved across yeast, mammals, and plants and consist of α, β, and γ subunits[53,54]. In yeast one α-subunit (Snf1), three β-subunits (Gal83, Sip1, and Sip2), and one γ-subunit (Snf3) have been identified [54]. In mammals, the Snf1 homolog is AMPK with two α-subunits (AMPKα1 and AMPKα2), two β-subunits (AMPKβ1 and AMPKβ2), and three γ-subunits (AMPKγ1, AMPKγ2, and AMPKγ3) that have been identified [55]. In plants, the Snf1 complex homologs are the Snf1 Related Kinase 1 (SnRK1) complexes. In *Arabidopsis*, two functional α-subunits (*At*SnRK1.1, aka AKIN10 and *At*SnRK1.2, aka AKIN11) as well as a third very lowly expressed α-subunit (*At*SnRK1.3, aka AKIN13), three β-subunits (*At*SnRK1 β1, β2, and β3, aka AKINβ1, β2, and β3), and two γ-subunits (*At*SnRK1 γ and *At*SnRK1βγ, aka AKIN γ and AKINβγ)[56]. The *At*SnRK1.1βγ is a special γ-subunit that also contains the Carbohydrate Binding Domain (CBD) of the β–subunits and is proposed to be the only functional γ-subunit in *Arabidopsis* [57]. In tomato, two α-subunits (*Sl*SnRK1.1 and *Sl*SnRK1.2), four α-subunits (*Sl*Gal83, *Sl*Sip1, *Sl*Tau1, and *Sl*Tau2), and one γ-subunit (*Sl*Snf4) has been discovered [58]. Besides the SnRK1 family complexes,

plants also have diverged SnRK2 and SnRK3 family complexes specific to plants that function in stress conditions like draught, salt, and cold [59].

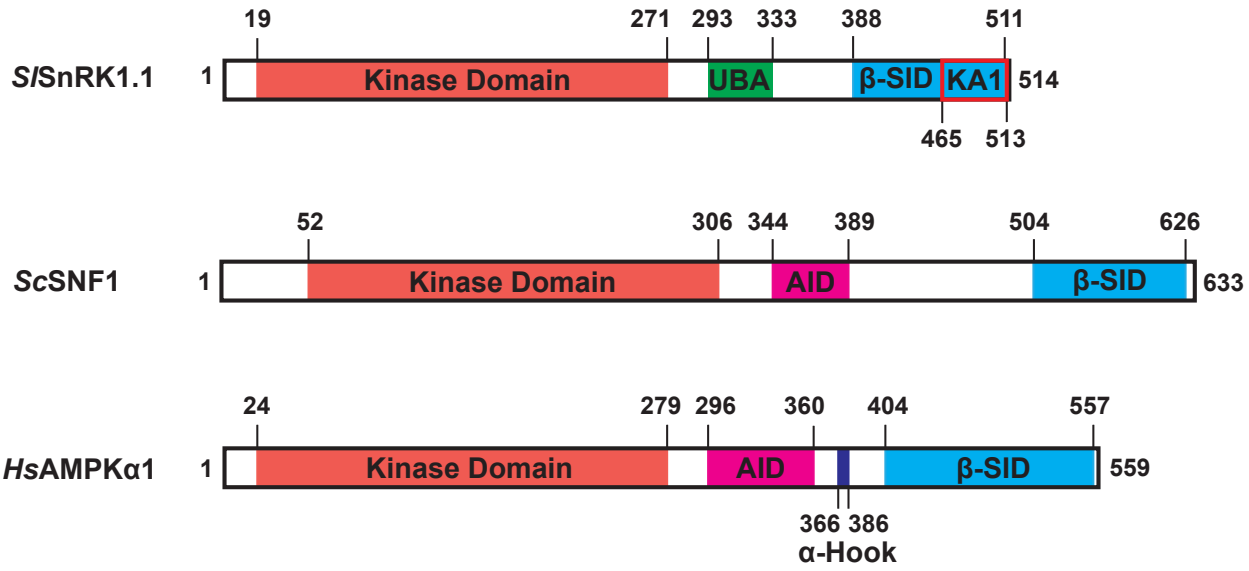

Figure 4. Conserved protein domains of plant SnRK1, yeast SNF1, and mammalian AMPK. Salmon colored box, kinase domain; green box, ubiquitin associated domain (UBA); magenta box, auto-inhibitory domain (AID); light blue box, β-subunit interaction domain (β-SID); dark blue box, α-hook domain, red box, KA1 motif. The kinase domain and β-SID are conserved across yeast, plant and mammals. In plants, there is a conserved KA1 domain within the β-SID domain. Only yeast and mammals have the AID domain that can bind to the unphosphorylated kinase domain for inhibition of kinase activity in the absence of ADP and AMP. The mammalian AMPK also contains an α-hook domain that interacts with the γ-subunit in the presence of ADP or AMP and regulates kinases activity.

1.4.2. Structure and regulation of the SnRK1 catalytic α-subunits

The SnRK1 α-subunits are the subunits that process the Ser/Thr kinase activity [53]. SNF1, AMPK, and SnRK1 α-subunits contain an N-terminal kinase domain and a C-terminal β-subunit interaction domain (β-SID) (Figure 4). Additionally, SnRK1 contains an ubiquitin-associated domain (UBA) (Figure 4, top panel), which has been suggested to bind to ubiquitinated proteins [60] and is not found in AMPK or Snf1. On the other hand, AMPK and Snf1 contain an autoinhibitory domain (AID) (Figure 4, middle and bottom panel) [61] that is not found in SnRK1. Phosphorylation of a conserved Threonine in the activation loop is required for activation of kinase activity. In SNF1, this is Thr 210 that can be phosphorylated by Tos3, Pak1, or Elm1 [62]. In mammal AMPKα, this is Thr172 that can be phosphorylated by LKB1, CaMKKβ, or Tak1 [55]. In *Arabidopsis At*SnRK1, this is Thr175 that can be phosphorylated by *At*SnRK1-activation kinase (*At*SnAK) [63]. In tomato, this is Thr175 for SlSnRK1.1 but the upstream activating kinase has not been identified [58].

1.4.3. Function and regulation of the SnRK1 β-subunits

Snf1/AMPK/SnRK1 β-subunits have been shown to have three conserved protein domains: an N-terminal variable region containing a myristoylation motif (N-Myr), a C-terminal association with Snf1 complex (ASN) domain, and a carbohydrate binding domain (CBD) in the middle of the protein (Figure 5A) [64]. The N-terminal variable region is proposed to determine substrate specificity and subcellular localization of the yeast Snf1 complex [65]. In yeast and mammals, the CBD domain can bind to glycogen so it is also termed the glycogen binding domain in yeast and mammals [66,67], while in plants the CBD domain can bind to starch [68].

The C-terminal ASN domain act as a scaffold of the SNF1/AMPK/SnRK1 complexes by binding to both the α and the γ-subunits.

Regulation of the β-subunits by phosphorylation has been well studied in mammals and yeast. The mammalian β-subunit AMPKβ1 is phosphorylated by the α-subunit AMPKα1 at Ser24/Ser25 and Ser108, as well as Ser182 by an unknown upstream kinase [69,70]. The phosphorylation at Ser108 increases AMPK complex kinase activity [70], while Ser24/Ser25 and Ser182 phosphorylation causes nuclear exclusion of the complex [69]. The yeast β-subunit *Sc*Gal83 can be phosphorylated by the yeast α-subunit Snf1 and casein kinase 2, however, the exact phosphorylation sites and the function of the phosphorylation is still unknown [71]. In plants the tomato β-subunit *Sl*Gal83 was shown to be phosphorylated at Ser26 by Adi3, while the other three tomato β-subunits did not show detectable phosphorylation by Adi3 [58]. This phosphorylation of *Sl*Gal83 by Adi3 has been shown to be the trigger for down regulating the kinase activity of the SnRK1 complex in tomato, possibly during pathogen defense responses [58].

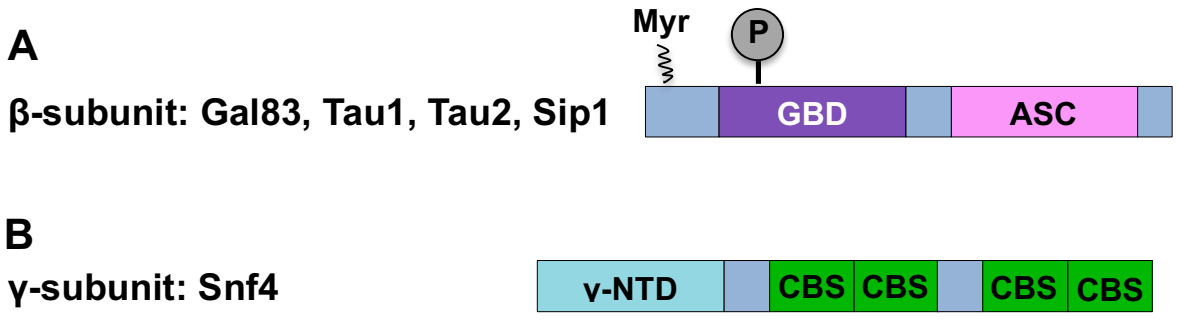

Figure 5. Structure models of SnRK1 complex β and γ subunits. (A) Structure model of SnRK1 β-subunits. Grey box, N-terminal variable region; purple box, glycogen binding domain (GBD), interacts with α-subunit; pink box, associate with snf1 complex domain (ASC); wavy line, N-terminal Myristoylation (Myr) site. (B) Structure model of SnRK1 γ-subunit. Light blue box, non-conserved N-terminal domain; green boxes, cystathionine-β-synthase (CBS) domains.

1.4.4. Function and regulation of the SnRK1 γ-subunits

The SnRK1 γ-subunits contains four repeats of cystathionine-β-synthase (CBS) domains (Figure 5B)[53]. In mammals, AMPKγ can bind to adenylates through its CBS domains one, three, and four [72]. Among these, CBS one and three bind adenylates reversibly, while CBS four binds AMP non-exchangeably [72]. Adenylates binding to these three CBS domains are proposed to regulate AMPK activity by both allosteric activation an enhanced phosphorylation by upstream kinases [73]. In fission yeast, the CBS three and four can bind adenylates interchangeably [74]. In plants, a recent study suggests the *Arabidopsis* βγ type γ-subunit contains only one binding site for adenylates [75]. However, unlike in mammals where binding to AMP/ADP activates AMPK activity, in plants the binding of AMP or ADP to the γ-subunits does not change the activity of the SnRK1 complex [75].

1.4.5. Snf1/AMPK/SnRK1 family proteins are an important part of energy sensing and signaling

Snf1/AMPK/SnRK1 complexes are involved in energy homeostasis. A classic example is the shift from fermentation to oxidative metabolism in the absence of glucose in yeast [52]. Snf1/AMPK/SnRK1 can sense cellular energy status by an increased ratio of ADP/AMP to ATP[76–78]. In mammals, this is achieved through AMP binding to the γ-subunits that both directly activates the α-subunit and increases activation by upstream kinase [73,79]. Additionally, binding of ADP and AMP to the γ-subunits can cause a conformational change that protects the complex against inactivation by phosphatases [73]. In yeast and plants, ADP has also been shown to protect the complex against phosphatases, however the exact binding site and mechanism is still under debate [75,80]. Besides direct regulation by AMP/ADP, Snf1/AMPK/SnRK1 complexes are also regulated by some metabolites, although in many cases

the exact mechanism is not known. In mammals, high concentration of glucose, citrate, glycogen, leucine, and glutamate can inhibit AMPK activity independent of the ADP/AMP to ATP ratio change, suggesting that AMPK can also sense the levels of energy reserves in addition to sensing ATP levels [67,81–83]. In plants, a major regulator of SnKR1 activity is trehalose-6-phosphate (T6P). T6P is considered a signaling molecule for the carbohydrate levels in plants [84]. T6P can inhibit SnRK1 kinase activity at the micromolar concentration range and this inhibition is mediated through a still unidentified factor that is separable from SnRK1 [85]. The inhibition by T6P has not been observed in yeasts, mammals, or mature plant leaves, indicating specificity for certain plant tissue and development stages [86].

1.4.6. Snf1/AMPK/SnRK1 roles in regulation of metabolism

The result of SnRK1 signaling is changes in a wide range of metabolic processes. The regulation is achieved by either direct phosphorylation of key enzymes in metabolic pathways or phosphorylation of transcription factors, some key examples are detailed below. In yeast and mammals, Snf1 and AMPK can inhibit fatty acid synthesis through direct phosphorylation and inhibition of acetyl-CoA carboxylase [87,88]. Plant SnRK1 and mammalian AMPK can inhibit the isoprenoid pathway by direct phosphorylation and inactivation of HMG-CoA reductase [89,90]. In plants, SnRK1 can also regulate sucrose synthesis, photosynthate partitioning, nitrogen assimilation, as well as stress and developmental signaling, through direct phosphorylation and inactivation of sucrose phosphate synthase, fructo-2,6-bisphosphatase, nitrate reductase (NR), and trehalose phosphate synthase 5, respectively [91–93]. Compared to direct phosphorylation, regulation of transcription factors by Snf1/AMPK/SnRK1 can result in large scale reprogramming of transcription. In yeast, Snf1 increases nuclear export of a

transcriptional repressor of glucose-repressed genes called Mig1, releasing glucose repression when glucose levels are low [94,95]. In plants, SnRK1 regulates S-group bZIP transcription factors, including bZIP1, bZIP2, bZIP11, bZIP44, and bZIP 53, which regulate responses to stresses including darkness and hypoxia [56]. One of the S-group bZIP transcription factors, bZIP11, has been shown to regulate amino acid metabolism through regulating expression levels of asparagine synthetase 1 and proline dehydrogenase 2[96].

1.4.6. Fight or flight, the dilemma of energy expenditure strategy

Pathogen defense is an energy intensive process; as a result, the affected cell will take up hexose sugars produced by cleavage of apoplastic sucrose by invertase ("fight") [97]. On the other hand, it has been shown that plants undergoing herbivorous attack will redistribute nutrition in the affected cell to other parts of the plant, preserving nutrients for other parts of the plant ("flight") [98]. Little is known about which strategy is used by incompatible plants during *Pst* infection. The SnRK1 complex is proposed to have a central role in regulating the synthesis of over a thousand proteins through regulation of transcription factors, chromatin remodeling, and direct modulation of metabolic enzyme activity [56,99,100]. Due to the central role of the SnRK1 complex in cell metabolism, it will be a good target to study in order to understand the energy strategy plants employ during resistant interactions with *Pst*.

1.6. Nitrate Reductase

1.6.1. Nitrate reductase structure and function

Nitrate reductase (NR) is a cytosolic enzyme that catalyzes the reduction of nitrate to nitrite, which is the first and rate limiting step of nitrate assimilation in fungi, algae, and plants

[101]. NR contains an N-terminal molybdenum cofactor (Moco) binding domain, followed by a dimerization domain, together these two domains form the nitrate reducing module; the center region contains the heme domain that is linked to the dimerization domain through hinge 1; the C-terminus contains the flavin adenine nucleotide cofactor associated (FAD) domain that is linked to the heme domain by hinge 2 [101]. Plant NR, depending on the species, either only use NADH or use both NADH and NADPH as the reducing agent [102]. NR is only active as a dimer since each molecule of nitrate needs two electrons in order to be reduced into nitrite, and each NR can only transport one electron at a time[103]. The catalytic process of NR starts with binding of two molecules of NADH or NADPH to the FAD domain, the electrons are transported from NADH or NADPH to the FAD domain, then through the heme domain to be finally transferred to one molecule of nitrate via the Moco domain, forming one molecule of nitrite (Figure 6) [104].

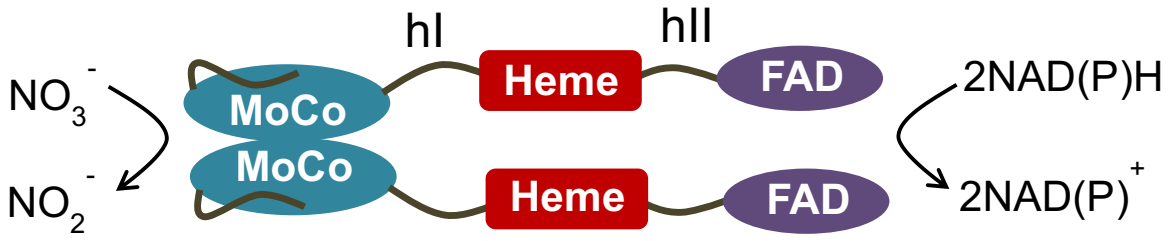

Figure 6. Structure and function of nitrate reductase (NR). NR is consisted of N-terminal molybdenum (MoCo) domain, Heme domain and C-terminal flavin adenine nucleotide cofactor associated (FAD) domain. These three domains are linked by two hind regions, hI and hII. NR function as homodimer. The FAD domains binds to two molecules of NAD(P)H, transporting electrons from NAD(P)H through heme and MoCo domain to reduce one molecule of NO_3^- to NO_2^-.

1.6.2. Regulation of nitrate reductase

NR activity is tightly regulated in plants, this is because: 1) nitrate reduction is a very energy intensive process that consumes about 20% of the reducing power produced by photosynthetic electron transport [105]; 2) the intermediate product, nitrite, is mutagenic, and nitrile ion can form nitrous acid that are highly toxic to the photosynthetic apparatus [106]. As a result, NR activity regulation is closely coupled to photosynthesis and NR could be rapidly inactivated under conditions that limit photosynthesis [107]. NR can be phosphorylated by multiple protein kinases including CDPK and SnRK1 [93,108] in the conserved motif R/K-S/T-X-pS-X-P in the hinge 1 domain [109,110]. It was previously thought that phosphorylation on the conserved motif inhibits NR activity[93]. Recent studies indicate that it is not the phosphorylation *per se* that caused the inhibition, but the phosphorylation on hinge 1 promotes binding of a 14-3-3 protein to the hinge 1 region and an N-terminal acidic motif, which in turn disrupt electron transport by changing NR conformation [111,112].

1.6.3. Nitrate reductase regulation by the SnRK1 complex

It has long been proposed that SnRK1 could phosphorylate NR in spinach [93,108]. More recent studies using cell free assays confirmed that *Arabidopsis* SnRK1.1 and SnRK1.2 α-subunits can bind *Arabidopsis* NR2 [113]. Moreover, *At*SnRK1β1 but not *At*SnRK1β2 can bind to NR2 through its ASC domain and this binding specificity is conferred by the β-subunit N-terminal domain [113]. Another study further demonstrated the link between the SnRK1 complex and NR activity regulation by the observation that overexpression of *At*SnRK1β1 strongly inhibits NR activity while a knockout of *At*SnRK1β1 increases NR activity [114].

CHAPTER II

METHODS

2.1. Cloning and Site Directed Mutagenesis

2.1.1. Cloning of, SlSnRK1.2, Tau2 and SlSnAK.

All primers used for cloning and site directed mutagenesis are listed in Table 1. The *Sl*SnRK1.2 α-subunit was identified by BLAST against the tomato proteome at the Sol Genomics Network (https://solgenomics.net) using the full-length amino acid sequence of *Sl*SnRK1.1 (NP_001304105.1) [58] as the query. The identified *SlSnRK1.2* sequence was used to designed primers for cloning of the ORF. Using tomato leaf total RNA and RT-PCR, a 1,512 bp full-length ORF for *Sl*SnRK1.2 was cloned that matched the *SlSnRK1.2* sequence (NM_001247396.3) identified in GenBank from a tomato cDNA sequencing project [115]. For the RT-PCR, first strand cDNA was produced using the SuperScript™ IV First-Strand Synthesis System (Invitrogen), and the *SlSnRK1.2* ORF was amplified from first strand cDNA using GoTaq Green (Promega). The *SlSnRK1.2* ORF was first cloned into the pGEMT vector by TA cloning, identity confirmed by sequencing, and the ORF sub-cloned into the pMAL-c2x vector using the *Eco*RI and *Sal*I restriction sites for expression of an N-terminal maltose binding protein (MBP) translational fusion protein in *E. coli*. The MBP-*Sl*SnRK1.2 recombinant protein was purified using amylose resin (NEB) in a gravity-fed column according to manufacturer instructions.

The *Sl*SnAK sequence was identified by BLAST against the tomato proteome in the NCBI database using the full-length amino acid sequence of *At*SnAK1 (NP_200863.2) and *At*SnAK2 (NP_566876.3) [63,116]. The *Arabidopsis* sequences identified two possible splicing

forms of a single *SlSnAK* (XM_010315107, XM_010315106). Although the two splice variants are different in the 5'-UTR regions, both contained the same full length 1,254 bp ORF and 3'-UTR regions. The *SlSnAK* ORF was isolated and cloned into pGEMT as described above for *SlSnRK1.2*. The *SlSnAK* ORF was sub-cloned into the pET28a vector using the *Eco*RI and *Sal*I restriction sites for expression of an N-terminal 6xHis translational fusing protein in *E. coli*. The His-*Sl*SnAK recombinant protein was purified using Ni-NTA agarose resin (QIAGEN) in a gravity-fed column according to manufacture instructions.

The *SlSnRK1.1* ORF was previously cloned [58] and purification of MBP-*Sl*SnRK1.1 followed published protocols.

The Tau2 sequence was identified by BLAST against the tomato genome at the Sol Genomics Network using the predicted translated ORF of the tomato *SlSip1* cDNA sequence (AF322108) [58]. A 819 bp full-length ORF for *SlTau2* (JQ846035) was identified and cloned by RT-PCR using tomato leaf total RNA. First strand cDNA was produced using the SuperScript™ III First-Strand Synthesis System (Invitrogen), and the *SlTau2* ORF was amplified from first strand cDNA using GoTaq Green (Promega). The SlTau2 ORF was cloned into the pGEMT vector by TA cloning, identity confirmed by sequencing.

Site directed mutagenesis of *SnRK1.2* and *Tau2* was performed using Pfu Turbo DNA Polymerase (Agilent Technologies) according to manufacturer instructions using primers listed in Table 1.

Table 1. Primers used in the study.

Primer Name	Sequence	Gene	Purpose
SnRK1.2-F	ATGAGTTCCAGAGGTGGTGG	SnRK1.2	Forward primer for SnRK1.2 from +1
SnRK1.2-R	TCATTGTGGCCCCTCTAGCTG	SnRK1.2	Reverse primer for SnRK2 to stop codon
SnRK1.1T175E-F	GATGGTCATTTTCTGAAGGAAAG TTGCGGAAGC	SNRK1.1	Forward primer to cause a T to E mutation in SnRK1.1
SnRK1.1T175E-R	GAGGTCATTTTCTGAAGGAAAGT TGCGGAAGC	SNRK1.1	Reverse primer to cause a T to E mutation in SnRK1.1
BamHI-SnRK1.1-F	CACGGATCCATGGACGGAAC	SnRK1.1	Forward primer to add BamHI site to the beginning of SnRK1.1
SnRK1.1NS-SalI-R	CTAGTCGACAAGTACTCGAAGCT GAGCAAG	SnRK1.1	Reverse primer to add SalI site to C-terminal of SnRK1.1 without stop codon
SnRK1.2-T173D-F	CCATTTTCTGAAGGATAGTTGTG GAAGTCCAA	SnRK1.2	Mutagenesis primer T173D
SnRK1.2-T173D-R	TTGGACTTCCACAACTATCCTTCA GAAAATGG	SnRK1.2	Mutagenesis primer T173D
SnRK1.2-T173E-F	CCATTTTCTGAAGGAGAGTTGTG GAAGTCCAA	SnRK1.2	MBP-SNRK1.2 T173E SDM forward primer

Table 1. Continued

Primer Name	Sequence	Gene	Purpose
SnRK1.2-T173E-F	TTGGACTTCCACAACTGTCCTTCAGAAAATGG	SnRK1.2	MBP-SNRK1.2 T173E SDM reverse primer
SNRK1.2-ECORI-F	GAATTCATGTCCAGAGG	SnRK1.2	Forward primer for SnRK2 adding a EcoRI restriction site to 5'-end
SnRK1.2-SalI-R	GTCGACTCATTGTGGCCCCTC	SnRK1.2	Reverse primer for SnRK1.2 adding a SalI restriction site to 3'-end
SnRK1.2-EcoRI+1-F	CACGAATTCGATGAGTTTCCAGAGGTG	SnRK1.2	Forward primer to add EcoRI site to the N-terminus of SnRK1.2 and cause a +1 frame shift.
SnRK1.2-NS-SalI-R	GTGATTGTCGACTTGTGGCCCCTC	SnRK1.2	Reverse primer adding SalI restrection site and eliminating stop codon
SnRK1.2 a78c-F	GAAAAACTCTTGGACATGGCTCCTTTGGTAAAG	SnRK1.2	Forward primer to mutate a78c to eliminate BamHI site
SnRK1.2 a78c-R	CTTTACCAAAGGAGCCATGTCCAAGAGTTTTTC	SnRK1.2	Reverse primer to mutate a78c to eliminate BamHI site
BamHI-SnRK1.2-F2	CACGGATCCATGAGTTCCAGAGGTGGTG	SnRK1.2	Forward primer to add BamHI site to the beginning of SnRK1.2 with BamHI site mutated
SnRK1.1R50A/K51A-F	ATCCTTAATCGGGCGGCAATGAAGACTCCAGAC	SNRK1.2	Forward primer for R50A/K51A mutation in putative NLS in SnRK1.2

Table 1. Continued

Primer Name	Sequence	Gene	Purpose
SnRK1.1R50A/K51A-R	GTCTGGAGTCTTCATTGCCGCCC GATTAAGGAT	SNRK1.2	Reverse primer for R50A/K51A mutation in putative NLS in SnRK1.2
SlSnAK-F	GGATGTCTGTGATGATGC	SlSnAK	Forward primer to amplify putative SnRK upstream kinase SnAK
SlSnAK-R	TCAAGTAGGGGTATCCTCTG	SlSnAK	Reverse primer to amplify putative SnRK upstream kinase SnAK
SlSnAK-EcoRI-F	CACGAATTCATGTCTGTGATGAT GC	SlSnAK	Forward primer to add EcoRI to tomato SnAK
SlSnAK-SalI-R	GTAGTCGACTCAAGTAGGGGTAT CCTC	SlSnAK	Reverse primer to add SalI to tomato SnAK
Tau2-3UTR-R	TGTCTAACACATTCCTCTGCTAC	Tau2	Reverse primer annealing to the 3'URT of Tau2 upstream of Tau2-3UTR-R1 for RT-PCR
Tau2-5UTR-F	CAAACTTTAATGGGGAATG	Tau2	Forward primer annealing on the 5'UTR and CDS of Tau2 for RT-PCR
SlTau2 - S244A - F	CATGCAGAAGGGAAAGGCTAAC CCATCTCTGGTAGC	Tau2	Mutagenesis primer replacing putative SnRK phosphorylation site on Tau2.
SlTau2 - S244A - R	GCTACCAGAGATGGGTTAGCCTT TCCCTTCTGCATG	Tau2	Mutagenesis primer replacing putative SnRK phosphorylation site on Tau2.

Table 1. Continued

Primer Name	Sequence	Gene	Purpose
SlTau2 - S247A - F	GGGAAAGAGTAACCCAGCTCTGGTAGCACTCAG	Tau2	Mutagenesis primer replacing putative SnRK phosphorylation site on Tau2.
SlTau2 - S247A - R	CTGAGTGCTACCAGAGCTGGGTTACTCTTTCCC	Tau2	Mutagenesis primer replacing putative SnRK phosphorylation site on Tau2.
Tau2S244/247A-F	GGGAAAGGCTAACCCAGCTCTGGTAGCACTCAG	Tau2	Forward mutagenesis primer for TAU2 S244A, S247A double mutation
Tau2S244/247A-R	CTGAGTGCTACCAGAGCTGGGTTAGCCTTTCCC	Tau2	Reverse mutagenesis primer for TAU2 S244A, S247A DOUBLE MUTATION
Tau2S32A-F	GAATTTATGGGTCAATATCCACCTTCAAGTC	Tau2	Forward primer to mutate Tau2 S32 to A
Tau2S32A-R	CTTGAAGGTGGATATTGACCCATAAATTCAC	Tau2	Reverse primer to mutate Tau2 S32 to A
NR-F	TCAATGGCGGCATCTGTG	NIA	forward prime to amplify tomato nitrate reductase from cDNA. With first 3 nucleotides in 5'UTR
NR-R	CCATCCAATTTAGAACAC	NIA	Reverse prime to amplify tomato nitrate reductase from cDNA.
NR-XbaI-F	CTATCTAGAATGGCGGCATCTGTGGA	NIA	Forward primer to add XbaI to the 5' end of NR, contains 3 extra bp for cutting enzyme binding
NR-PstI-R	CTGCAGTTAGAACACCAATAGTTC	NIA	reverse primer to add PstI to the 3' of tomato nitrate reductase

2.1.2. Cloning of tomato Nitrate Reductase

Primers for the nitrate reductase ORF (*SlNIA*) (CAA32218) was designed based on previously reported gene sequence[117]. A 911 bp full-length ORF for *SlNIA* (CAA32218) was identified and cloned by RT-PCR using tomato leaf total RNA. First strand cDNA was produced using the SuperScript™ IV First-Strand Synthesis System (Invitrogen), and the *SlNIA* ORF was amplified from first strand cDNA using Phusion High-Fidelity DNA Polymerase (NEB). The *SlNIA* ORF was cloned into the *Xba*I and *Pst*I sites of the pMAL-c2x vector.

2.2. Recombinant Protein Expression and Purification

SlSnRK1.2 and *SlTau2* were sub-cloned into the *EcoR*I and *Sal*I sites of the pMAL-c2x (NEB) vector for expression of an N-terminal maltose binding protein (MBP) translational fusion protein. *SlNIA* was cloned into the *Xba*I and *Pst*I sites of the pMAL-c2x (NEB) vector for expression of an N-terminal MBP translational fusion protein. *E. coli* BL21 Star (DE3) was used for fusion protein expression. Recombinant proteins were purified using amylose resin (NEB) in a gravity-fed column according to manufacturer instructions.

The *SlSnAK* ORF was sub-cloned into the *EcoR*I and *Sal*I sites of the pET28a vector for expression of an N-terminal 6xHis translational fusing protein in *E. coli*. The His-*Sl*SnAK recombinant protein was purified using Ni-NTA agarose resin (QIAGEN) in a gravity-fed column according to manufacture instructions.

The *SlSip1*, *SlGal83*, *SlTau1*, *SlSnf4*, and *SlSnRK1.1* ORF was previously cloned and purification of MBP-*Sl*Sip1, MBP-*Sl*Gal83, MBP-*Sl*Snf4, and MBP-*Sl*SnRK1.1 followed published protocols [58].

All eluted proteins were concentrated using Amicon Ultra Centrifugal Filter Units (Millipore Sigma), mixed with storage buffer (50mM Tris-HCl pH7.5, 50% glycerol, 0.5mM EDTA, 50 mM NaCl), and stored at -80 °C. Protein concentrations were quantified using Bradford protein assay (Bio-Rad) before protein assay.

SlSnRK1.1 and *SlSnRK1.2* were cloned in to the pFLAG-CTC vector (Sigma-Aldrich) for expression of C-terminal FLAG tagged *Sl*SnRK1.1 and *Sl*SnRK1.2 for pull-down assays. *E. coli* BL21 Star (DE3) cells expressing recombinant proteins were aliquoted and flash frozen by liquid nitrogen, then stored at -20 °C.

2.3. Yeast Knockout Complementation Assay

SlSnRK1.1 and *SlSnRK1.2* were subcloned for a C-terminal FLAG tag into the MBB263 vector (uracil selection) modified for expression control under the *glyceraldehyde-3-phosphate dehydrogenase* promotor. The yeast *SNF1* knockout strain BY4741 (*MATa snf1Δ::KanMX his3Δ1 leu2Δ0 met15Δ0 ura3Δ0*) was obtained from Dharmacon, and was transformed with the above *SlSnRK1.1* and *SlSnRK1.2* constructs using the lithium acetate/PEG method. The transformants were screened on synthetic complete (SC) media lacking uracil with 2% glucose at 30 °C. Recovered colonies were grown in liquid SC -uracil media with 2% glucose for 40 hrs, adjusted to the same OD_{600} spotted on SC -uracil plates containing either 2% glucose or 2% sucrose in 5-fold serial dilutions, and incubated at 30 °C for 48 hrs or 144 hrs, respectively, before imaging.

2.4. Pull Down Assays

E. coli BL21 Star (DE3) cells expressing recombinant MBP-*Sl*SnRK1.1 and MBP-*Sl*SnRK1.2 were lysed in lysis buffer (10 mM Tris-HCl pH8.0, 150mM NaCl, 5mM EDTA, 0.1% TritonX-100, 1x protease inhibitor). The cell lysate was centrifuged at 14,000 *g* at 4°C for 10 mins. The supernatant containing MBP-*Sl*SnRK1.1 and MBP-*Sl*SnRK1.2 was incubated with Amylose Resin (NEB) for 1 hour on a rocking platform shaker at 4°C in the presence or absence of MBP-tagged *Sl*Sip1, *Sl*Gal83, *Sl*Tau1, *Sl*Tau2, or *Sl*Snf4. Resin incubated with MBP-*Sl*SnRK1.1 was washed 5 times with washing buffer 1 (10 mM Tris-HCl pH8.0, 150mM NaCl, 5mM EDTA, 0.1% TritonX-100), while resin incubated with MBP-*Sl*SnRK1.1 was washed 5 times with washing buffer 2 (10 mM Tris-HCl pH8.0, 500mM NaCl, 5mM EDTA, 0.1% TritonX-100). After wash the resin was boiled at 95 °C in SDS-PAGE sample buffer, resolved by 8% SDS-PAGE, and transferred onto Amersham Hybond P 0.45 PVDF membrane (GE Healthcare). For western blot, 1:1000 diluted α-FLAG-HRP (Sigma-Aldrich), 1:5000 diluted α-MBP (NEB), and 1:10000 diluted α-mouse-HRP was used. Western blot detection was performed using Amersham ECL prime (GE Healthcare) and the chemiluminescent signal was detected using an Amersham Imager 600 (GE Healthcare).

2.5. Kinase Assays

2.5.1. Autophosphorylation and phosphorylation of the β-subunits

*Sl*SnRK1.1 autophosphorylation and phosphorylation of the β-subunits was carried out in a buffer containing 10 mM DDT, 10 mM Tris-HCl pH 8.0, and 10 mM $MgCl_2$. *Sl*SnRK1.2 autophosphorylation and phosphorylation of the β-subunits was carried out in a buffer containing 10 mM DDT, 10 mM Tris-HCl pH 7.5, and 10 mM $MnCl_2$. Reactions were initiated by addition

of 2 μCi of γ-[^{32}P]ATP (6,000 Ci/mmole) and non-radioactive ATP to a final concentration of 100 μM. Four mg of *Sl*SnRK1.1 or *Sl*SnRK1.2 and 4 mg of *Sl*Gal83, *Sl*Sip1, *Sl*Tau1, or *Sl*Tau2 were used in each reaction as indicated. The reactions were carried out at either 30 °C for 15 min for *Sl*SnRK1.1 or 14 hrs at 20 °C for *Sl*SnRK1.2, after which the reaction was terminated with the addition of 10ul 4x SDS-PAGE sample buffer. Proteins were resolved by 8% SDS-PAGE, the gel dried, and the gel exposed to a phosphorimager screen for different lengths of time as specified in the figure legends. Incorporated radioactivity was visualized and quantified using a phosphorimager (Typhoon FLA7000, GE Healthcare Life Sciences) and quantification software (ImageQuant TL, GE Healthcare Life Sciences). Band volume of each phosphorylated protein was calculated by integrating the area below the peak of each band and above the background as determined using the rolling ball method (Figure 7). In order to determine suitable exposure times for different kinase assays, an initial 24 hr exposure was analyzed and subsequent exposure times were adjusted so that the signal from different reactions were all in the same range.

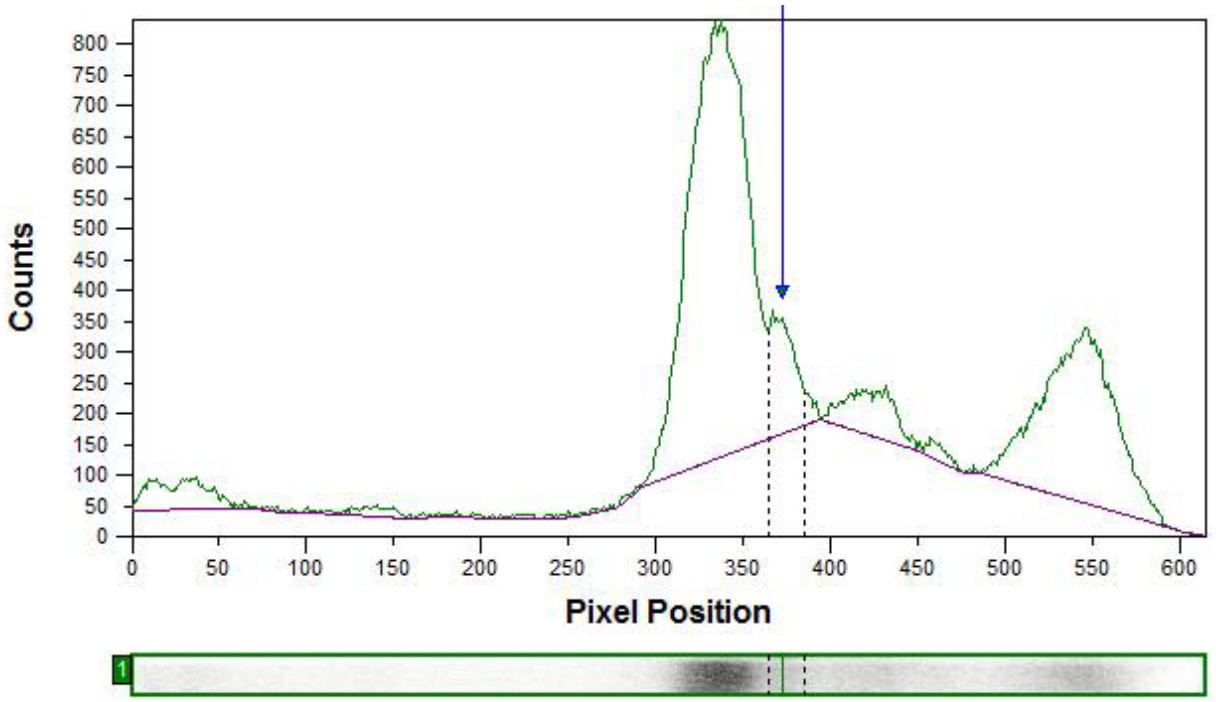

Figure 7. Analysis of phosphorimage band volume using ImageQuant TL. Bottom panel, a single phosphor image scan lane in horizontal orientation Top panel, signal counts for the bottom panel. Green peaks, signal counts at each pixel position of the single gel lane; purple line, background subtraction using rolling ball method; blue arrow, detection peak for target protein phosphorylation signal; dotted line, cut-off for phosphorylation peak of target protein by slope detection. Band volume of target protein phosphorylation is calculated by integrating the area below the green peak and above the purple line.

2.5.2. SlSnAK activation of SlSnRK1.1 and SlSnRK1.2 for β-subunit phosphorylation

For *Sl*SnAK activation reactions, 4 mg of *Sl*SnRK1.1 or *Sl*SnRK1.2 were pre-incubated with 1 mg of *Sl*SnAK in the presence of 50 μM non-radioactive ATP at 30 °C for 15 min. Each β-subunit was then added and the phosphorylation reactions initiated by the addition of 2 μCi of γ-[^{32}P]ATP (6,000 Ci/mmole) and non-radioactive ATP to a final concentration of 100 μM, including the initial 50 μM non-radioactive ATP used for *Sl*SnAK activation. Due to the relatively high level of *Sl*SnAK autophosphorylation, *Sl*SnRK1.2 reactions that contain *Sl*SnAK were only carried out for 30 min at 30 °C instead of the usual 14 hrs at 20 °C to avoid the overly strong signal from *Sl*SnAK autophosphorylation. Reactions were terminated with the addition of 10 ul 4x SDS-PAGE sample buffer and protein phosphorylation levels were analyzed as described above.

2.5.3. SlSnAK activation of SlSnRK1.1 and SlSnRK1.2 complexes for peptide substrate-based kinase assays

Four mg of *Sl*SnRK1.1 or *Sl*SnRK1.2, 4 mg of *Sl*Gal83, *Sl*Sip1, *Sl*Tau1, or *Sl*Tau2, and 4 mg of *Sl*Snf4 were used to reconstitute the *Sl*SnRK1 complex. The complexes were activated by the addition of 1 mg of *Sl*SnAK and 50 μM non-radioactive ATP at 30 °C for 15 min. After activation, 2 μCi of γ-[^{32}P]ATP (6,000 Ci/mmole) with non-radioactive ATP to a final concentration of 100 μM, including the initial 50 μM non-radioactive ATP used for *Sl*SnAK activation, and 100 μM AMARA peptide [118] (GenScript) were added to each reaction. The *Sl*SnRK1.1 reaction was incubated at 30 °C for 15 min, while *Sl*SnRK1.2 was incubated at 30 °C for 30 min. The reactions were terminated by heating at 95 °C for 10 min. Each reaction was spotted on a 2 cm x 2 cm piece of P81 paper (Reaction Biology Corp), washed three times with

74 mM phosphoric acid, and washed one time with acetone to bind the phosphorylated peptide to the filter paper while removing all other proteins. The filter paper was then submerged in scintillation fluid (Bio Safe II, RPI) in a scintillation vial and the incorporated radioactivity detected using a liquid scintillation counter (LSC) (Tri-Carb 2910R, Perkin Elmer). The count per minute (CPM) reading was converted to nmol of ATP incorporated per minute per mg of *Sl*SnRK1.1 or *Sl*SnRK1.2 as previously described [119]. Due to the possibility of residual phosphorylated proteins adhering to the filter paper, CPMs from reactions containing each protein combination but no AMARA peptide were used as a background level, and this background from each protein combination was subtracted from each corresponding full reaction CPM to obtain net AMARA phosphorylation levels. Reactions containing all components except *Sl*SnRK1.1 or *Sl*SnRK1.2 were carried out as negative controls.

2.5.3. AMARA peptide assay with crude plant extract

A plant crude extract was prepared as described previously [120] with modifications. Five grams of tomato leaves were ground in liquid nitrogen and then suspended in 200 ul plant total protein extraction buffer (50mM Tris 8.2, 1mM EDTA,1mM EGTA, 1mM DTT, 50mM NaCl, 8% (v/v) glycerol, 1xphosphatase inhibitor (P9599, Sigma-Aldrich) and 1xprotease inhibitor (P0044, Sigma-Aldrich). The mixture was centrifuged at 14,000 *g*, 4°C for 15 min. PEG 8,000 was added to the supernatant to 11% w/v. The mixture was stirred on ice for 20 min then centrifuged at 14,000 *g*, 4°C for 30 min. The pellet was resuspended in extraction buffer and 2 ug of total protein was added to kinase buffer (40 mM HEPES, pH 7.0, 0.8 mM EDTA, 1 mM EGTA, 50 mM NaCl, 1 mM DTT, 1x protease inhibitor (P9599, Sigma-Aldrich), 1x phosphatase inhibitor (P0044, Sigma-Aldrich), 8% [v/v] glycerol, 5 mM $MgCl_2$, 200 mM AMARA peptide),

Reactions were initiated by the addition of 2 μCi of γ-[^{32}P]ATP and non-radioactive ATP in a final concentration of 100 μM. The reactions were carried out at 30 ℃ for 2 hrs. After incubation, the reaction was spotted on a 2 cm × 2 cm piece of P81 paper (Reaction Biology Corp), washed three times with 74 mM phosphoric acid, and washed one time with acetone to bind the phosphorylated peptide to the filter paper while removing all other proteins. The filter paper was then submerged in scintillation fluid (Bio Safe II, RPI) in a scintillation vial and the incorporated radioactivity detected using a Liquid Scintillation Analyzer (Tri-Carb 2910R, Perkin Elmer).

2.7 Mass Spectrometry

After preforming the *in vitro* phosphorylation assay, Tau2 and its mutants were separated by 8-16% gradient SDS-PAGE. Protein bands corresponding to Tau2 were cut out and in-gel digested with trypsin overnight. Phosphopeptides were enriched using a NuTip metal oxide phosphoprotein enrichment kit (Glygen). The enriched phosphopeptides were analyzed by LC-MS/MS using an LTQ Orbitrap XL mass spectrometer (Thermo Scientific), using collision induced dissociation (CID) method. The MS/MS spectra were analyzed using Mascot Server (Matrix Science).

2.8. *Agrobacterium* and *Pseudomonas syringe* pv. *tomato* Infiltration

Empty pBTEX vector or pBTEX vector containing C-terminally FLAG-tagged AvrPto were transformed in to *Agrobacterium tumefaciens* GV3101 by electroporation using a MicroPulser Electroporator following manufacturer's instructions (Bio-Rad). Transformed *Agrobacterium* were grown at 28 °C in LB media overnight, pelleted, then resuspended in ice

cold infiltration media (10 mM MES, pH5.5, 10 mM $MgCl_2$, 200 μM). The resuspended *Agrobacterium* was allowed to recover at 28 °C for 1 hour, then adjusted to final OD_{600} of 0.2 or 0.5 before infiltration. The agrobacterium solution was infiltrated from the lower epidermis of PtoR or *prf-3* tomato leaves using a syringe.

Pseudomonas syringe pv. *tomato (Pst)* strains DC3000, DC3000*ΔavrPto*, DC3000*ΔavrPtoB* and DC3000*ΔavrPtoΔavrPtoB*, were produced previously by Lin et, al [121]. *Pst* was grown on King's B plates overnight at 37 °C. The colonies were scraped from the plate and resuspended in 10 mM $MgCl_2$. The CFU of the *Pst* suspension was estimated by cell counting under microscope and adjusted to 10^6 CFU/ml before infiltration. The *Pst* solution was infiltrated from the lower epidermis of PtoR or *prf-3* tomato leaves using a syringe.

2.9. Protoplast Protein Expression and Microscopy

The *SlSnRK1.2* ORF was cloned into the *Bam*HI and *Sal*I restriction sites of pTEX-eGFP containing the 35S promoter, which will produce a C-terminal GFP fusion on *Sl*SnRK1.2. Site directed mutagenesis was performed on pTEX-*SlSnRK1.2*-eGFP to yield the double mutation of $SnRK1.2^{R53A/K54A}$. pTEX-eGFP containing wild type and $SnRK1.2^{R53A/K54A}$ was purified by CsCl gradient centrifugation[122] and stored at -20 °C.

Tomato protoplasts were isolated from PtoR tomato plants that are 4-weeks-old. The leaves were cut into 5 mm squares and floated on the surface of digestion buffer (20 mM MES pH5.7, 1.5% wt/vol cellulose R10, 0.4% wt/vol macerozyme R10, 0.4 M mannitol, 20 mM KCl, 10 mM $CaCl_2$, 0.1% BSA) in a petri dish in dark at 25 °C for 12 hrs. Protoplasts were released by slowly shaking on an orbital shaker for 30 min, then filtered through a 40 mesh tissue sieve to remove debris. A layer of W5 buffer (154 mM NaCl, 5.55 mM glucose, 125 mM $CaCl_2$, 5.36

mM KCl) was added to the top of the protoplast and then centrifuged at 400 *g*, at 20 °C for 3 mins, so that live protoplasts float to the interface with the W5 buffer. The live cells at the interface were collected and washed again with W5 buffer, then recovered on ice for 2 hrs. After recovery, the percent of live protoplasts were counted by staining 100 ul of protoplasts with 0.1% Evans blue and counting live cells using a hemocytometer under a light microscope. The live protoplasts were resuspended in MMM buffer (0.4 D-mannitol, 15 mM $MgCl_2$, 4 mM MES pH5.7) at a concentration of 7.5 x 10^5 cells/ml. Protoplasts were transformed by adding 200 ul of cells to a tube along with 25 ug of CsCl purified plasmid, then an equal volume of PEG solution (0.8 M D-mannitol, 1M $Ca(NO_3)_2$, 40%w/v PEG4000) was added and incubated for 5 mins. After transformation, the protoplasts were washed with W5 buffer and resuspended in 400 ul WI solution (0.5 M D-mannitol, 4 mM MES pH5.7, 20 mM KCl). Protoplasts in WI solution were incubated in the dark at 20 °C for 16 hours to express protein, then visualized using a Zeiss Axioplan 2 fluorescent microscope.

2.10. Ion Leakage Test

Pst strains DC3000, DC3000*ΔavrPto*, and DC3000*ΔavrPtoΔavrPtoB* were infiltrated into PtoR tomato leaves at 10^6 CFU/ml. Four hours after infiltration, four 6 mm diameter leaf discs per plant was taken from the infiltrated leaf area with a hole punch (Staples). The leaf discs were washed twice in sterile MilliQ water for 15 mins each in a shaker at 250 rpm at 20 °C . After washing, the discs from each plant were submerged in 6ml sterile MilliQ water and incubated for 1 hr at 20 °C. The conductivity of the solutions after incubation were measured using a CON 6+ meter (Oakton Instruments). Leaf discs taken from tomato leaves infiltrated with infiltration buffer only (10 mM $MgCl_2$) were used as control.

2.11. Nitrate Reductase Assay

Leaf crude extracts were prepared fresh each time by first freezing 200 mg of leaf tissue in liquid nitrogen in a 1.5 ml Eppendorf tube. 400 ul of grinding buffer (50 mM Tris-HCl pH7.5, 10 mM $MgCl_2$, 1 mM EDTA, 1.5 mM DTT, 0.1% TritonX-100), 100 ug of 1 mm diameter stainless steel beads, and five 3 mm diameter stainless steel beads were added to each tube, and the leaf tissue was homogenized using Bullet Blender® (HOMOGENIZERS) at the highest setting for 10 min. Homogenized sample were centrifuged at 10, 000 *g* for 10 min at 4 °C. The protein concentration of the supernatant was tested with a Bradford assay (Bio-Rad) and adjusted to 2 mg/ul. Ten mg of crude protein extract was mixed with 40 ul of assay solution (25 mM phosphate buffer pH 7.5, 10 mM KNO_3), the reaction was started by the addition of 5 ul NADH solution (2.5 mM NADH in pH7 sodium phosphate buffer). The reaction was carried out for 30 min at 30 °C, then terminated with the addition of 2.5 ul of 0.1 M ZnOAc followed by boiling at 95 °C for 5 mins. The precipitants formed by ZnOAc was removed by centrifugation. The remaining NADH was removed by addition of 2.5 ul of 1 mM phenazine methosulfate to the supernatant of each reaction and incubated at 20 °C in the dark for 10 mins.

The color reagent was made right before detection by mixing 1% sulfanilamide (in 1.5 M HCl) and 0.02% N-1(naphthyl)-ethylenediamine hydrochloride (in water). The KNO_2 produced in each reaction was detected by adding 50 ul of the color reagent to each reaction, mixing, and incubating at 20 °C for 15 min. The color reaction was detected by reading the absorbance at 540 nm and each reading was the average of three duplicates.

CHAPTER III

IN VITRO ACTIVITY CHARACTERIZATION OF THE TOMATO SNRK1 COMPLEX PROTEINS[2]

3.1. Introduction

SnRK1 (Sucrose non-Fermenting Related Kinase1) is the plant homolog of the mammalian AMP-activated protein kinase (AMPK) and the yeast sucrose non-fermenting 1 (Snf1) kinase, and these kinases regulate cellular carbon metabolism such as usage of glucose in yeast and mammals, ATP production in mammals, and sucrose utilization in plants [99]. SnRK1 was originally discovered through its sequence homology to Snf1 and ability to complement the yeast *SNF1* knockout [123]. Like AMPK and Snf1, SnRK1 exists as a heterotrimeric complex consisting of a kinase active α-subunit termed SnKR1, a β-subunit for regulating substrate specificity, and a γ-subunit needed for full kinases activity [124]. Recent studies indicate the plant SnRK1 complex regulates a variety of metabolic processes besides sucrose metabolism, including nitrogen assimilation, sterol synthesis, starch synthesis, and photosynthate partitioning [100].

The SnRK1 α-subunit has been studied from many plant species including *Arabidopsis thaliana*, *Solanum lycopersicum* (tomato), *Solanum tuberosum* (potato), *Oryza sativa* (rice), *Sorghum biocolor* (sorghum), *Hordeum vulgare* (barley), and *Nicotiana tabacum* (tobacco) [58,125–128]. The SnRK1 protein contains an N-terminal kinase domain and a C-terminal β-subunit interaction domain (β-SID), both of which are conserved in AMPK and Snf1 (Figure 4). Plant SnRK1s also

[2] Part of the data reported in this chapter is reprinted with permission from S. Dongyin, T.P. Devarenne, *In vitro* activity characterization of the tomato SnRK1 complex proteins, BBA-Proteins and Proteomics (2018), DOI.10.1016/j.bbapap.2018.05.010, © 2018 Elsevier B.V.

contain a kinase associated (KA1) domain embedded within the β-SID domain (Figure 4), which is identified by homology to the KA1 domains in mammalian microtubule-associated proteins [129]. The KA1 domain is a common motif in protein kinases and has been shown to bind to anionic phospholipids and upstream phosphatases, which could play a role in membrane localization and regulation of kinase activity [130,131]. Additionally, SnRK1 contains an ubiquitin-associated domain (UBA), which has been suggested to bind to ubiquitinated proteins [60] and is not found in AMPK or Snf1 (Figure 4). AMPK and Snf1 contain an autoinhibitory domain (AID) for regulation of α-subunit kinase activity [61] that is not found in SnRK1 (Figure 4). Finally, only AMPK has an α-hook domain (Figure 4), which regulates interaction with the γ-subunit in an ADP/AMP dependent manner [72].

The SnRK1 α-subunit from *Arabidopsis* has been studied the most in relation to regulation of kinase activity. Three *Arabidopsis* SnRK1 α-subunits have been identified so far and only two of them, *At*SnRK1.1 (a.k.a. AKIN10) and *At*SnRK1.2 (a.k.a. AKIN11), have been found to be active kinases [56]. The third *Arabidopsis* α-subunit, *At*SnRK1.3 (a.k.a. AKIN12), has been shown to be expressed at low levels in pollen, developing embryos, and seeds [120,132]. *At*SnRK1.1 and *At*SnRK1.2 are activated *in vitro* and *in vivo* by the upstream kinases *At*SnAK1 and *At*SnAK2 (a.k.a. GRIK1 and GRIK2), which phosphorylate the conserved Thr175 or Thr176 residues in the kinase domain T-loop region of *At*SnRK1.1 or *At*SnRK1.2, respectively [133]. Compared to *At*SnAK1, *At*SnAK2 shows higher kinase activity on both *At*SnRK1.1 and *At*SnRK1.2 [63,116]. *At*SnAK1 and *At*SnAK2 can autophosphorylate *in vitro* on Thr153 or Thr154, respectively, while phosphorylation of Ser260 or Ser261 in *At*SnAK1 or *At*SnAK2, respectively, by *At*SnRK1.1 inhibits their activity and functions as a negative feedback control [63].

In tomato, only one α-subunit, *Sl*SnRK1.1, has been functionally studied [58,134]. *Sl*SnRK1.1 was first isolated from a tomato seed cDNA library by hybridization analysis using the tobacco SnRK1 α-subunit NPK5 as a probe, and was shown to be constitutively expressed in seed and leaves [134]. *Sl*SnRK1.1 can bind to and phosphorylate the tomato yellow leaf curl China virus β-satellite βC1 protein at Ser33 and Thr78 to attenuate the viral infection [135]. Later studies found *Sl*SnRK1.1 was also able to interact with the tomato cell death suppressor AGC Ser/Thr protein kinase Adi3, which plays a role in the defense against the bacterial pathogen *Pseudomonas syringae* [58]. While the βC1 protein interaction did not affect *Sl*SnRK1.1 function [135], Adi3 has been proposed to inhibit *Sl*SnRK1 complex kinase activity *in vitro* and *in vivo* [58]. These studies indicate SnRK1 may also play a role in pathogen resistance.

Four tomato SnRK1 complex β-subunits have been identified: *Sl*Gal83, *Sl*Sip1, *Sl*Tau1, and *Sl*Tau2 [58]. Plant SnRK1 β-subunits have been shown to have three conserved protein domains: an N-terminal variable region containing a myristoylation motif (N-Myr), a C-terminal association with Snf1 complex (ASN) domain, and a carbohydrate binding domain (CBD) in the middle of the protein [64]. All four tomato β-subunits have these conserved domains (Figure 8).

Regulation of the SnRK1 β-subunits by phosphorylation has been shown in mammals, yeast, and plants, but has been best studied in mammals and yeast. The mammalian β-subunit AMPK β1 is phosphorylated by the α-subunit AMPKα1 at Ser24/Ser25 and Ser108, as well as Ser182 by an unknown upstream kinase [69,70]. The phosphorylation at Ser108 increases AMPK complex kinase activity [70], while Ser24/Ser25 and Ser182 phosphorylation causes nuclear exclusion of the complex [69]. The yeast β-subunit *Sc*Gal83 can be phosphorylated by the yeast α-subunit Snf1 and casein kinase 2, however, the exact phosphorylation sites and the

function of the phosphorylation is still unknown [71]. In plants the tomato β-subunit *Sl*Gal83 was shown to be phosphorylated at Ser26 by Adi3, while the other three tomato β-subunits did not show detectable phosphorylation by Adi3 [58]. This phosphorylation of *Sl*Gal83 by Adi3 has been shown to be the trigger for down regulating the kinase activity of the SnRK1 complex in tomato, possibly during pathogen defense responses [58].

Here we report the identification and characterization of a second SnRK1 α-subunit from tomato, *Sl*SnRK1.2. We show that *Sl*SnRK1.2 has substantially different kinase activity in terms of autophosphorylation and *trans*-phosphorylation of the tomato β-subunits compared to the tomato SnRK1.1 α-subunit. Interestingly, this lower activity of SnRK1.2 may be conserved among Solanaceous plants. Potential implication of these findings for *in vivo* function of SnRK1.2 are discussed.

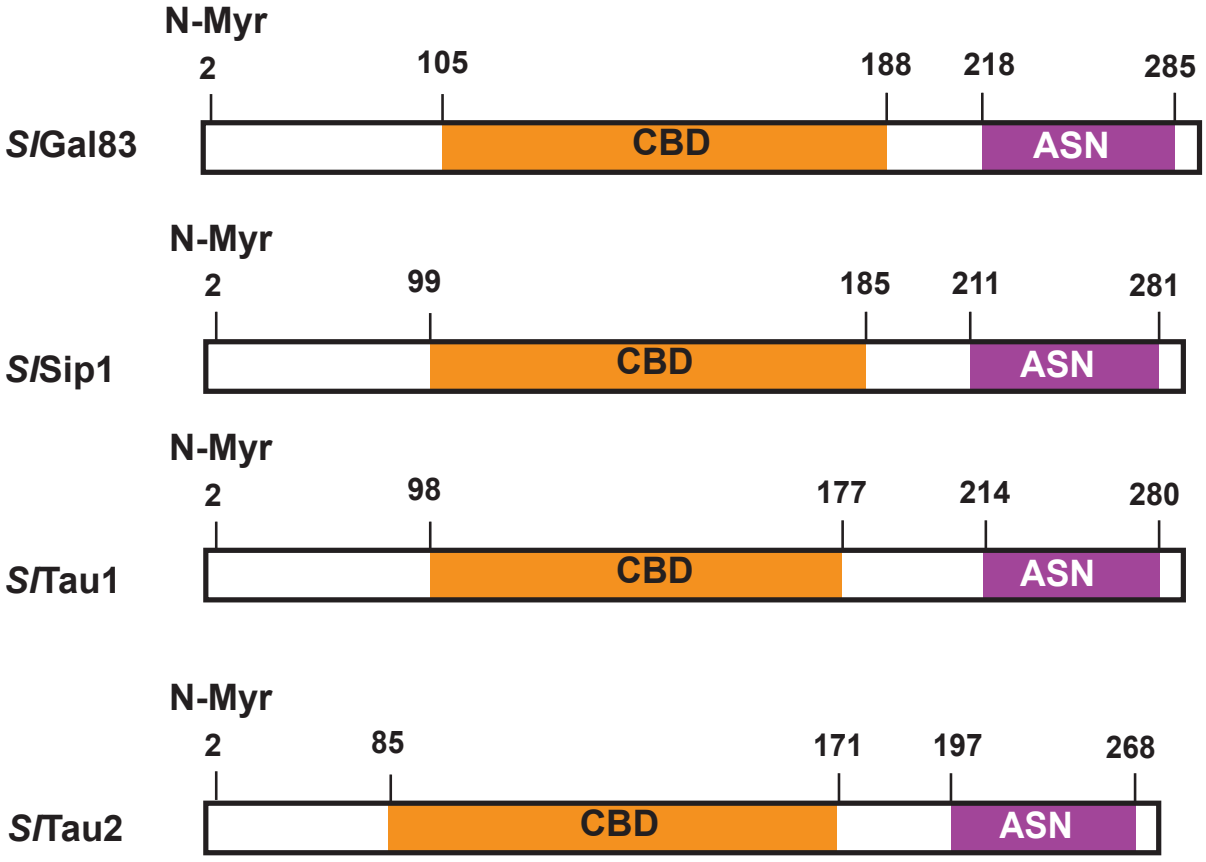

Figure 8. Conserved protein domains of tomato SnRK1 β-subunits *Sl*Gal83, *Sl*Sip1, *Sl*Tau1, and *Sl*Tau2. There is a proposed myristoylation (N-Myr) site at N-terminus. Orange box, carbohydrate binding domain (CBD); purple box, association with Snf1 complex (ASN) domain.

3.2. Identification of a Second Tomato SnRK1 Complex α-subunit

Most plants have at least two α-subunits for the SnRK1 complex including *Arabidopsis*, potato, rice, sorghum, and barley [125,126]. However, for tomato only one α-subunit has been characterized at the protein level [58,134]. Thus, we undertook a search for additional tomato *Sl*SnRK1 complex α-subunits. A BLAST search of the tomato proteome using the Sol Genome Database with *Sl*SnRK1.1 as the query returned one additional α-subunit sequence we termed *Sl*SnRK1.2. The *Sl*SnRK1.2 protein showed conservation of all SnRK1 domains and showed 69% identity to *Sl*SnRK1.1, with high conservation within the catalytic domain, the UBA domain, and the KA1 domain (Figure 9). The *Sl*SnRK1.2 sequence also showed very high identity (98%) to the potato homolog, PKIN1 [136], and to (99%) the predicted SnRK1 from wild tomato (*Solanum pennellii*) *Sp*Kin10like (Figure 9).

A phylogenetic analysis of SnRK1.1 and SnRK1.2 sequences from 28 plant species showed the monocot and dicot sequences could be distinguished from each other, and the Solanaceae sequences formed two distinct Group A and Group B clades (Figure 10). Interestingly, while the monocot SnRK1.1 and SnRK1.2 sequences clustered together, as well as the *Arabidopsis* homologs *At*SnRK1.1 and *At*SnRK1.2 [137], the Solanaceae SnRK1.1 and SnRK1.2 sequences distinctly clustered into the distantly related Group B and Group A clades, respectively (Figure 10). Also, the three *Solanum* SnRK1.2 sequences *Sl*SnRK1.2, potato PKIN1, and *S. pennellii Sp*Kin10like all clustered together in a subclade (Figure 10). This may suggest the Solanaceae SnRK1.2 proteins have functions divergent from those proposed for SnRK1.1.

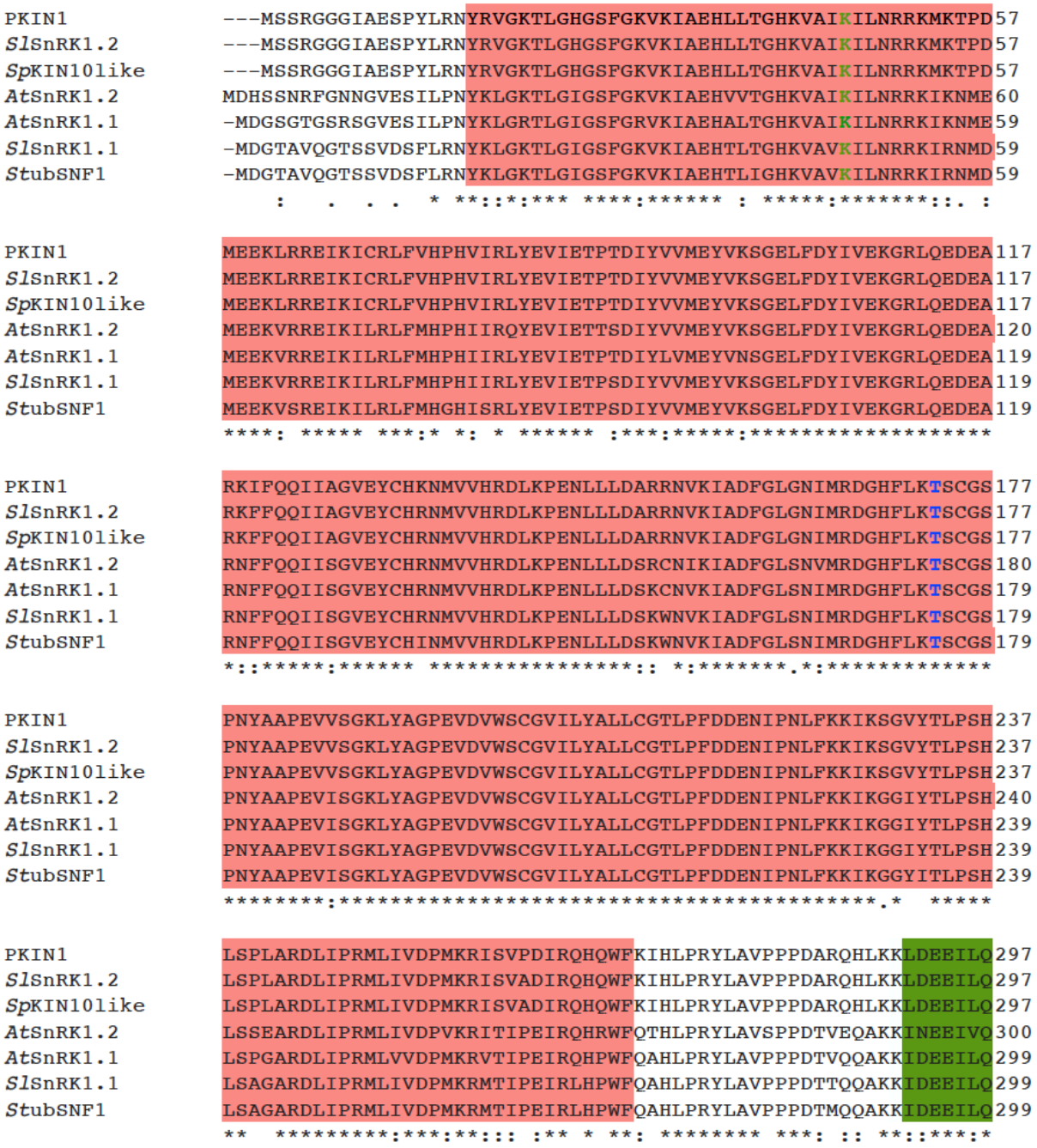

Figure 9. Alignment of *Arabidopsis*, tomato, and potato SnRK1 α-subunits. Protein sequences of SnRK1 α-subunits of *Arabidopsis* (*At*SnRK1.1, *At*SnRK1.2), tomato (*Sl*SnRK1.1, *Sl*SnRK1.2), wild tomato (*Solanum pennellii*, *Sp*Kin10like), and potato (PKIN1, StubSnf1) were aligned using Clustal Omega. The Lysine in Green shows the conserved key residue for ATP binding. The Threonine in dark blue shows the conserved phosphorylation site for activation. The kinase domain is highlighted in salmon, the UBA domain is highlighted in green, the β-SID domain is high lighted in light blue, and the KA1 domain is highlighted by the red box.

Percent Identity Matrix

	PKIN1	*Sl*SnRK1.2	*Sp*KIN10like	AtSnRK1.2	AtSnRK1.1	*Sl*SnRK1.1	*Stub*SNF1
PKIN1	100.00	98.02	98.41	67.74	68.73	68.92	67.73
*Sl*SnRK1.2	98.02	100.00	99.21	67.74	68.92	69.12	67.73
*Sp*KIN10like	98.41	99.21	100.00	67.74	69.12	69.12	67.73
AtSnRK1.2	67.74	67.74	67.74	100.00	81.10	79.02	77.25
AtSnRK1.1	68.73	68.92	69.12	81.10	100.00	84.93	83.37
*Sl*SnRK1.1	68.92	69.12	69.12	79.02	84.93	100.00	97.67
*Stub*SNF1	67.73	67.73	67.73	77.25	83.37	97.67	100.00

Figure 9. Continued.

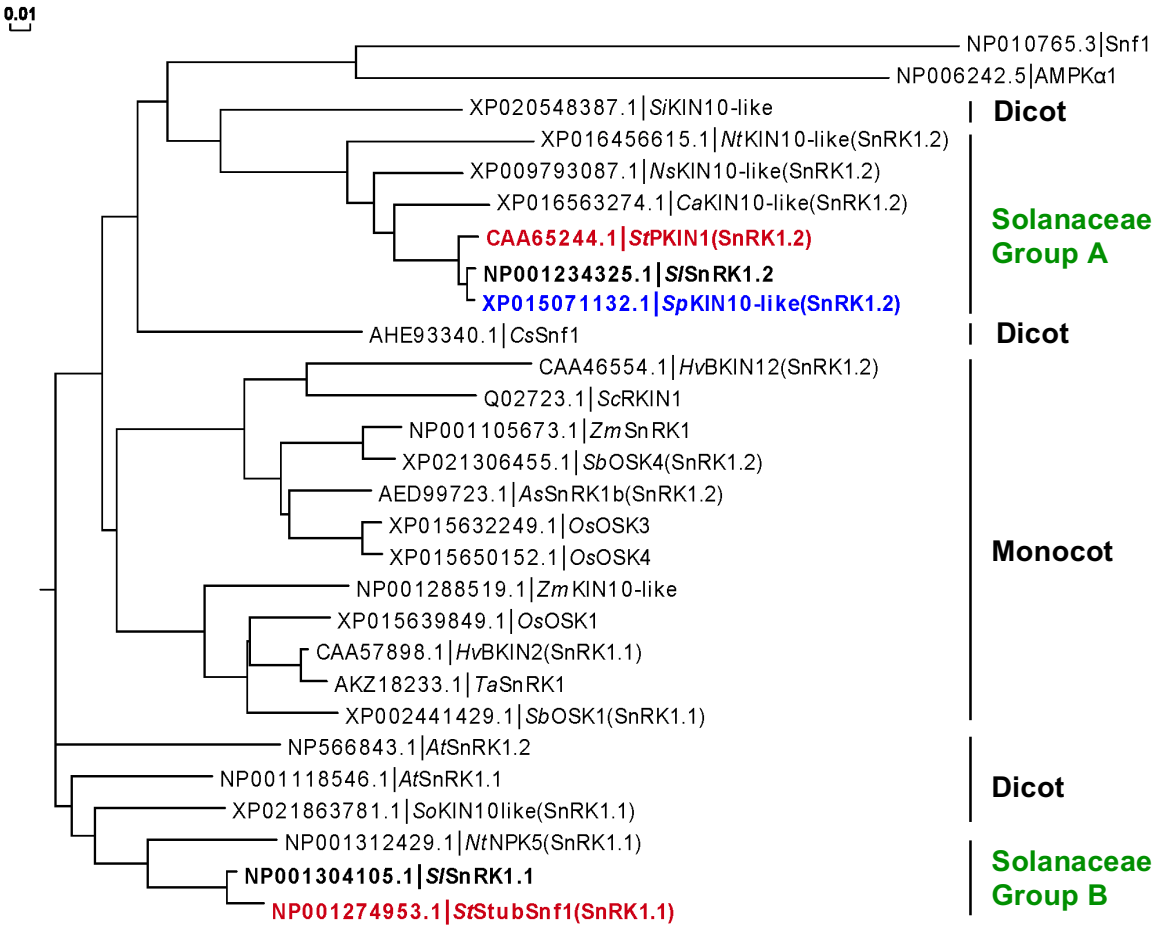

Figure 10. Phylogenetic tree of SnRK1 family proteins. This is a Neighbor-joining tree without distance corrections generated using Clustal Omega and visualized by EvolView. Scale bar indicates branch length. If SnRK1.1 or SnRK1.2 is not given in the protein name this designation is indicated in parentheses after the protein name. This designation is not known for some proteins. *At*, *Arabidopsis thaliana*; *As*, *Avena sativa*; *Ca*, *Capsicum annuum*; *Cs*, *Camellia sinensis*; *Hv, Hordeum Vulgare*; *Nt*, *Nicotiana tabacum*; *Ns*, *Nicotiana sylvestris*; *Os, Oryza sativa*; *Sb*, *Sorghum bicolor*; *Sc, Secale cerea*l; *Si*, *Sesamum indicum*; *Sl*, *Solanum lycopersicum*; *So*, *Spinacia oleracea*; *Sp*, *Solanum pennellii*; *St, Solanum tuberosum*; *Ta*, *Triticum aestivum*; *Zm*, *Zea mays*.

Most plant SnRK1 α-subunit proteins have been confirmed as functional Snf1-like proteins by successfully complementing the yeast *SNF1* knockout line (*snf1Δ*) [126,128,138]. Thus, the ability of *Sl*SnRK1.2 to complement *snf1Δ* was tested to confirm it as a functional Snf1-like protein. Indeed, *Sl*SnRK1.2 was able to confer complementation for growth on sucrose when expressed in the yeast *snf1Δ* line (Figure 11). However, *Sl*SnRK1.2 was not able to complement to the extent of *Sl*SnRK1.1 (Figure 11), This suggests that while *Sl*SNRK1.2 may function as an SnRK1 α-subunit, it may not have full Snf1-like activity.

3.3. *Sl*SnRK1.2 Has Weak Kinase Activity Compared to *Sl*SnRK1.1

Autophosphorylation is prevalent in eukaryotic protein kinases [139] and both *Arabidopsis* and tomato SnRK1 α-subunit proteins have been shown to autophosphorylate [58,138]. In order to confirm *Sl*SnRK1.2 as a functional protein kinase, we first determined its autophosphorylation ability under several different reaction conditions by varying the pH, temperature, reaction time, and preference for divalent cations of Mg^{+2} or Mn^{+2}. While the differences between the conditions were minimal, the experiments (not shown) showed the optimal conditions to be pH 7.5, 20 °C, 14-hour reaction time, and preference for Mn^{+2}. This differs from the *Sl*SnRK1.1 reaction conditions of pH 8.0, 30 °C, 30 minute reaction time, and preference for Mg^{+2} [58]. The main difference between the reaction conditions for the two kinases is the reaction time, which suggests *Sl*SnRK1.2 is a much weaker kinase than *Sl*SnRK1.1.

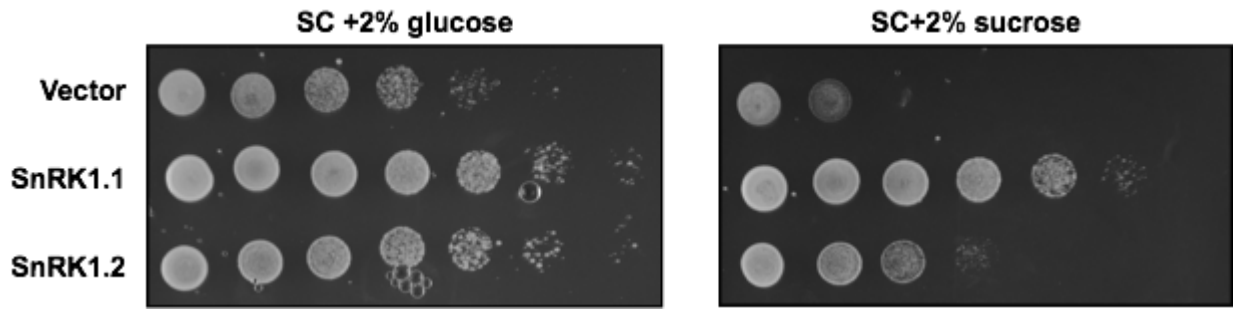

Figure 11. *Sl*SnRK1.2 is able to compliment a yeast *SNF1* knock-out. *snf1Δ* yeast cells were transformed with empty vector, FLAG-tagged *Sl*SnRK1.1, or FLAG-tagged *Sl*SnRK1.2 and spotted in 5-fold dilutions on SC-Ura plates containing either 2% glucose (left panel) or 2% sucrose (right panel).

Using the optimal reaction conditions, *Sl*SnRK1.2 autophosphorylation activity was analyzed for comparison to *Sl*SnRK1.1. Wild-type (WT) *Sl*SnRK1.2 autophosphorylation was shown to be much weaker than that of WT *Sl*SnRK1.1 (Figure 12A and B, lane 1). In fact, the *Sl*SnRK1.2 autophosphorylation signal was only slightly detectable after 168 hours of exposure to the phosphorimager screen (Figure 12B, lane 1). We previously identified *Sl*SnRK1.1 Lys48 as the key amino acid involved in ATP binding and mutation of this residue to Gln eliminates autophosphorylation [58] (Figure 12A, lane 2). The corresponding residue in *Sl*SnRK1.2 is Lys46 (Figure 9) and mutation to Gln also eliminated autophosphorylation activity (Figure 12B, lane 2).

In *Arabidopsis*, upstream kinases are known to phosphorylate *At*SnRK1.1 and *At*SnRK1.2 at the conserved Thr175 or Thr176, respectively, for activation [63]. In the case of *Sl*SnRK1.1 and *Sl*SnRK1.2 this residue is Thr175 and Thr173, respectively (Figure 9). Mutation of these residues in *Sl*SnRK1.1 and *Sl*SnRK1.2 to the phosphomimetic Asp or Glu significantly increased autophosphorylation of both kinases (Figure 12A and B, lanes 3, 4). The T175D mutation in *Sl*SnRK1.1 conferred higher autophosphorylation activity compared to the T175E mutation (Figure 12A, lanes 3, 4), while the *Sl*SnRK1.2 T173E mutation resulted in higher autophosphorylation activity compared to the T173D mutation (Figure 12B, lanes 3, 4). It should be noted that in all the kinase assays in Fig. 1 the *Sl*SnRK1.1 activity was much higher than that of *Sl*SnRK1.2.

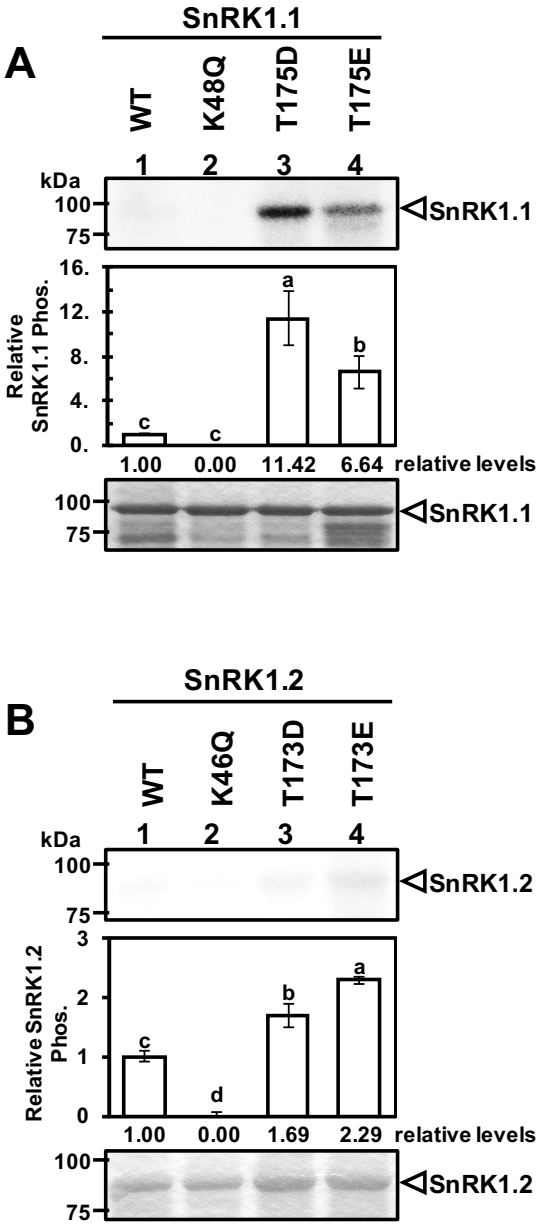

Figure 12. Autophosphorylation of *Sl*SnRK1.1 and *Sl*SnRK1.2. In (A) and (B), the indicated proteins were incubated with γ-[^{32}P]ATP in an *in vitro* kinase assay. Top panel, phosphorimage; middle panel, quantification of autophosphorylation from four repeats, error bars indicate standard error, average value is shown under each column; bottom panel, Coomassie blue-stained gel. Statistical analysis was carried out using the Fisher LSD test and samples with the same letter above the bars are not significantly different ($p < 0.05$). (A) *Sl*SnRK1.1 autophosphorylation. The reaction was carried out at 30°C for 30 min and the gel was exposed to the phosphorimager screen for 24 hrs. (B) *Sl*SnRK1.2 autophosphorylation. The reaction was carried out at 20°C for 14 hrs and the gel was exposed to the phosphorimager screen for 168 hrs.

3.4 *Sl*SnRK1.1 and *Sl*SnRK1.2 *in vitro* Interaction with β- and γ-subunits

To determine the interaction of *Sl*SnRK1.1 and *Sl*SnRK1.2 with the β-subunits, MBP tagged β-subunits were immunoprecipitated using amylose resin, and then their ability to pull-down FLAG-tagged α-subunits with and without the Snf4 γ-subunit was tested. Among all the β-subunits, Tau1 showed the strongest interaction with both *Sl*SnRK1.1 and *Sl*SnRK1.2 (Figure 13A, lane 4 and 8; Figure 13B, lane 4 and 8). this was followed by Gal83 and Tau2 showing a medium level of interaction with *Sl*SnRK1.1 and *Sl*SnRK1.2 (Figure 13A, lane 3 and 9; Figure 13B, lane 3 and 9), while Sip1 showed the lowest level of interaction with *Sl*SnRK1.1 and *Sl*SnRK1.2 (Figure 13A, lane 6 and 10; Figure 13B, 6 and 10). The Snf4 γ-subunits was also able to weakly interact with both α-subunits (Figure 13A, lane 2; Figure 13B, lane 2). Combining β and γ-subunits did not increase the ability of any β-subunit to pull-down either α-subunits (Figure 13A and B, comparing lane 2-6 with 7-10). This indicates that Tau1 has the strongest and most stable interaction with the α-subunits while Snf4 and Sip1 have weaker and more transient interactions with the α-subunits.

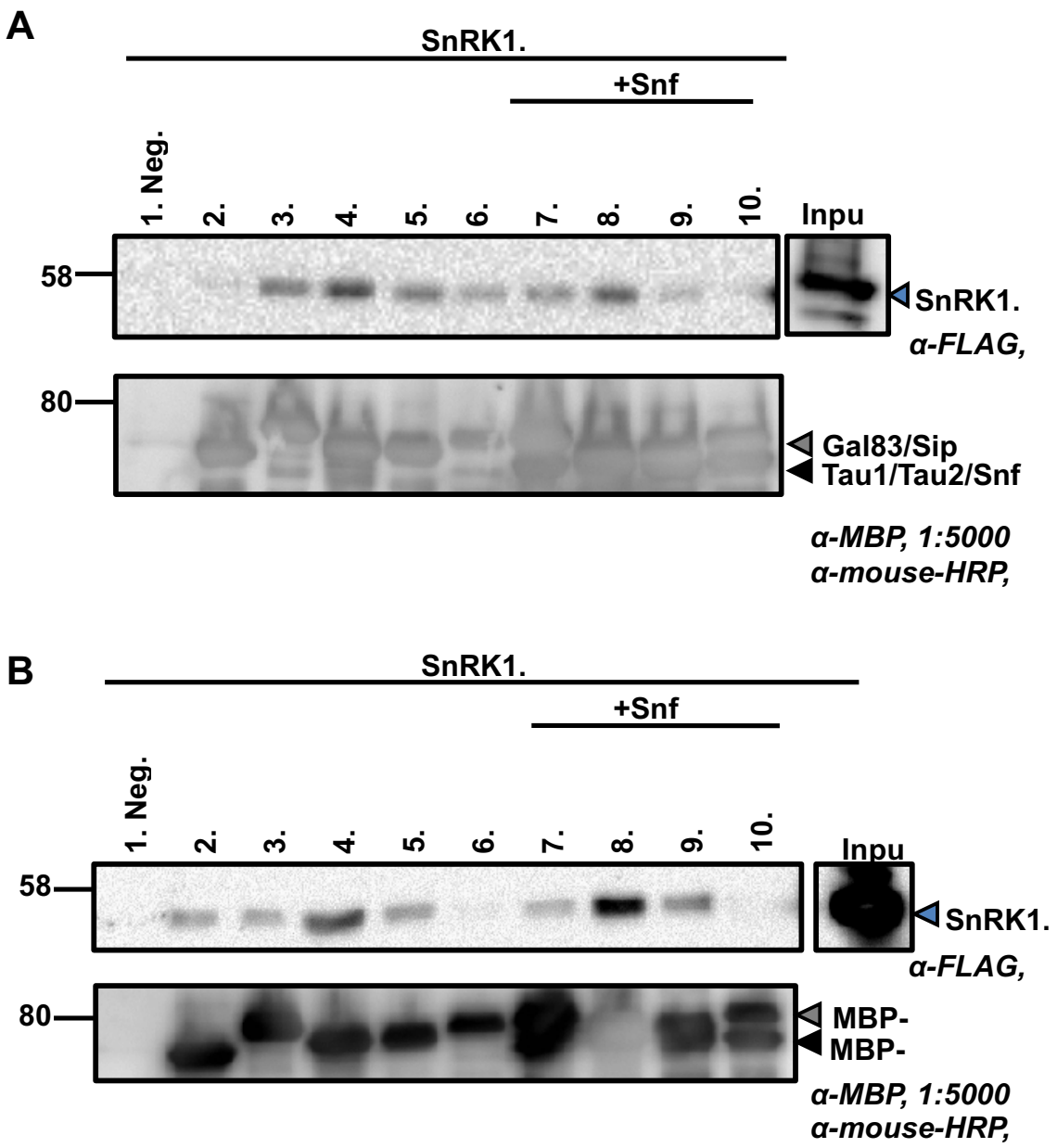

Figure 13. *Sl*SnRK1.1 and *Sl*SnRK1.2 interaction with β- and γ-subunits *in vitro*. Recombinant MBP tagged proteins immobilized on amylose resin pulls down FLAG tagged SnRK1.1 and SnRK1.2. Both A and B, top panel, pull-down of FLAG-tagged SnRK1.1 or SnRK1.2 detected by anti-FLAG antibody; bottom panel, detection of MBP-tagged β- and γ-subunit proteins used for pull-down. Among the β-subunits, Tau1 shows strongest interaction with both α-subunits whereas α-subunit interactions with Sip1 are the weakest. Interaction between Snf4 and SnRK1.2 is stronger than that of SnRK1.1.

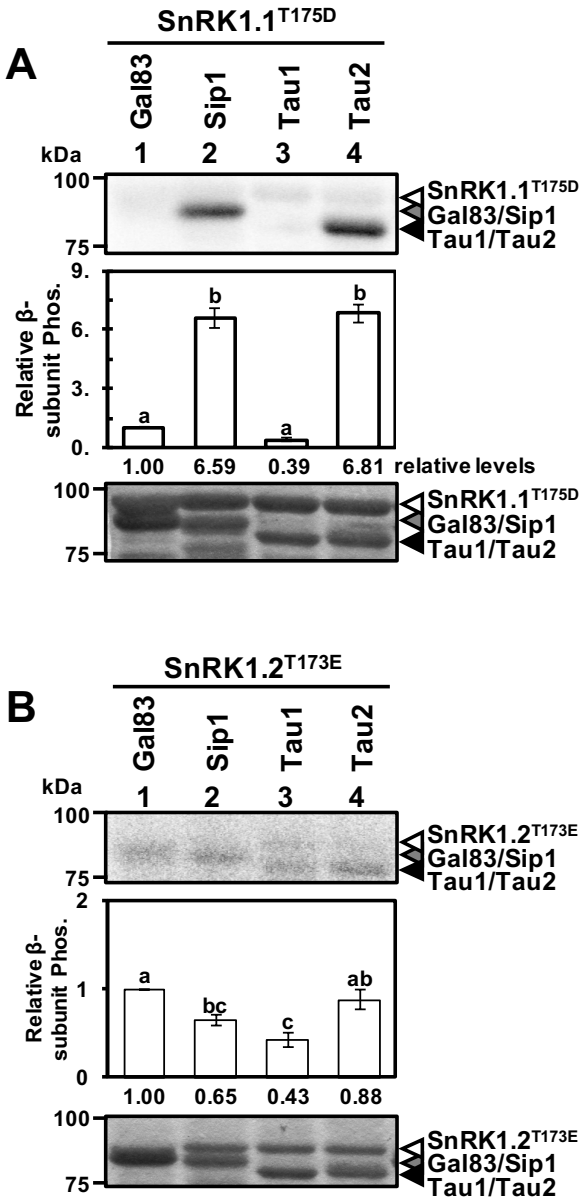

Figure 14. *Sl*SnRK1.1^{T175D} and *Sl*SnRK1.2^{T173E} have different preferences for β-subunit phosphorylation. In (A) and (B), the indicated proteins were incubated with γ-[^{32}P]ATP in an *in vitro* kinase assay. Top panel, phosphorimage; middle panel, quantification of β-subunit phosphorylation from four repeats, error bars indicate standard error, average value is shown under each column; bottom panel, Coomassie blue-stained gel. Statistical analysis was carried out using the Fisher LSD test and samples with the same letter above the bars are not significantly different ($p < 0.05$). (A) *Sl*SnRK1.1^{T175D} phosphorylation of different β-subunits. The reaction was carried out at 30℃ for 15 min and the gel was exposed to the phosphorimager screen for 24 hrs. (B) *Sl*SnRK1.2^{T173E} phosphorylation of different β-subunits. The reaction was carried out at 20 °C for 14 hrs and the gel was exposed to the phosphorimager screen for 168 hrs.

3.5. *Sl*SnRK1.1 and *Sl*SnRK1.2 Differentially Phosphorylate the β-subunits *in vitro*

Previous studies have shown that the α-subunits of the Snf1 and AMPK complexes are capable of phosphorylating their respective β-subunits [70,71]. Thus, given the different kinase activity levels between *Sl*SnRK1.1 and *Sl*SnRK1.2 the ability of each of these kinases to phosphorylate the tomato β-subunits was analyzed using the phosphomimetic kinases with the highest activity, *Sl*SnRK1.1^{T175D} and *Sl*SnRK1.1^{T173E}. While *Sl*SnRK1.1^{T175D} was able to phosphorylate each β-subunit, Sip1 and Tau2 (Figure 14A, lanes 2, 4) were phosphorylated over 6 times stronger than Gal83 and Tau1 (Figure 14A, lanes 1, 3). For *Sl*SnRK1.2^{T173E} all β-subunits were phosphorylated within 50% of each other (Figure 14B) with Gal83 and Tau2 having the highest phosphorylation levels (Figure 14B, lanes 1, 4). As was seen in the autophosphorylation assays, *Sl*SnRK1.2 β-subunit phosphorylation was much weaker than that of *Sl*SnRK1.1 (Figure 14A, B).

3.6. Identification of the Tomato Upstream Kinase for the *Sl*SnRK1 Complex α-subunits

It has been shown in *Arabidopsis* that replacing Thr175 or 176 in *At*SnRK1.1 or *At*SnRK1.2, respectively, with a phosphomimetic mutation is not enough to fully activate these kinases, and the upstream kinase *At*SnAK2 is required for full activation [75]. Since the *Sl*SnRK1.2 phosphomimetic mutations contained quite low auto- and *trans*-phosphorylation activity (Figure 12, Figure 14), a tomato *SnAK* sequence was identified to test the ability of the encoded kinase to confer higher *Sl*SnRK1.2 kinase activity. The *Arabidopsis* SnAK1 and SnAK2 sequences (*At*SnAK1, *At*SnAK2; [63,116]) were used in a BLAST search of the tomato proteome to identify any homologous tomato sequences. The results identified only a single *Sl*SnAK sequence that showed 62% identity to *At*SnAK1 and 65% identity to *At*SnAK2 (Figure

15). *Sl*SnAK was able to activate both *Sl*SnRK1.1 and *Sl*AnRK1.2, though the activation of *Sl*SnRK1.2 was much weaker than that of *Sl*SnRK1.1 (Figure 16).

3.7. *Sl*SnAK Activation of *Sl*SnRK1.1 and *Sl*SnRK1.2 Kinase Activity

The ability of *Sl*SnAK phosphorylation to activate *Sl*SnRK1.1 and *Sl*SnRK1.2 *trans*-phosphorylation was tested using the β-subunits as substrate. The *Sl*SnAK activated *Sl*SnRK1.1 showed a dramatic increase in its ability to phosphorylate all β-subunits, reducing the phosphorimager screen exposure time from 24 hours for the phosphomimetic *Sl*SnRK1.1^{T175D} (Figure 14A) to 2 hours (Figure 17A). The preference of *Sl*SnAK activated *Sl*SnRK1.1 for phosphorylating the different β-subunits did not change when compared to the phosphomimetic *Sl*SnRK1.1^{T175D} (Figure 14A, 3A).

```
SlSnAK      MSVMMHSVDEVTEMGCCGCFGFSFARKPKKEIRPNRGYGNSWSHEPLLQQEAEEVEDDGF    60
AtSnAK1     --MFRDSFLFARTIGCFGCFGSSGSRNQQS---PKPYDDDTHSCDSDVTSTAR-------    48
AtSnAK2     --MFCDSFAFAQVMSCFGCFGGSE-RSRHS---PNPYDDDTYSHDSGETSNPG-------    47
              :: .*.  .  :.* **** *  *. :.   *:   .:: * :    .

SlSnAK      DSGDIIDTGSE-DDEVCHSPVKRYQEILMERAQNGLICREIPVKETHKVVRTEDEDGNKM    119
AtSnAK1     --GEE-E--EDEEEVEQKSRSKRSEEILKYRLDNGLICRHIPVRETNELIRGEDENGDKT    103
AtSnAK2     --GDD-EEGEEEEEVEELSRSKRSEEILKCKLQNGLVCRQFPVKETNKLTRGEDEDGNKT    104
              *:  :  .: ::    *  ** :***  : :***:**.:**:**::: * ***:*:*

SlSnAK      VNEYVREHKIGAGSYGKVVLYRSCTDGKHYAIKAFHKSHLSKMRVAPSETAMGDVLREVS    179
AtSnAK1     INEYVRVCKIGSGSYGKVVLYRSTLDGQYYAIKAFHKSHLLRLRVAPSETAMSDVLREVM    163
AtSnAK2     INEFVRERKIGSGSYGKVVLYRSTVDDKHYAIKAFHKSHLSRLRVAPSETAMGDVLREVM    164
            :**:**  ***:***********  *.::*********** ::*********.******

SlSnAK      IMKMLCHPNIVNLVEVIDDPETDNFYMVLEYVEGKWVCEDSGPPCVLEENKARLYLRDIV    239
AtSnAK1     IMKILEHPNIVNLIEVIDDPETDHFYMVLEYVDGKWVYDGSGPPGALGEKTARKYLRDIV    223
AtSnAK2     IMKTLEHPNIVNLIEVIDDPEFDDFYMVLEYVDGKWAYDDSGPPGALGEITARKYLRDVV    224
            *** * *******:******* *.********:***. :.**** .* * .** ****:*

SlSnAK      SGLMYLHSHNIIHGDIKPDNLLVSAAGKVKIGDFSVSQVFEDDNDKLRRSPGTPVFTAPE    299
AtSnAK1     TGLMYLHAHDVIHGDIKPDNLLVTSSGTVKIGDFSVSQVFKDDDDQLRRSPGTPVFTAPE    283
AtSnAK2     AGLMYLHAHNVIHGDIKPDNLLVTSTGRVKIGDFSVSQVFKDDDDQLRRSPGTPVFTAPE    284
            :******:*::************:::* ************:**:*:**************

SlSnAK      CCV--GDRYHGKCADTWAVGVTLYCMILGKYPFLGETLQDTYDKIVNNPIILPDDMNPLL    357
AtSnAK1     CCLVSGITYSGRAADTWAVGVTLYCMILGQYPFLADTLQDTYDKIVNNPLIIPDGLNPLL    343
AtSnAK2     CCL--GITYSGRSADTWAVGVTLYCMILGQYPFLGDTLQDTYDKIVHNPLIIPEGLNPRL    342
            **:  *  * *:.****************:****.:**********:**:*:*:.:** *

SlSnAK      KNLLEGLLCKDPTQRLTLESVCQHEWFLGDEGPIPQFSCWCQRQKLQKDVQDGSAEDTPT    417
AtSnAK1     RDLIEGLLCKDPSQRMTLKNVSEHPWVIGEDGHVPEYFCWCKRNAASKIEEGEANGISET    403
AtSnAK2     RDLIEGLLCKDPNQRMTLKAVAEHPWITGEDGAISEYCCWCKRKAEEEEDQNHS------    396
            ::*:********.**:**: *.:* *. *::* : :: ***:*:  .:  :. :

SlSnAK      ----417
AtSnAK1     SDPN407
AtSnAK2     ----396
```

Percent Identity Matrix

	SlSnAK	AtSnAK1	AtSnAK2
SlSnAK	100.00	62.25	64.56
AtSnAK1	62.25	100.00	79.95
AtSnAK2	64.56	79.95	100.00

Figure 15. Protein sequence alignment of tomato SnAK and *Arabidopsis* SnAK1 and SnAK2 using Clustal Omega. *Sl, Solanum lycopersicum*; *At, Arabidopsis.thaliana.*

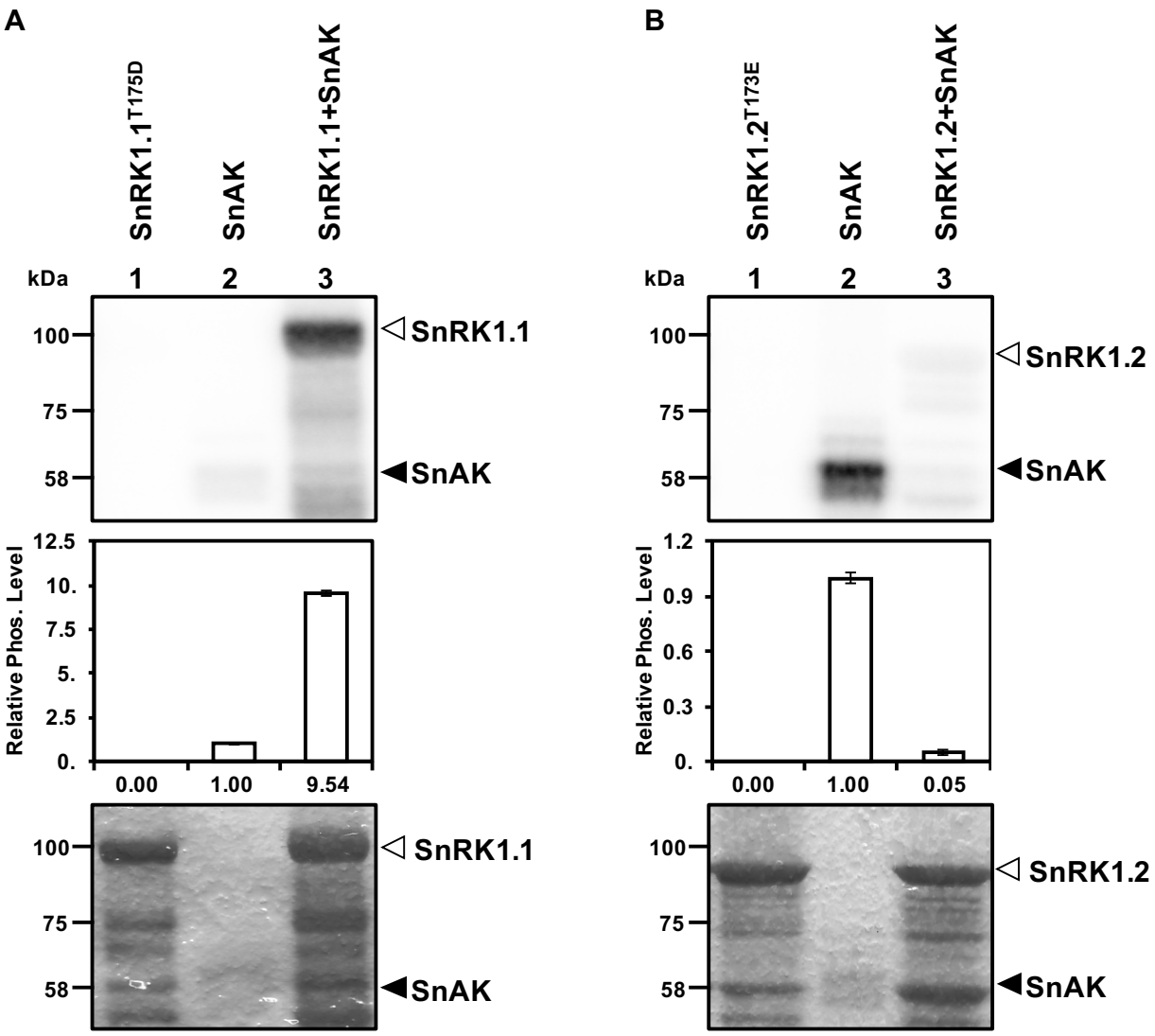

Figure 16. *Sl*SnAK activates *Sl*SnRK1.1 and *Sl*SnRK1.2. *Sl*SnRK1.1(4mg), *Sl*SnRK1.1^{T175D}(4mg), and *Sl*SnAK(1mg) were incubated in combination as indicated above each lane with γ-[^{32}P]ATP in an *in vitro* kinase assay at 30℃ for 15 min, the gel was exposed to the phosphorimager screen for 18 hrs. (B) *Sl*SnAK activation of *Sl*SnRK1.2. *Sl*SnRK1.2(4mg), *Sl*SnRK1.2^{T173E}(4mg), and *Sl*SnAK(1mg) were incubated in combination as indicated above each lane with γ-[^{32}P]ATP in an *in vitro* kinase assay at 30℃ for 15 min, the SnRK1.2 gel was exposed to the phosphorimager screen for 48 hrs. In Both (A) and (B) top panel, phosphorimage; middle panel, quantification of phosphorylation from four independent assays, error bars indicate standard error, average value is relative to *Sl*SnAK and shown under each column. Bottom panel, Coomassie blue-stained gel.

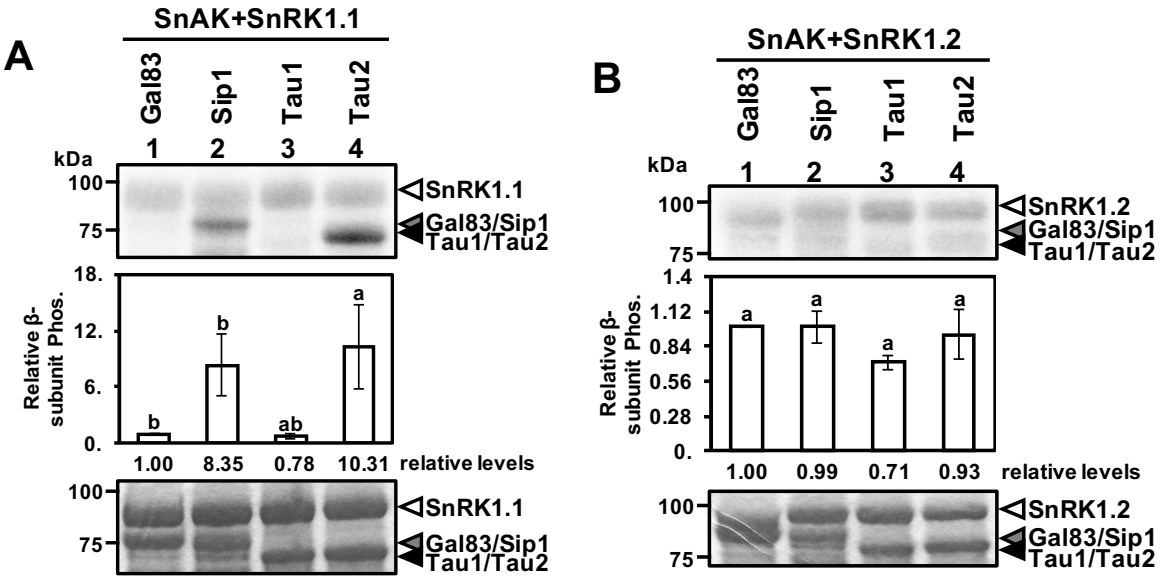

Figure 17. *Sl*SnAK activated *Sl*SnRK1.1 and *Sl*SnRK1.2 phosphorylation of β-subunits. In (A) and (B), the indicated proteins were incubated with γ-[^{32}P]ATP in an *in vitro* kinase assay. Top panel, phosphorimage; middle panel, quantification of β-subunit phosphorylation from four repeats, error bars indicate standard error, average value is shown under each column; bottom panel, Coomassie blue-stained gel. Statistical analysis was carried out using the Fisher LSD test and samples with the same letter above the bars are not significantly different ($p < 0.05$). (A) *Sl*SnAK activated *Sl*SnRK1.1 phosphorylation of different β-subunits. *Sl*SnRK1.1 was pre-incubated with *Sl*SnAK in the presence of non-radioactive ATP at 30 °C for 15 min, followed by addition of γ-[^{32}P]ATP with incubation at 30 °C for 15 min, and the gel was exposed to the phosphorimager screen for two hrs. (B) *Sl*SnAK activated *Sl*SnRK1.2 phosphorylation of different β-subunits. *Sl*SnRK1.2 was pre-incubated with *Sl*SnAK in the presence of non-radioactive ATP at 30 °C for 15 min, followed by addition of γ-[^{32}P]ATP with incubation at 30 °C for 30 min, and the gel was exposed to phosphorimager screen for 48 hrs. The phosphorylation levels of different β-subunits are not significantly different according to the Fisher LSD test.

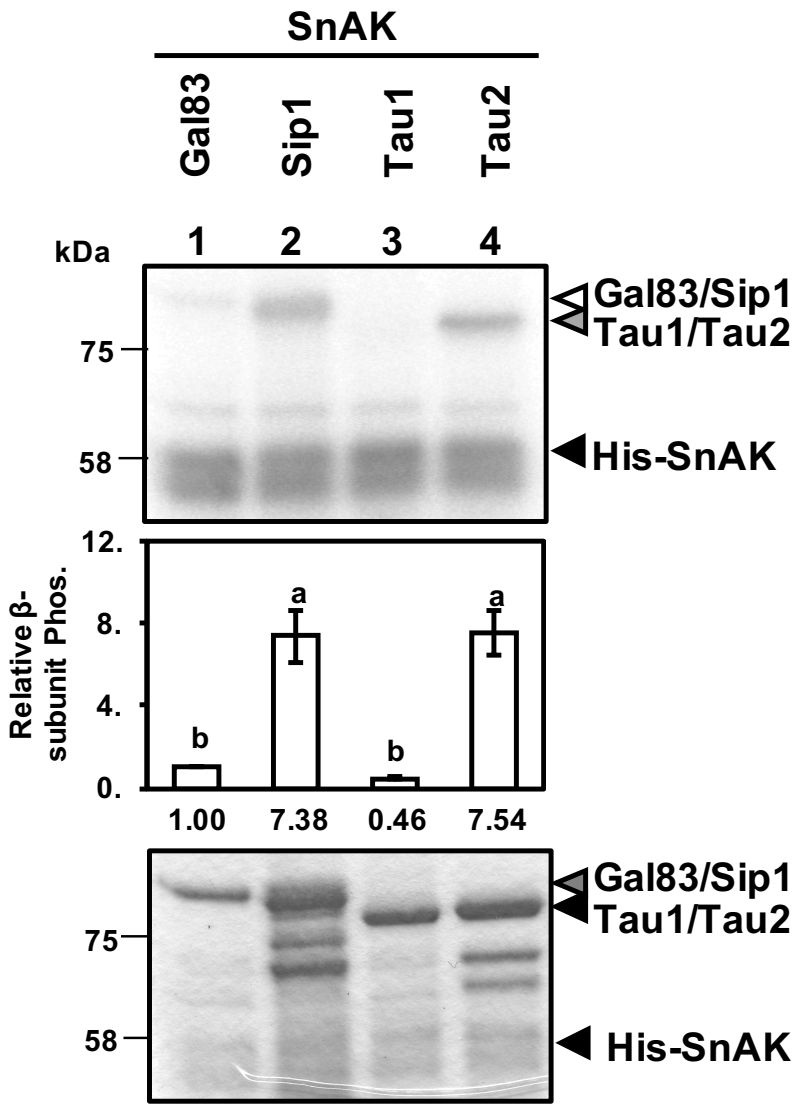

Figure 18. *Sl*SnAK can slightly phosphorylate the *Sl*SnRK1 complex β-subunits.
*Sl*SnAK(1mg) were incubated with different β-subunit (4mg) as indicated in presence of γ-[^{32}P]ATP in an *in vitro* kinase assay at 30℃ for 15 min, the gel was exposed to the phosphorimager screen for 96 hrs. Top panel, phosphorimage; middle panel, quantification of β-subunit phosphorylation from four independent assays, error bars indicate standard error, average value is shown under each column. Statistical analysis was carried out using Fisher LSD and samples with the same letter above the bars are not significantly different ($p < 0.01$). Bottom panel, Coomassie blue-stained gel.

For *Sl*SnRK1.2, activation by *Sl*SnAK also conferred a significant increase in the ability of *Sl*SnRK1.2 to phosphorylate the β-subunits, decreasing the optimal phosphorimager screen exposure time to 48 hours (Figure 17B) from 168 hours for the phosphomimetic *Sl*SnRK1.2^{T173E} (Figure 14B). The *Sl*SnAK activated *Sl*SnRK1.2 showed decreased phosphorylation specificity for the β-subunits with roughly equal phosphorylation of all β-subunits expect Tau1 (Figure 17B) compared to favoring Gal83 and Tau2 for the phosphomimetic *Sl*SnRK1.2^{T173E} (Figure 14B). *Sl*SnAK could also slightly phosphorylate the β-subunits, although the phosphorylation level was extremely low with low detection after 96 hours of exposure to the phosphorimager screen (Figure 18), and this level of phosphorylation was below the detection limit for the data presented in Figure 17.

3.8. *Sl*SnRK1.1 and *Sl*SnRK1.2 Show Differential Substrate Phosphorylation Dependent on the β-subunit Used

Finally, the kinase activity of the *Sl*SnAK activated *Sl*SnRK1 complex was tested with either the *Sl*SnRK1.1 or *Sl*SnRK1.2 α-subunit in combinations with the four different β-subunits. The γ-subunit is required for full kinase activity of the SnRK1 complex *in vitro* [58], so the only γ-subunit so far identified in tomato, *Sl*Snf4, was included in the *in vitro* assays to reconstitute the *Sl*SnRK1 complex. We previously demonstrated the ability to reconstitute the *Sl*SnRK1 complex *in vitro* for testing complex kinase activity [58]. The complex kinase activity was assessed using the AMARA peptide (AMARAA<u>S</u>AAALARRR; phosphorylation site underlined), which is an artificial substrate developed according to the consensus phosphorylation sequence identified for AMPK/Snf1 substrates [118]. Similar to *At*SnAKs [63,140], no phosphorylation of the AMARA peptide was observed with *Sl*SnAK alone (data not

shown). When using *Sl*SnAK activated *Sl*SnRK1.1 as the α-subunit, the reconstituted complex with Sip1 had the lowest kinase activity (Figure 19A, lane 2), while the complexes reconstituted with the other three β-subunits had an equal level of kinase activity (Figure 19A, lanes 1, 3, 4). In contrast, when *Sl*SnAK activated *Sl*SnRK1.2 was used as the α-subunit the complex reconstituted with Sip1 showed the highest kinase activity (Figure 19B, lane 2), while the complex reconstituted with Tau2 showed the lowest kinase activity (Figure 19A, lane 4). Kinase activity with Gal83 and Tau1 showed an intermediate level of activity (Figure 19A, lanes 1, 3). Additionally, when comparing kinase activity between complexes with *Sl*SnRK1.1 or *Sl*SnRK1.2 the *Sl*SnRK1.1 containing complexes showed activity 86 to 210 times higher than *Sl*SnRK1.2 containing complexes (Figure 19A, B). These data indicate the α-subunit in combination with the β-subunits dictate substrate phosphorylation levels, and the *Sl*SnRK1.1 α-subunit confers overall higher activity for the complex.

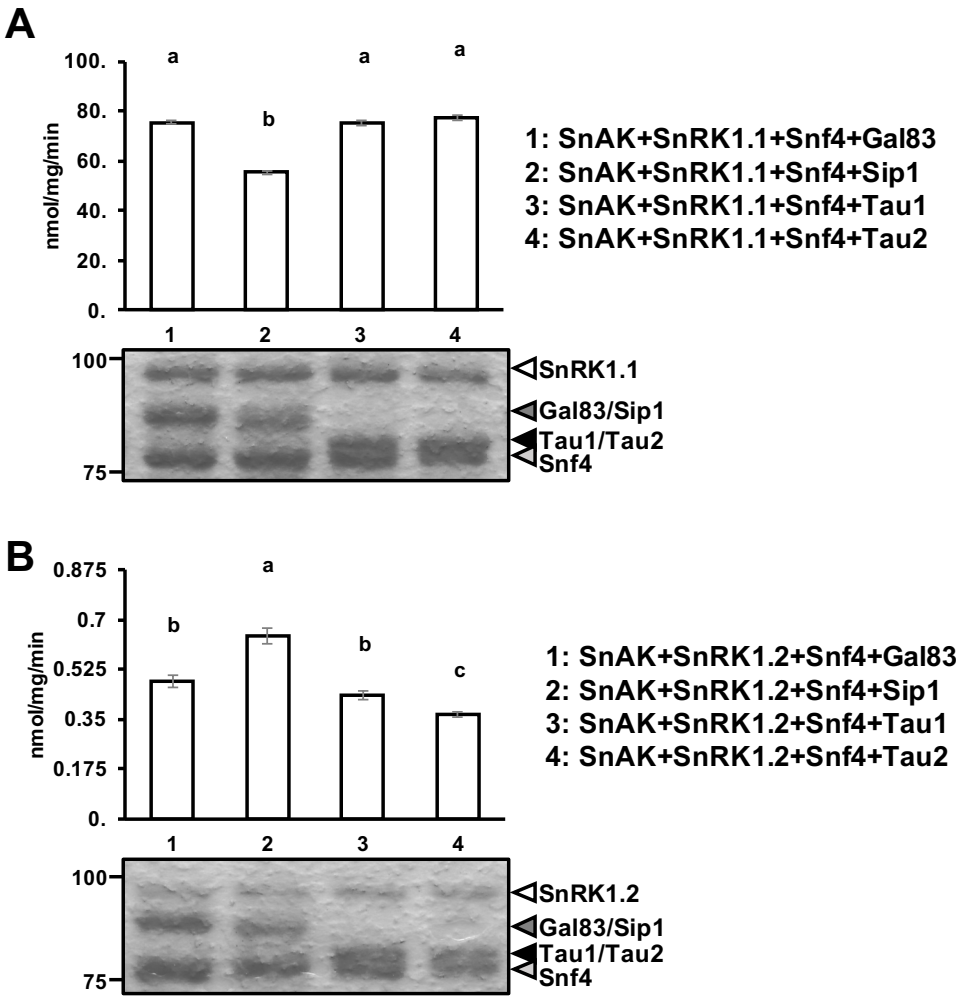

Figure 19. *Sl*SnAK activated *Sl*SnRK1.1 and *Sl*SnRK1.2 phosphorylation of the AMARA peptide. In (A) and (B), the indicated proteins were incubated with the AMARA peptide in the presence of γ-[^{32}P]ATP in an *in vitro* peptide substrate-based kinase assay. Top panel, quantification of scintillation counts for AMARA peptide phosphorylation from four repeats, values are shown as pmol phosphate incorporated mg^{-1} SnRK1 protein min^{-1}, error bars indicate standard error; bottom panel, Coomassie blue-stained gel of proteins put in the assay. Statistical analysis was carried out using the Fisher LSD test and samples with the same letter above the bars are not significantly different ($p < 0.05$). (A) *Sl*SnAK activated *Sl*SnRK1.1 phosphorylation of the AMARA peptide in the presence of different β-subunits. *Sl*SnRK1.1 were pre-incubated with SnAK in the presence of non-radioactive ATP at 30 °C for 15 min, followed by addition of γ-[^{32}P]ATP with incubation at 30 °C for 15 min and the gel was exposed to the phosphorimager screen for two hrs. (B) *Sl*SnAK activated *Sl*SnRK1.2 phosphorylation of the AMARA peptide in the presence of different β-subunits. *Sl*SnRK1.1 were pre-incubated with SnAK in the presence of non-radioactive ATP at 30 °C for 15 min, followed by addition of γ-[^{32}P]ATP with incubation at 30 °C for 30 min, and the gel was exposed to phosphorimager screen for 48 hrs.

Figure 20. Possible Tau2 phosphorylation sites according to conserved phosphorylation sequence of SnRK1 family proteins. (A) Conserved SnRK1 family protein phosphorylation sequence[93]. Black box, phosphorylation site; gray box, amino acids required for phosphorylation; X, any amino acid. (B) Possible Tau2 phosphorylation site deducted from the conserved phosphorylation sequence of SnRK1.2. Ser244 and Ser247 highly matches the conserved phosphorylation sequence, while Ser32 only partially match the conserved sequence.

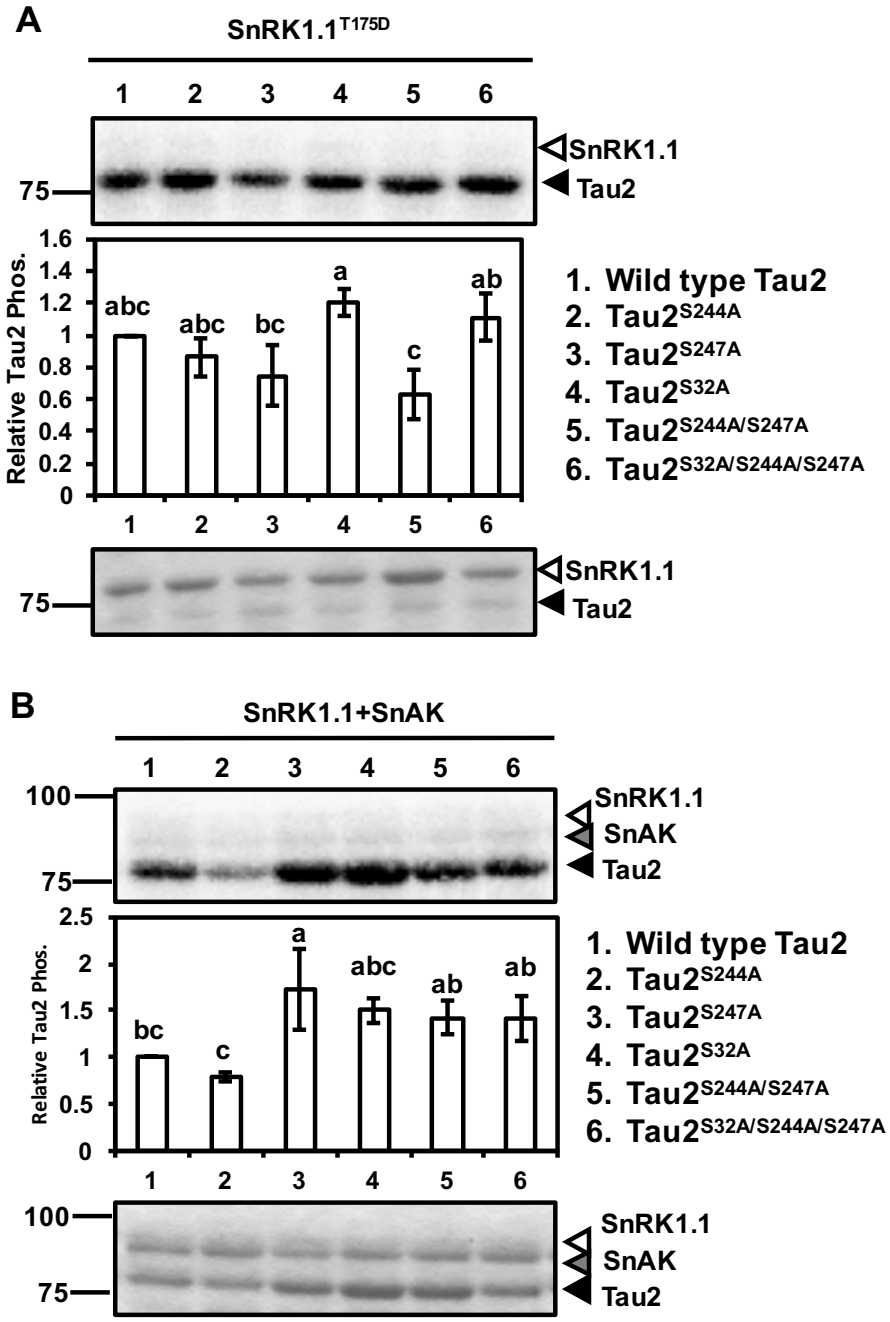

Figure 21. Identification of phosphorylation site of Tau2 by serine mutations. Tau2 containing indicated Ser to Ala mutations was phosphorylated in *in vitro* kinases assay containing γ -[32 P]ATP by (A) kinase-active MBP-SnRK1.1^{T175D} or (B) SnRK1.1 pre-activated by SnAK. ImageQuant TL software was used to analyze the phosphorylation levels of Tau2 in each assay. Top panels, phosphorimage. Middle panels, relative Tau2 phosphorylation levels are calculated by normalizing to wild type Tau2 phosphorylation levels and are the average of three independent experiments. Error bars are standard error of the mean. Bottom panels, Coomassie stained gel.

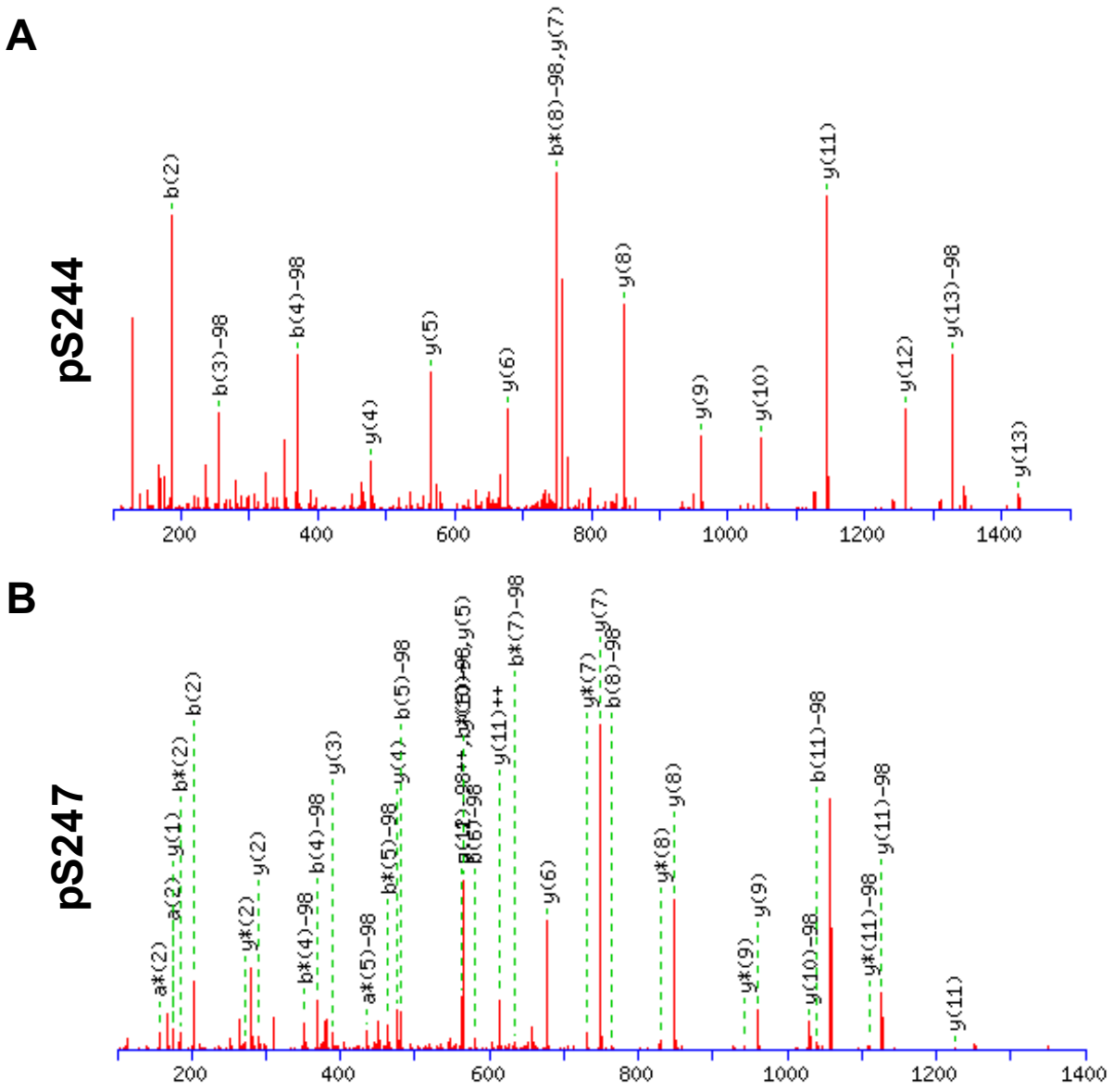

Figure 22. MS identification of Tau2 phosphorylation sites *in vitro* by *Sl*SnRK1.1. Wild type Tau2 (A and B) or double mutant Tau2$^{S244A/S247A}$ (C and D) was phosphorylated by SnAK pre-activated SnRK1.1 *in vitro*, separated by 6-12% gradient gel, digested with trypsin, passed over an IMAC column, and eluted peptides analyzed by MS/MS. (A) Identification of Ser244 and Ser247 phosphorylation in peptide GKSNPSLVALSSTNR. (B) Identification of Ser244 and Ser247 phosphorylation in peptide and SNPSLVALSSTNR. (C) Identification of Ser108 phosphorylation in peptide DIAVEGSWDNWKSR. (D) Identification of S115 phosphorylation in peptide SGKDFTILK (phosphorylated Serine underlined).

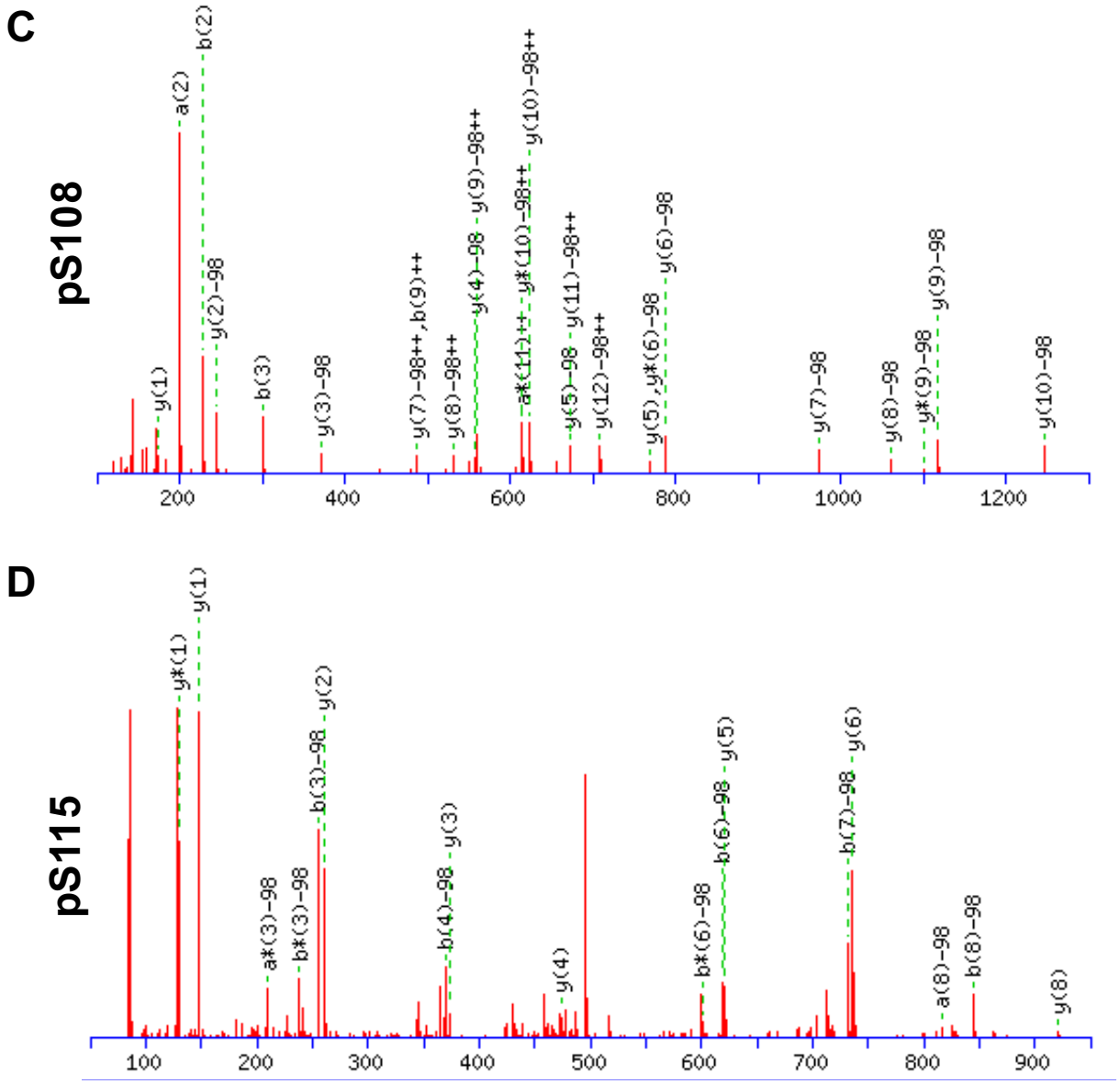

Figure 22. Continued.

3.9. Identification of Phosphorylation Sites of Tau2

As the β-subunit that has the highest level of *Sl*SnRK1.1phosphorylation, Tau2 represents a good target for the study of β-subunit phosphorylation regulation, substrate binding, and subcellular localization. Using the SnRK1 phosphorylation consensus sequence (Figure 20A) [93], we identified three potential Serine residues in Tau2, Ser32, Ser244, and Ser247 (Figure 20B), as potential phosphorylation site by *Sl*SnRK1.1. Tau2 single, double, and triple Serine to Alanine mutations at these sites were generated and their ability to be phosphorylated by *Sl*SnRK1.1 was tested in *in vitro* kinase assays. Both kinase-active *Sl*SnRK1.1^{T175D} and wild type *Sl*SnRK1.1 pre-activated by *Sl*SnAK was tested for their ability to phosphorylated Tau2 and its mutants. Although S244A and S247A single and double mutations decreased Tau2 phosphorylation levels by *Sl*SnRK1.1, they did not eliminate phosphorylation by *Sl*SnRK1.1 (Figure 21A, lane 2, 3, 5 and B lane 2). Surprisingly, the S32A mutation increased Tau2 phosphorylation to higher than wild type (Figure 21A and B, lane 4, and 6), which could be a result of major conformational changes that opened up potential phosphorylation sites that are otherwise buried inside of the protein.

To further elucidate any additional Tau2 phosphorylation sites, mass spectrometry (MS) analysis of trypsin digested *Sl*SnRK1.1 phosphorylated Tau2 was preformed to identify phosphorylated peptides. MS analysis of *in vitro* phosphorylated wild type Tau2 identified Ser244 and Ser247 phosphorylation in peptides GKSNPSLVALSSTNR and SNPSLVALSSTNR (phosphorylated Serine underlined, Figure 22 A and B). This confirms that Ser244 and Ser247 as *Sl*SnRK1.1 phosphorylation sites. We then analyzed the Tau2$^{S244A/S247A}$ double mutant to find additional phosphorylation sites. MS analysis of *in vitro Sl*SnRK1.1phosphorylated Tau2$^{S244A/S247A}$ identified Ser108 phosphorylation in peptide DIAVEGSWDNWKSR and Ser115

phosphorylation in peptide SGKDFTILK (phosphorylated Serine underlined, Figure 22 C and D).

3.10. Discussion

Although many plants have more than one SnRK1 α-subunit, the importance of having multiple SnRK1 α-subunits has not been well studied. In tomato, *Sl*SnRK1.1 is the only α-subunit that had been studied at the protein level. Here, we characterized the *in vitro* activity of an additional tomato α-subunit, *Sl*SnRK1.2. Overall, compared to *Sl*SnRK1.1 *Sl*SnRK1.2 is a much weaker kinase in relation to its ability to autophosphorylate and phosphorylate the β-subunits and AMARA peptide. For *Sl*SnRK1.1, the T175D phosphomimetic mutation increased its kinase activity 11.42 times, while for *Sl*SnRK1.2 the T173E phosphomimetic mutation only increased kinase activity 2.29 times (Figure 12A, B). Similarly, *Sl*SnRK1.2 kinase activity on the β-subunits or the AMARA peptide is much weaker than that of *Sl*SnRK1.1 even after *Sl*SnAK activation (Figure 17A, B). One possible reason for the lower kinase activity of *Sl*SnRK1.2 could be the presence of autoinhibitory domains in the protein. While the autoinhibitory domains found in AMPK and Snf1 are not found in plant SnRK1 α-subunits, a recent study raised the possibility that kinase activity of the *Arabidopsis* α-subunit *At*SnRK1.1 could be negatively regulated by its C-terminus, but *At*SnRK1.2 did not show such regulation [75]. It is possible the *Sl*SnRK1.2 C-terminal region negatively regulates its kinase activity similar to *At*SnRK1.1 through a yet to be identified domain, while the *Sl*SnRK1.1 C-terminal region does not have a negative regulatory function. It will be interesting to see whether the C-termini of *Sl*SnRK1.1 and *Sl*SnRK1.2 have different regulatory functions as seen in *Arabidopsis*.

*Sl*SnRK1.2 did show different preferences for β-subunit phosphorylation compared to *Sl*SnRK1.1. Sip1 and Tau2 are highly phosphorylated by *Sl*SnRK1.1 (Figure 14, Figure 17),

while *Sl*SnRK1.2 could phosphorylate *Sl*Gal83 and *Sl*Tau2 to a higher extent than the other two β-subunits (Figure 14, Figure 17). On the other hand, when phosphorylating the AMARA peptide, *Sl*SnRK1.2 kinase activity is the highest when the heterotrimer was reconstituted using Sip1 as the β-subunit (Figure 19B), while *Sl*SnRK1.1 kinase activity is the lowest when Sip1 was used as the β-subunit (Figure 19A).

There are a few possible ways these differences in *Sl*SnRK1.1 and *Sl*SnRK1.2 activity could have physiological importance. It is possible the activity differences relate to different *in vivo* functions for these two kinases, specifically for *Sl*SnRK1.2, which along with other Solanaceous SnRK1.2 sequences appear to be quite different phylogenetically from the other plant SnRK1.2 sequences (Figure 10). In potato, the *Sl*SnRK1.1 α-subunit homolog, StubSNF1, can interact with the potato Gal83 β-subunit and complement the yeast *snf1*Δ knockout [126], similar to what we have seen for *Sl*SnRK1.1 [58]. On the other hand, the potato *Sl*SnRK1.2 α-subunit homolog, PKIN1, does not interact with Gal83 or compliment the yeast *snf1*Δ knockout [126]. These data may suggest unique functions for Solanaceous SnRK1.2 α-subunit kinases.

*Sl*SnRK1.1 and *Sl*SnRK1.2 could also be differentially regulated at distinct plant developmental stages. Transcriptome analysis of various tomato tissues showed that while *Sl*SnRK1.1 and *Sl*SnRK1.2 expression levels are similar in the leaf, *Sl*SnRK1.2 expression levels increased more than three fold in developing fruit before reaching the green mature stage [141]. The expression levels for *Sl*SnRK1.1 only increase about 20% at the same fruit developmental stage [141]. This could indicate differences in regulation, and possibly function, for *Sl*SnRK1.1 and *Sl*SnRK1.2 during the carbohydrate storage process in fruit.

Additionally, *Sl*SnRK1.1 and *Sl*SnRK1.2 could be differentially regulated under stress conditions. In *Arabidopsis* under phosphate starvation conditions, *At*SnRK1.2 kinase activity

decreased 35%-40% and is selectively degraded, while *At*SnRK1.1 activity increased one fold at the same time [120]. We have found that *Sl*SnRK1.1 interacts with the tomato cell death regulatory kinase Adi3 [58] which helps to regulate the cell death associated with resistance to the causative agent of bacterial spec disease, *P. syringae* [47–49]. This interaction is speculated to regulate *Sl*SnRK1.1 for the reallocation of nutrients during the resistance cell death. Thus, it will be interesting to determine how biotic stresses such as *P. syringae*, or even abiotic stresses, will cause changes in *Sl*SnRK1.1 and *Sl*SnRK1.2 transcript and protein levels as well as differential regulation of kinase activity.

CHAPTER IV

NITRATE REDUCTASE PHOSPHORYLATION AND REGULATION BY *Sl*SNRK1.1

4.1. Rationale

Plant SnRK1 family proteins have been shown to directly or indirectly regulate over a thousand proteins [56]. Among them, nitrate reductase (NR) is a very important target due to its function in nitrogen assimilation. NR catalyzes the reduction of NO_3^- to NO_2^- using NADH as the electron donor[142]. Since nitrate reduction consumes ~20% of the e^- produced by photosynthetic electron transport and the nitrite produced by NR is cytotoxic and mutagenic, NR activity needs to be tightly regulated and coordinated with carbon synthesis and plant growth to ensure balance in energy expenditure and the pool of reducing e^- [105]. We chose NR as a focus to study the effects on the regulation of SnRK1 substrate phosphorylation during the resistance response to *Pst* due to the potential changes in energy expenditure during PCD. In Arabidopsis, NR has been shown to interact with AKINβ1, the β-subunit homolog in *Arabidopsis* [113]. In spinach, NR activity is inactivated by the spinach SnRK1 homolog through direct phosphorylation [76]. SnRK1 and NR both respond to stresses like darkness, so it will be interesting to see how SnRK1 regulates NR under PCD inducing conditions such as resistance to pathogens. 14-3-3 proteins are required for the inactivation of NR in the presence of upstream kinase[112]. In *Arabidopsis*, the 14-3-3 protein isoforms ω, κ, and λ showed strong inhibition activity on *Arabidopsis* NR2 [111]. However, in tomato the specific 14-4-3 proteins responsible for NR inactivation have not been identified. As a result, crude leaf extracts were used for *in vitro* NR reactions instead of purified proteins so that potential regulating 14-3-3 proteins could be included.

4.2. Phosphorylation of NR by *Sl*SnRK1.1

NR phosphorylation by upstream kinases is an important step in the regulation of NR catalytic activity [112]. Phosphorylation of a conserved motif on the NR hinge 1 is required for 14-3-3 protein binding and NR inactivation results from this binding [112]. Although NR has been shown to be phosphorylated by SnRK1 family proteins in spinach, NR phosphorylation by tomato SnRK1 has not been experimentally tested [76]. Moreover, there have been reports that *At*SnRK1.1 could bind to the *Arabidopsis* NR2 *in vitro* [113]. However, NR phosphorylation in tomato has not been well studied and there is no study on tomato SnRK1 phosphorylation of NR to our knowledge. Before analyzing how *Sl*SnRK1.1 regulates NR activity, the ability of *Sl*SnRK1.1 to phosphorylate NR needs to be confirmed. Tomato NR is about 103 kD and the large size caused low and truncated expression in the *E. coli* expression system. There have been reports of successful expression of *Arabidopsis* NR in a yeast called *Pichia pastoris* [143]. However, in our hands the *Pichia* expression system did not generate expression of NR. As a result, a mixture the full length and truncated *E. coli* expressed, N-terminally MBP-tagged NR were used for further experiments (Figure 23). In the *Sl*SnRK1.1 kinases assay, *Sl*SnRK1.1 by itself only weakly phosphorylated NR (Figure 24, lane 3). After activation by *Sl*SnAK, as indicated by the increased *Sl*SnRK1.1 phosphorylation band, *Sl*SnRK1.1 can significantly phosphorylate NR (Figure 24, lane 4). On the other hand, NR did not show phosphorylation by *Sl*SnAK (Figure 24, lane 2).

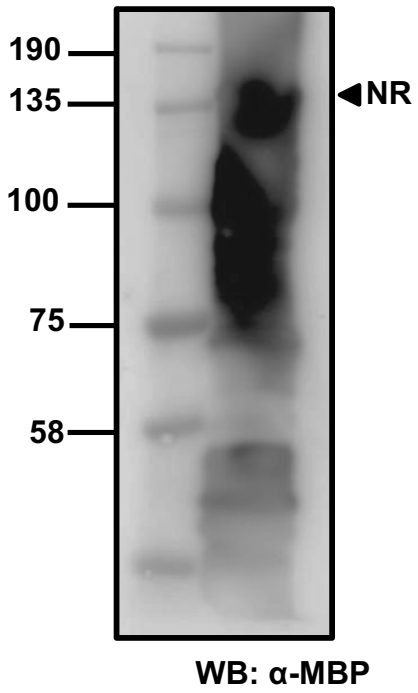

Figure 23. Expression of MBP-tagged NR in E. coli. N-terminally MBP-tagged NR was expressed in E. coli, purified by amylose affinity column. Presence of NR was confirmed by western blot against MBP tag. Due to the large size of NR with N-terminal MBP tag (about 145 kD), the NR expression level is relatively low and several truncated versions of NR was detected.

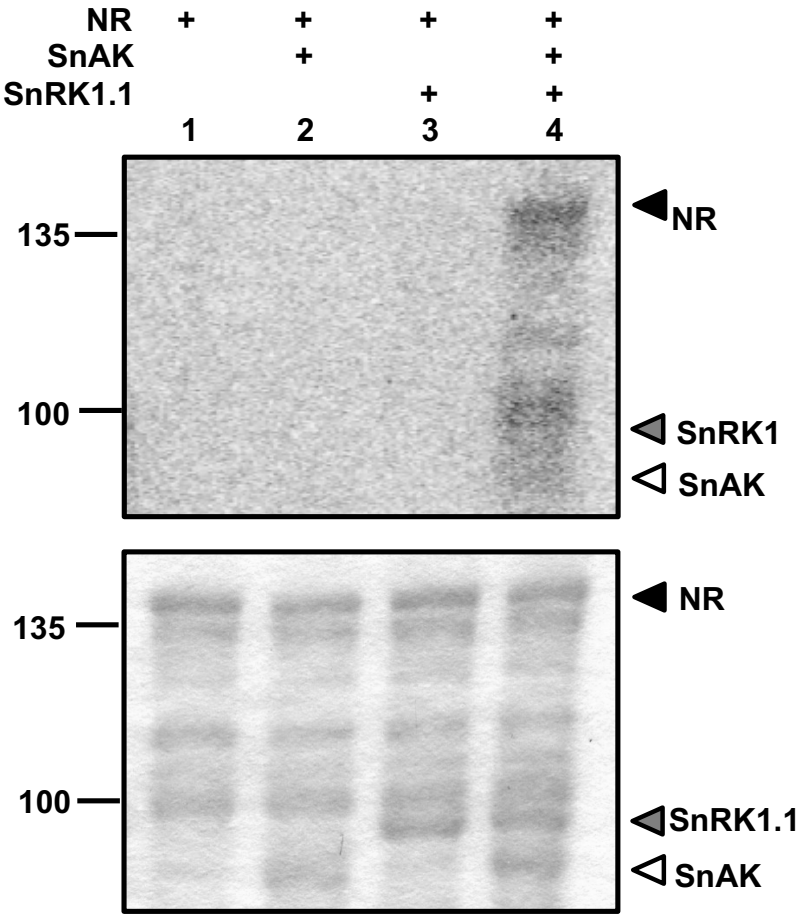

Figure 24. NR is phosphorylated by *Sl*SnRK1.1. Top panel, proteins added to each reaction; middle panel, phosphor image; bottom panel, Coomassie stained gel. Each reaction contains 4ug NR, 4 ug SnRK1.1, or 2 ug SnAK as indicated on top of each lane. Kinase Reaction was carried out at 20°C for 45 mins. Gel was exposed on phosphor screen for 24 hrs.

4.3. Effects of Gal83 and Adi3 on NR Phosphorylation

The closest homolog of the tomato Gal83 β-subunit, *Arabidopsis* SnRK1β1, has been shown to interact with NR [113]. Moreover, tomato Gal83 has been shown to be phosphorylated by Adi3 at Ser26 [58]. It will be interesting to find out whether tomato Gal83 can interact with NR, and most importantly, whether Gal83 phosphorylation by Adi3 can influence NR phosphorylation by *Sl*SnrK1.1. To analyze the effect of Gal83 phosphorylation status on NR phosphorylation by *Sl*SnrK1.1, we carried out the NR phosphorylation assay with different phosphorylation status forms of Gal83. Addition of wild type Gal83 did not change *Sl*SnrK1.1 phosphorylation of NR compared to *Sl*SnRK1.1 alone (Figure 25, lane 2). Gal83^{S26D}, which is a phosphomimetic for Adi3 phosphorylation, caused a very slight decrease in NR phosphorylation (Figure 25, lane 3), indicating the phosphomimetic mutation at Ser26 alone is not enough to influence *Sl*SnRK1.1 activity on NR. Alanine mutation of either the Adi3 phosphorylation site Ser26 or the *Sl*SnRK1.1 phosphorylation site Ser45 on Gal83 did not produce significant changes in NR phosphorylation levels (Figure 26, lane 5 and 7). On the other hand, Gal83 phosphorylated by the constitutively active Adi3$^{S539D/S212D}$ caused a significant increase in NR phosphorylation by *Sl*SnRK1.1 (Figure 26, lane 6), indicating phosphorylation by Adi3 is required for Gal83 to increase NR phosphorylation by *Sl*SnRK1.1. Interestingly, addition of the constitutively active Adi3$^{S539D/S212D}$ alone to *Sl*SnRK1.1 also caused a moderate increase in NR phosphorylation (Figure 26, lane 2). A possible explanation for this is that the interaction between Adi3 and *Sl*SnRK1.1 influences *Sl*SnRK1.1 activity, or the interaction alters how SnRK1.1 binds with NR.

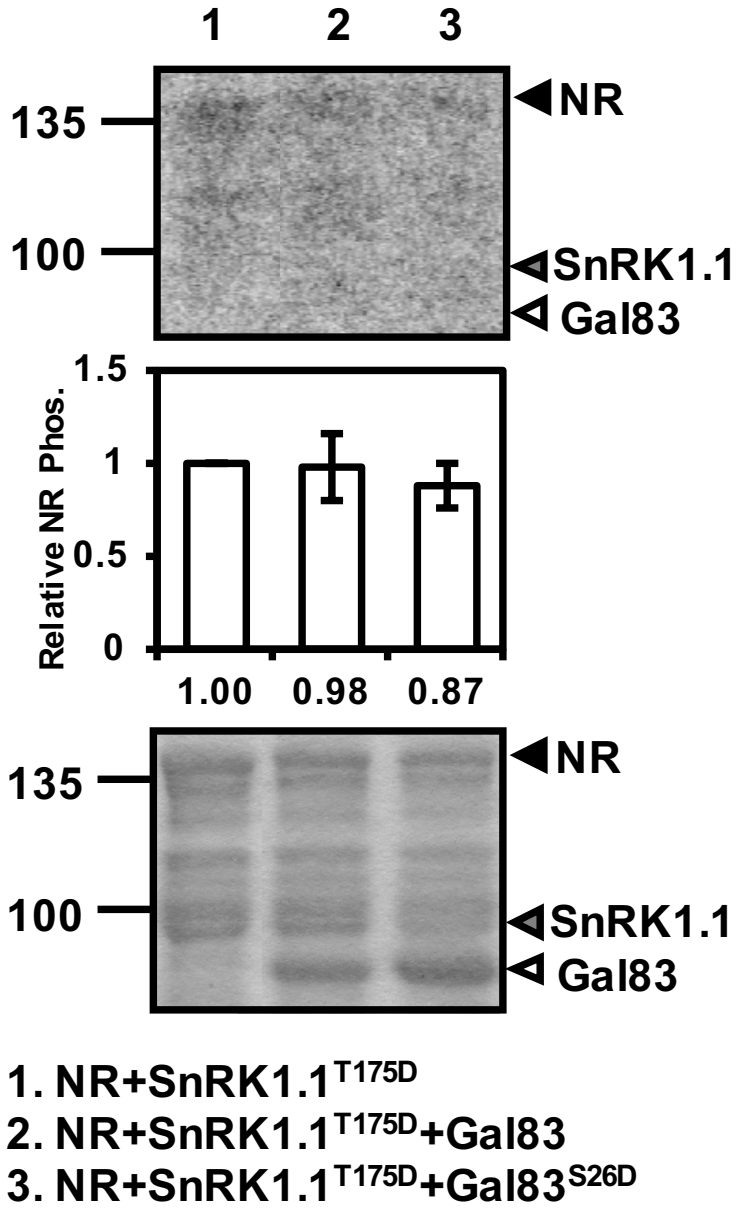

Figure 25. Effect of Gal83S26D on NR phosphorylation by SnRK1.1. Top panel, phosphor image; middle panel, quantification of relative NR phosphorylation level compared to SnRK1.1^{T175D} only; bottom panel, Coomassie stained gel. Kinase Reaction was carried out at 20°C for 45 mins. Gel was exposed on phosphor screen for 24 hrs. Black arrow, MBP-tagged NR; gray arrow, MBP-tagged SnRK1.1^{T175D}; white arrow, MBP-tagged Gal83 or Gal83^{S26D}.

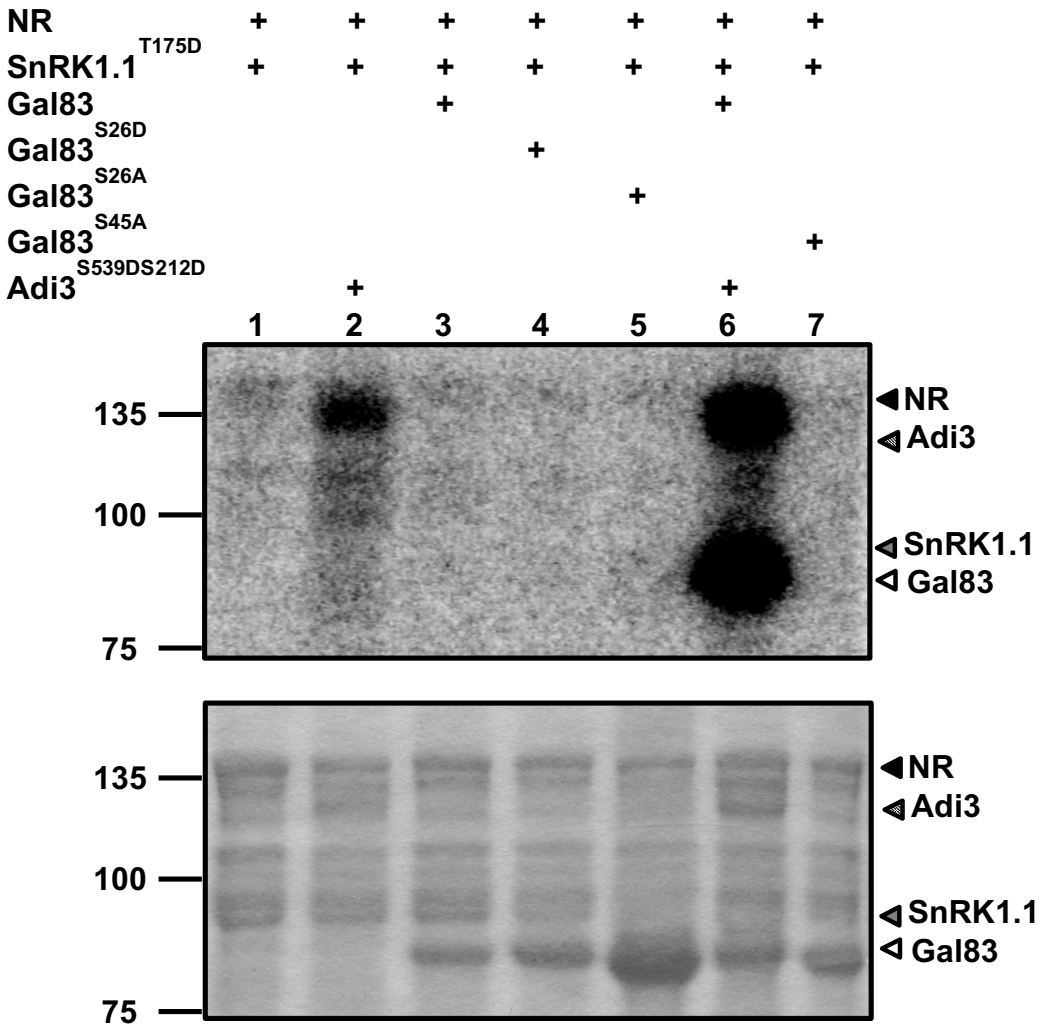

Figure 26. Adi3 phosphorylated Gal83 increased NR phosphorylation by *Sl*SnRK1.1. Top panel, proteins added to each reaction; middle panel, phosphor image; bottom panel, Coomassie stained gel. Kinase Reaction was carried out at 20°C for 45 mins. Gel was exposed on phosphor screen for 24 hrs. Black arrow, MBP-tagged NR; striped arrow, MBP-tagged Adi3$^{S539D/S212D}$; gray arrow, MBP-tagged SnRK1.1; white arrow, MBP-tagged Gal 83 and mutants.

4.4. Effects of *Sl*SnRK1.1 and Gal83 on NR Activity from Leaf Extracts

Since Gal83 and its phosphomimetic mutant Gal8^{3S26D} appear to slightly decrease NR phosphorylation by *Sl*SnRK1.1, we want to know if this change in NR phosphorylation will influence NR activity. To test the effect of *Sl*SnRK1.1 phosphorylation on NR activity as well as the regulation of this phosphorylation by Gal83, we performed *in vitro* NR activity assays using tomato leaf extracts pre-incubated with phosphomimetic *Sl*SnRK1.1^{T175D} and wild type or phosphomimetic mutant Gal83. Incubation with Gal83 alone did not change the NR activity from a tomato leaf extract (Figure 27, bar 1 and 2). Surprisingly, pre-incubation with the constitutively active *Sl*SnRK1.1^{T175D} increased NR activity from a tomato leaf extract (Figure 27, bar 3). Similarly, addition of wild type Gal83 or phosphomimetic Gal8^{S26D} also increased NR activity from a tomato leaf extract (Figure 27, bar 4 and 5). These observation, contrary to previous reports [76], indicate that phosphorylation by *Sl*SnRK1.1 increases NR activity. This is likely because the inactivation of NR is not through the phosphorylation event *per se*, but through binding to 14-3-3 proteins at the NR phosphorylation site that leads to NR degradation [112]. Under our *in vitro* assay conditions, NR binding with a 14-3-3 protein and/or NR degradation could be inhibited. As a result, the phosphorylated NR appears to have increased activity *in vitro*.

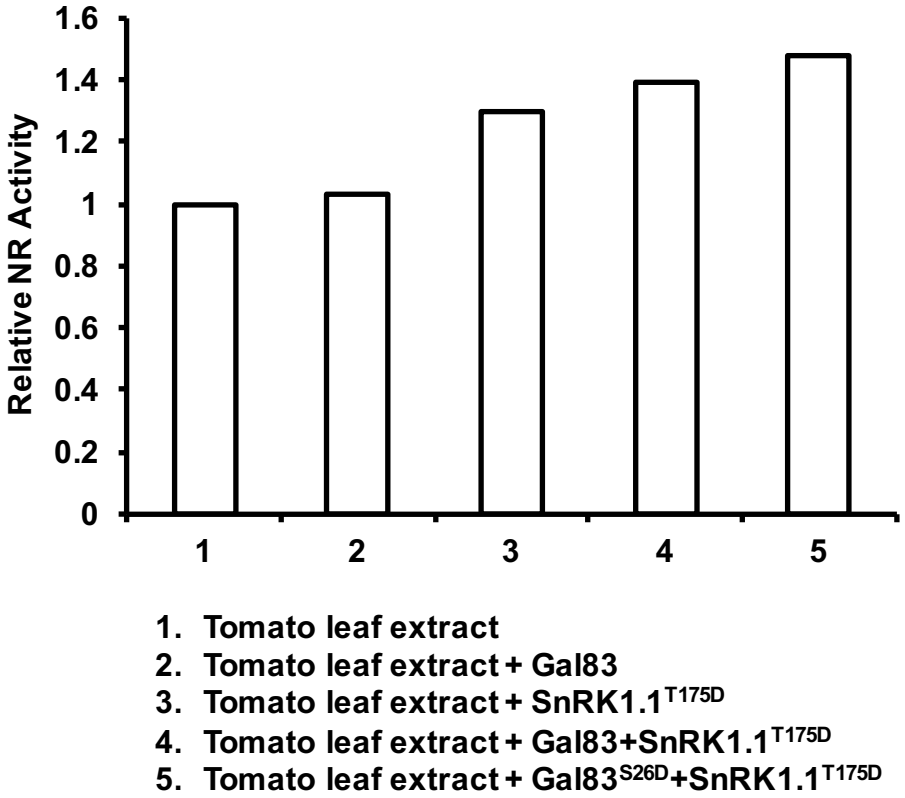

Figure 27. Effect of *Sl*SnRK1.1 and Gal83 on NR activity from Leaf Extract. Tomato leaf extract was pre-incubated with phosphor-mimic SnRK1.1^{T175D} and wild type or mutant Gal83 at 20°C for 45 mins before used for NR activity assay. NR activity is measured by its ability to convert KNO_3 to KNO_2. The production of KNO_2 is measured by the Griess color reaction. Relative NR activity is calculated comparing to tomato leaf extract without additional protein.

4.5. Discussion

We were able to express and partially purify tomato nitrate reductase from the *E. coli* expression system and show that tomato SnRK1.1 was indeed able to phosphorylate NR. This phosphorylation is further enhanced by *Sl*SnAK activation of *Sl*SnRK1.1. Tomato Gal83 is a good candidate for studying the mechanism of NR regulation by *Sl*SnRK1.1 under PCD inducing conditions because: 1) The closest homolog to *Sl*SnRK1.1 in *Arabidopsis*, SnRK1β1, can specifically interact with NR *in vitro* [113]; 2) tomato Gal83 is phosphorylated by the PCD inhibitor Adi3 [58]. Thus, Gal83 could potentially be a controller of nitrate assimilation under PCD conditions. To test this hypothesis, we first tested whether Gal83 phosphorylation status could change NR phosphorylation levels. Addition of constitutively active Adi3$^{S539D/S212D}$, which has been shown to phosphorylate Gal83, significantly increased NR phosphorylation by *Sl*SnRK1.1, indicating phosphorylated Gal83 promotes NR phosphorylation. However, we cannot rule out the possibility that constitutively active Adi3$^{S539D/S212D}$ directly influenced *Sl*SnRK1.1 activity, since reactions containing Adi3$^{S539D/S212D}$ but no Gal83 also showed a slight increase in NR phosphorylation. Interestingly, phosphomimetic mutation of the Adi3 phosphorylation site of Gal83 did not result in significant change of NR phosphorylation level. This could be due to either secondary Adi3 phosphorylation sites on Gal83, or that Adi3 itself plays a role in NR phosphorylation.

So far there is contradicting evidence regarding the regulation of NR by SnRK1 β-subunits. Studies with tomato Gal83 indicates Gal83 is a negative regulator of SnRK1 activity [58], and decreased SnRK1 activity could mean increased NR activity due to lower phosphorylation induced inactivation. On the other hand, studies in *Arabidopsis* showed that SnRK1β1 negatively regulates NR activity *in vivo* [114]. In our hands, addition of purified Gal83

to the cell free assay did not cause a change in NR activity, further obscuring the effect of β-subunits. The apparent uncoupling of NR phosphorylation and inactivation in our cell free assay could be a result of decreased 14-3-3 protein binding. However, this hypothesis cannot be tested with the involved 14-3-3 proteins being identified. Further study of NR in tomato, especially the identification of regulating proteins should greatly help us understand NR regulation during PCD.

CHAPTER V

REGULATION OF TOMATO SNRK1 ACTIVITY IN RESPONSE TO AVRPTO AND AVRPTOB

5.1. Rationale

The interaction of *Sl*SnRK1 complex subunits with Adi3 raises the possibility that the *Sl*SnRK1 complex could regulate metabolism during bacterial infection. There are two possible modes of regulation: one is that the infected cell spends more energy to fend off the infection; the other is the infected cell could relocate its nutrients to neighboring un-infected cells. To understand which mode resistant and susceptible plants employ during bacterial infection, the first step is to study the change in SnRK1 activity in the presence of effector proteins or bacteria. In the presence of AvrPto or AvrPtoB, Adi3 no longer localizes to the nucleus and PCD occurs [49]. Although it has been shown that Adi3 and SnRK1 complex subunits can interact [58], the sub-cellular location of the interaction is not known.

5.2. *Sl*SnRK1 Activity in Response to Agrobacterium Mediated Expression of AvrPto

5.2.1. Effect of AvrPto expression on SlSnRK1 kinase activity in PtoR tomato

To test the effect of AvrPto on *Sl*SnRK1.1 activity, we first tried to transiently express AvrPto in plant leaves using *Agrobacterium*. *Agrobacterium* carrying either the empty pBTEX vector or pBTEX vector containing FLAG-tagged AvrPto was infiltrated at either OD_{600}=0.2 or OD_{600}=0.5. Expression of AvrPto from infiltration at OD_{600}=0.2 and OD_{600}=0.5 was detectable at similar levels after 44 hrs (Figure 28). To minimize the effect of *Agrobacterium*, OD_{600}=0.2 was selected for further infiltrations. The PtoR plants start to show cell death symptoms around 32

hrs post infiltration. By 48 hrs post infiltration, cells in the infiltrated areas were completely dead (Figure 29).

To test the effect of AvrPto expression on *Sl*SnRK1.1 kinase activity, crude tomato leaf extracts from infiltrated leaf areas was tested for the ability to phosphorylate the AMARA peptide. The *Agrobacterium* carrying empty vector caused a gradual increase of kinase activity on the AMARA peptide (Figure 30), possibly due to a response to the *Agrobacteria* infiltration. On the other hand, *Agrobacterium* expressing AvrPto suppressed such an increase in kinase activity (Figure 30). There was an initial peak of AMARA phosphorylation at 8 hrs post infiltration, possibly due to a response to the *Agrobacteria*. However, after the initial response, the kinase activity remained lower than empty vector control (Figure 30). AvrPto transient expression by *Agrobacterium* appeared to attenuate the effect of bacterial infiltration on *Sl*SnRK1.1 kinase activity.

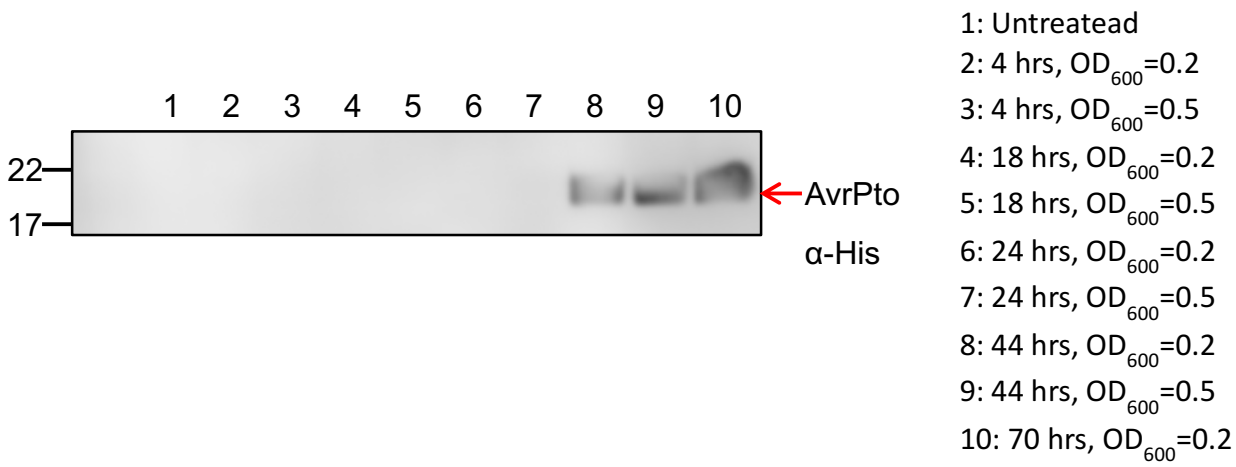

Figure 28. Agrobacterium mediated AvrPto expression in tomato leaves. Agrobacterium carrying His-tagged AvrPto was infiltrated into tomato leaves at OD600 0.2 or 0.5. Leaf samples were collected at different time points as indicated in the figure. The expression of AvrPto was detected by α-His antibody after 44 hrs of infiltration.

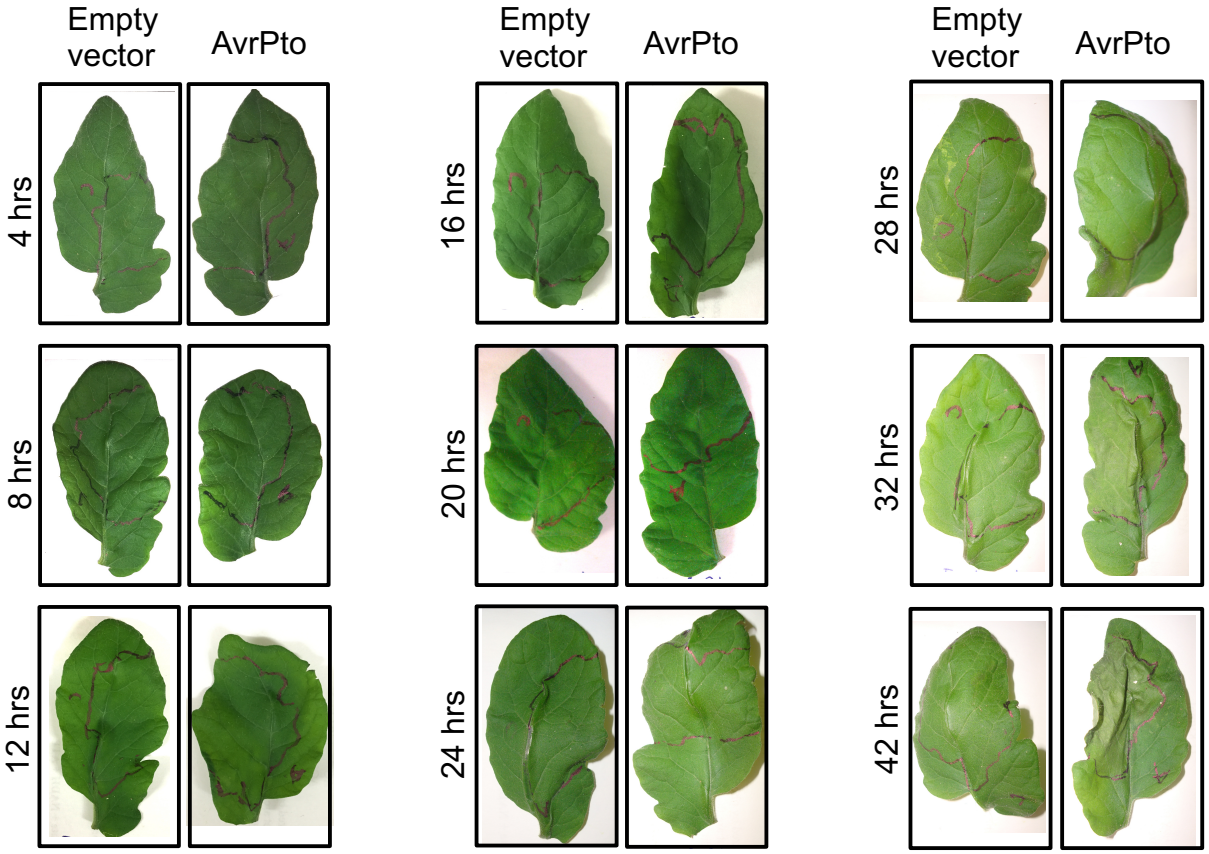

Figure 29**. Tomato leaf response to agrobacterium mediated transient expression of AvrPto.** Tomato leaves was infiltrated with agrobacterium carrying either empty vector or His-tagged AvrPto at OD_{600}=0.2. Leaf samples was taken at 4, 8, 12, 16, 20, 24, 28, 32, and 42 hrs after infiltration. Cell death was first observed 32 hrs after infiltration.

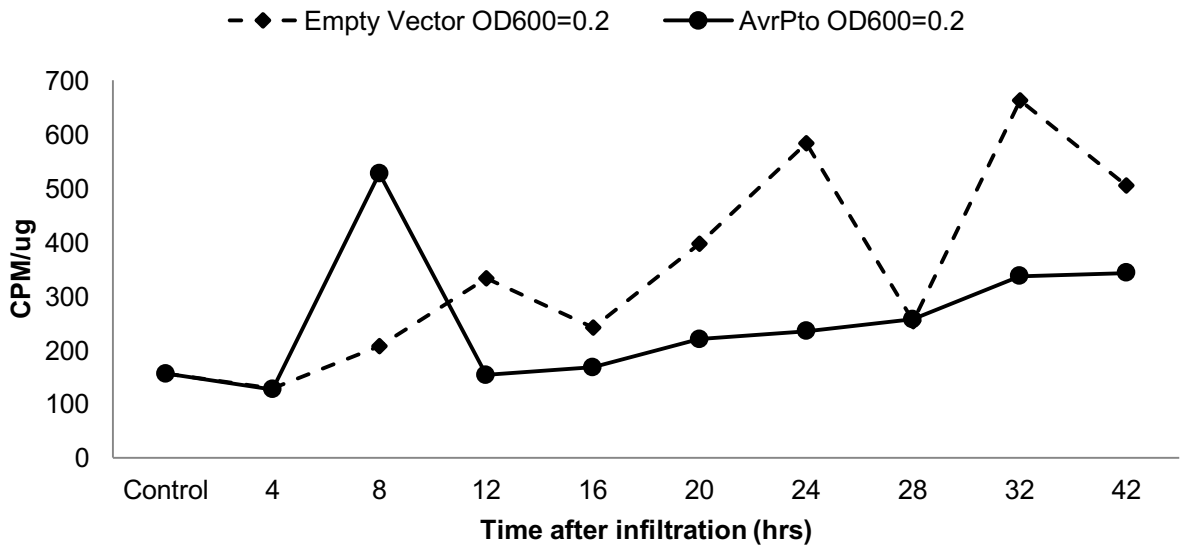

Figure 30. *Sl*SnRK1.1 kinase activity changes in response to AvrPto expression. Agrobacterium carrying either empty pBTEX vector or pBTEX vector containing FLAG-tagged AvrPto was infiltrated into tomato leaves at OD_{600}=0.2. Leaf disc samples was taken from infiltrated areas at 4, 8, 12, 16, 20, 24, 28, 32, 42 hrs after infiltration. A sample from untreated area is taken as control. Leaf crude protein preparation and AMARA kinase assay was carried out as described in the methods section. CPM: count per minute.

5.2.2. Effect of AvrPto expression on SlSnRK1.1 kinase activity in prf-3 tomato

To further elucidate the pathway involved in AvrPto suppression of *Sl*SnRK1.1 kinase activity, the *prf-3* mutant tomato plant was used. Prf is an NBS-LRR protein that is activated in response to AvrPto-Pto interaction and is required for induction of the hypersensitive response [42]. As a result, AvrPto cannot trigger the hypersensitive response in *prf-3* plants. Indeed, *prf-3* tomato leaves transiently expressing AvrPto did not cause any visible symptom on the leaf and no hypersensitive response was observed (Figure 31). We further tested *Sl*SnRK1.1 kinase activity of *prf-3* leaf crude extracts. Interestingly, *Sl*SnRK1.1 kinase activity remained low after *Agrobacterium* infiltration and AvrPto expression (Figure 32). A possible explanation is that *Sl*SnRK1.1 activation is regulated by a component upstream of Prf. As a result, AvrPto can still suppress *Sl*SnRK1.1 kinase activity even though the hypersensitive response did not occur. It has been shown that AvrPto can inhibit Pto kinase activity [42], which may result in reduced activation of *Sl*SnRK1.1 through so far unknown components.

Figure 31. *Prf-3* mutant tomato leaves did not show any symptom in response to AvrPto expression. *prf-3* mutant tomato leaves was infiltrated with agrobacterium carrying either empty vector or His-tagged AvrPto at OD_{600}=0.2. Leaf samples was taken at 24, 48 and 72 hrs after infiltration. Cell death was not observed 72hrs after infiltration.

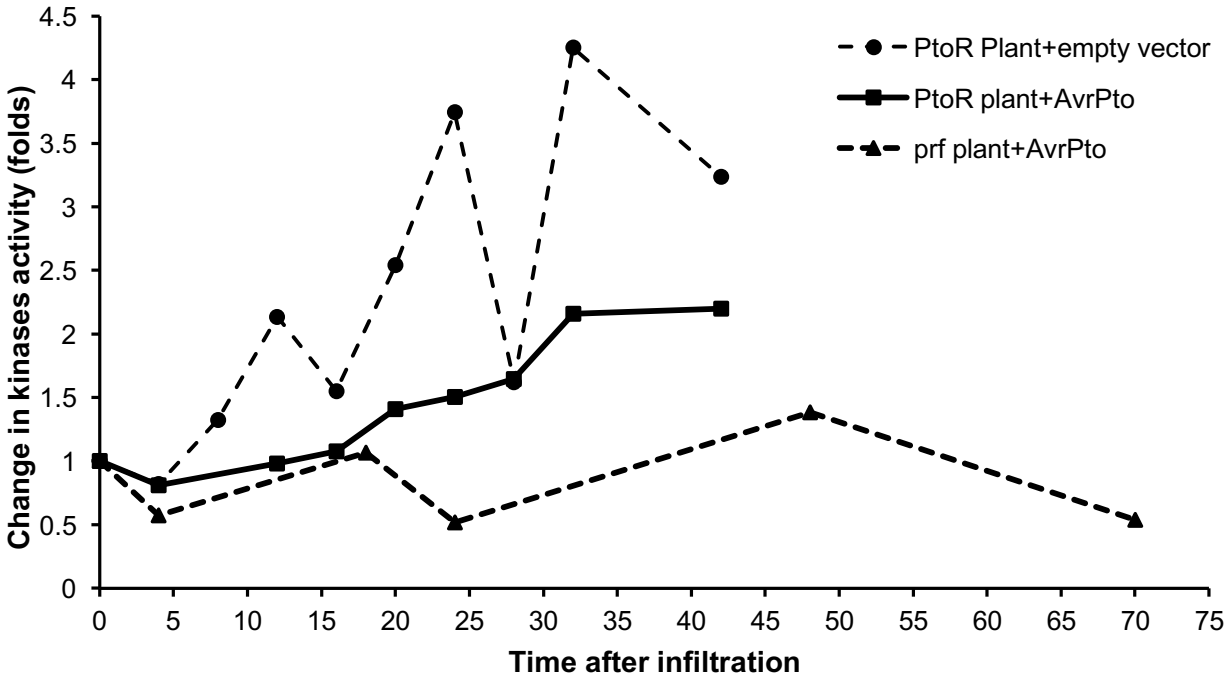

Figure 32. Changes in *Sl*SnRK1.1 kinases activity in *prf-3* tomato leaves expressing AvrPto. PtoR leave discs infiltrated with either empty pBTEX vector or pBTEX containing AvrPto and *prf-3* tomato leaves discs expressing AvrPto was collected at different time points after infiltration. A sample from untreated area is taken as control. Leaf crude protein preparation and AMARA kinase assay was carried out as described in the methods section. Changes in SnRK1 kinase activity on AMARA peptide for empty vector, AvrPto expression in PtoR tomato, and AvrPto expression in *prf-3* plants was calculated comparing to no treatment control.

5.3. *Sl*SnRK1.1 Activity During Interaction with *Pst* DC3000

5.3.1. Tomato leaf phenotype after Pst infiltration

Agrobacterium mediated transient expression of AvrPto provides an easy way to test the effect of AvrPto on *Sl*SnRK1 complex activity. However, the downside of using *Agrobacterium* is that due to the delay of the expression, it is hard to pin point the onset of HR response. Moreover, *Agrobacterium* mediated expression levels might be much higher than physiological levels, and possibly lead to artifacts in the result. In order to mitigate these problems, we used wild type *Pst* DC3000 which contains a functional AvrPto and AvrPtoB, and mutants of *Pst* that have single or double knockouts of AvrPto and/or AvrPtoB; i.e. *ΔavrPto*, *ΔavrPtoB*, *ΔavrPtoΔavrPtoB*. Using this system, we can tease apart how AvrPto, AvrPtoB, and all other factors from *Pst* influence the kinase activity of the *Sl*SnRK1 complex.

We first tested the acute leaf phenotype caused by DC3000 infiltration in both PtoR and *prf-3* plants. As expected, *prf-3* plants did not show a hypersensitive response when wild type or mutant versoins of DC3000 were infiltrated (Figure 33). DC3000 wild type, *avrPto*, or *ΔavrPtoB* infiltration in PtoR tomato leaves showed different levels of HR response. DC3000*ΔavrPto* showed the strongest HR response that was observable 15 hrs after infiltration (Figure 33 panel 2). Both DC3000 wild type and DC3000*ΔavrPtoB* started to show visible HR response 22 hrs after infiltration (Figure 33 panel 1 and 3). In agreement with previous reports [121], DC3000*ΔavrPtoΔavrPtoB* infiltration of PtoR leaves did not how visible HR response (Figure 33 panel 4).

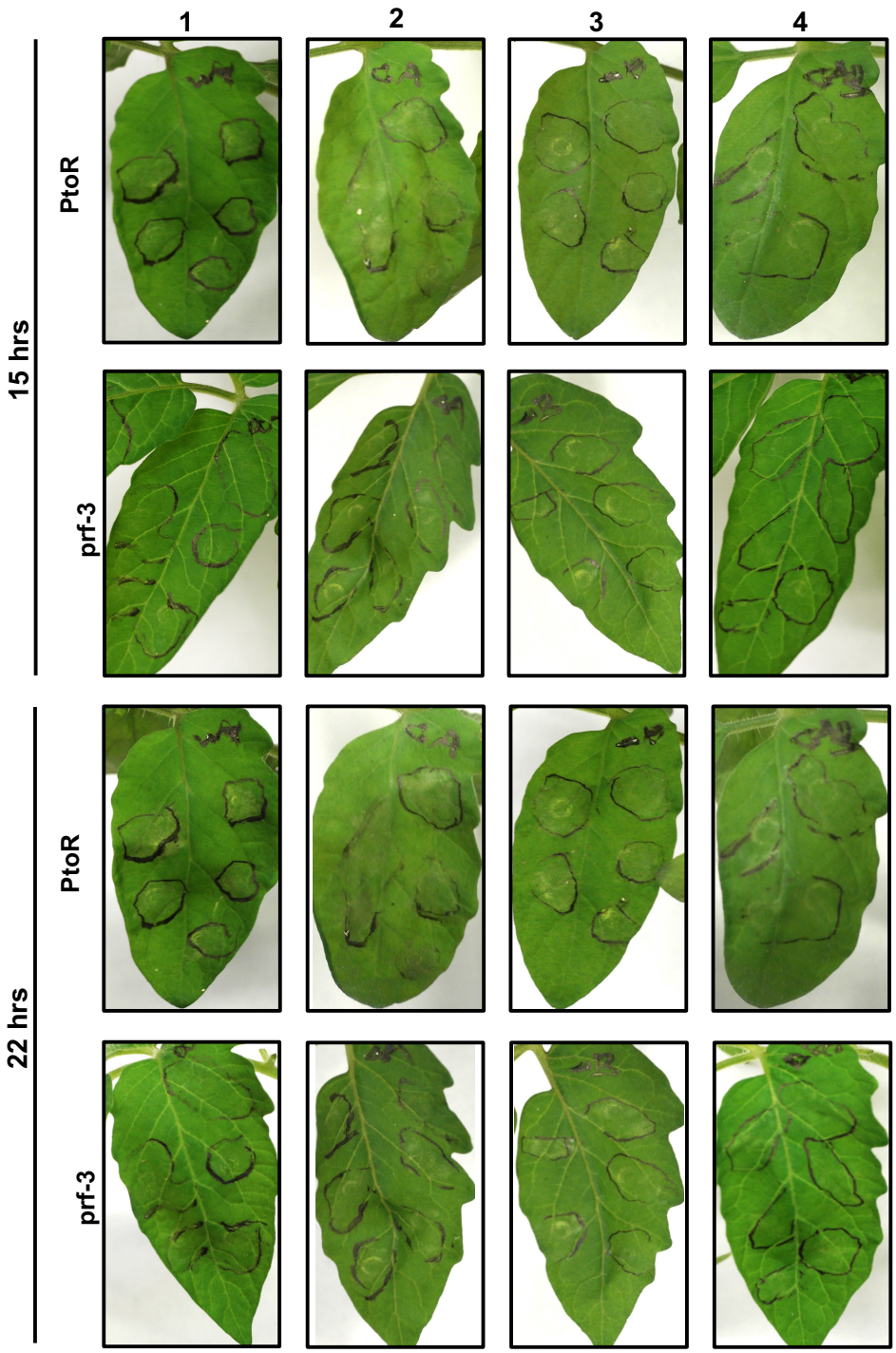

Figure 33. Tomato response to *Pst* DC3000 infiltration. Wild type and mutant *Pst* DC3000 was infiltrated into PtoR and *prf-3* tomato leaves at 10^6 CFU/ml. Photograph was taken at 15 and 22 hrs after infiltration. Infiltrated areas were marked by black outline. 1, DC3000; 2, DC3000*ΔavrPto*; 3, DC3000*ΔavrPtoB*; 4. DC3000*ΔavrPtoΔavrPtoB*.

5.3.2. Ion leakage test

During the PCD response increased plasma membrane permeability causes ion leakage and the conductivity of the surrounding solution of a leaf disc undergoing PCD can be a semi-quantitative indicator of PCD. To detect the early onset of the HR response in leaves infiltrated with *Pst* DC3000, we tested the solution conductivity of leaf discs shortly after infiltration. *Pst* DC3000 wild type and DC3000*ΔavrPtoB* infiltration induced a high level of ion leakage, while the ion leakage induced by DC3000*ΔavrPto* and DC3000*ΔavrPtoΔavrPtoB* are relatively low (Figure 34). This indicates that knockout of AvrPto and AvrPtoB from *Pst* DC3000 almost abolished the HR response. Previous reports showed that *ΔavrPto* has a higher effect on reducing the HR response than *ΔavrPtoB* [121]. However, in our hands, *ΔavrPtoB* had a stronger effect on reducing the HR response than *ΔavrPto*, suggesting AvrPto is the main factor in inducing HR response.

5.3.3. SnRK1 kinase activity in response to Pst

To test the effect of *Pst* DC3000 on *Sl*SnRK1.1 kinase activity in PtoR plants we preformed kinase activity assays using crude protein extracts from DC3000 infiltrated leaves using the artificial SnRK1 peptide substrate AMARA. Due to the fast HR response to *Pst* DC3000, samples were only collected within 24 hrs after infiltration. For PtoR plants infiltrated with wild type *Pst* DC3000 and *ΔavrPto*B, *Sl*SnRK1.1 kinase activity was slightly lower than the no treatment control (Figure 35). On the other hand, PtoR plants infiltrated with *ΔavrPto* or *ΔavrPtoΔavrPto*B showed increased kinase activity (Figure 35). Taking into consideration that *Agrobacterium* mediated AvrPto expression attenuated *Sl*SnRK1.1 kinase activity increased due

to *Agrobacterium* growth, these observations further support the hypothesis that AvrPto inhibits *Sl*SnRK1.1 kinase activity that would otherwise increase in the presence of bacteria infiltration.

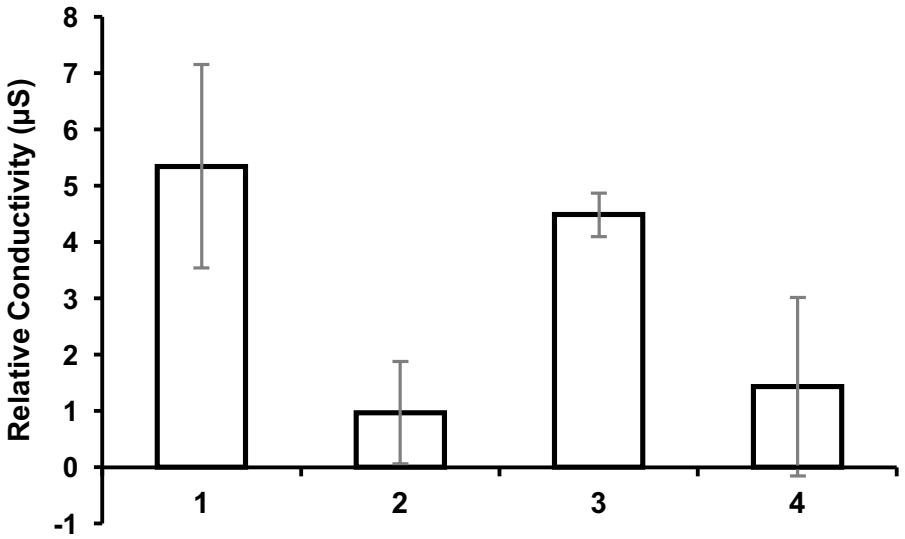

Figure 34. Ion leakage test for HR response. PtoR tomato leaves was infiltrated with wild type or mutants of *Pst* DC3000. 4 hrs after infiltration, leaf discs were taken from infiltrated areas and ion leakage was tested by measuring conductivity of incubating solution. The relative conductivity was obtained by subtracting value of infiltration buffer control from treated sample conductivity. The levels shown are average of three repeats, error bar indicates standard error of the mean of three repeats. 1, PtoR+DC3000; 2, PtoR+DC3000*ΔavrPto*; 3, PtoR+DC3000*ΔavrPtoB*; 4. PtoR+DC3000*ΔavrPto ΔavrPtoB*.

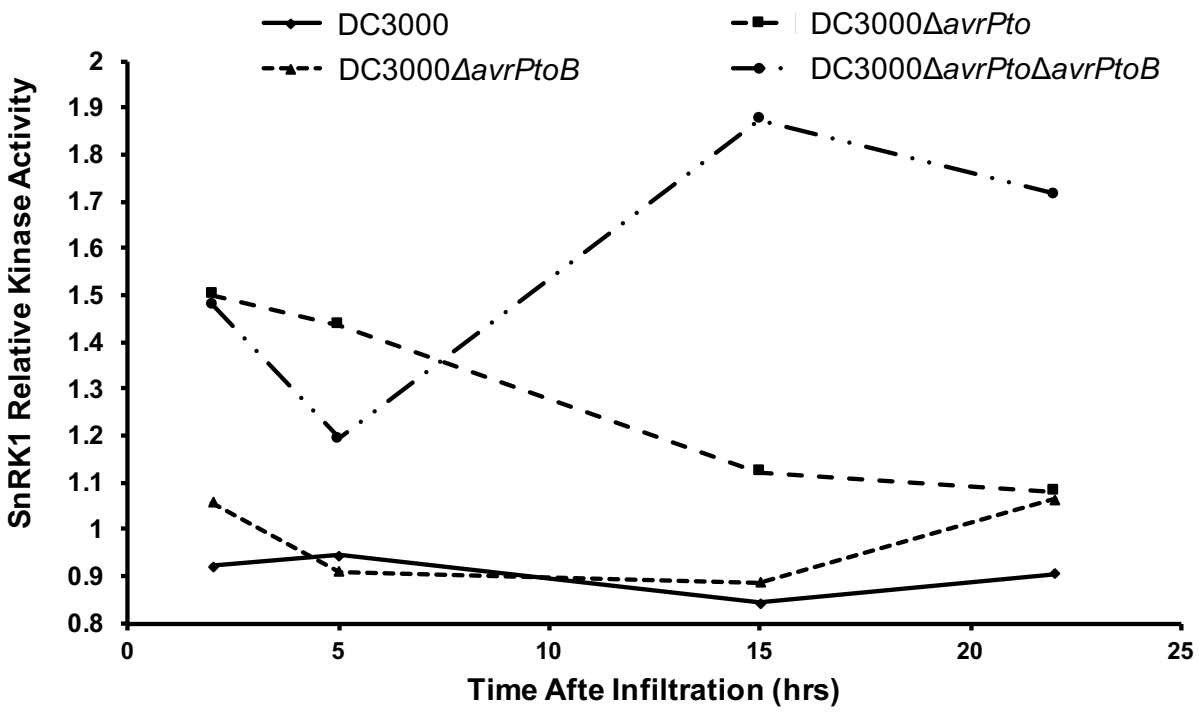

Figure 35. Relative *Sl*SnRK1.1 kinase activity after wild type or mutant *Pst* DC3000 infiltration. Leaf discs within wild type or mutant *Pst* DC3000 infiltrated areas were collected at 2, 5, 15, 22 hrs after infiltration. Leaf crude protein preparation and AMARA kinase assay was carried out as described in the methods section. Relative *Sl*SnRK1.1 kinases activity was calculated using untreated areas as control.

5.4. *Sl*SnRK1 NLS and Localization

5.4.1. Identification of a possible NLS in SlSnRK1.1 and SlSnRK1.2

The SnRK1 complex has been observed to localize to both the cytosol and nucleus [144], however, the mechanism for SnRK1 nuclear localization is not well studied. There are two possible ways for SnRK1 α-subunits to localize to the nucleus. The first is co-localization through interaction with proteins that are transported into the nucleus. The second is nuclear transport through recognition of a nuclear localization signal (NLS) in the SnRK1 α-subunit. The first possibility is supported by the fact that SnRK1 α-subunit localization can change when bound to different β-subunits and substrate [144,145]. However, the two possible nucleus localization mechanisms may not necessarily be exclusive. Previous analysis did not find a traditional NLS in the *Sl*SnRK1.1 amino acid sequence. With the recent increase in nuclear transport mechanisms, more NLS sequences have been proposed with less confined sequence requirements [146]. Using the online localization tool LOCALIZER [146], we identified a non-classical bipartite NLS [147] in the N-terminus of both *Sl*SnRK1.1 and *Sl*SnRK1.2 (Figure 36). As the name suggests, this non-classical bipartite NLS contains two conserved sequences linked by a 10-amino acids linker region (Figure 36). The first conserved part of the NLS consists of two amino acids that are either Arg or Lys [147]. The second conserved part of the NLS is a stretch of 5 amino acids containing at least three Arg or Lys [147]. Although there is no strict requirement for specific amino acids in the 10 amino acids linker region, acidic residues are favored in the center region, and proline as well as basic and hydrophobic residues are favored in the terminal regions [148].

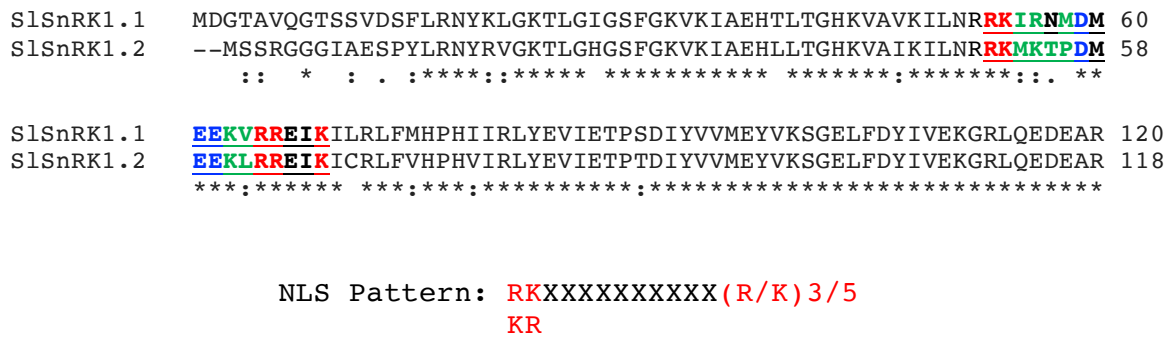

Figure 36. Proposed SnRK1 nucleus localization sequence and alignment. Both *Sl*SnRK1.1 and *Sl*SnRK1.2 contains bipartite nucleus localization sequence (NSL). The conserved pattern of the bipartite NLS is two Arg or Lys followed by a 10 amino acids linker region linked to a stretch of 5 amino acids containing at least three Arg or Lys. The bipartite NLS are underlined in the *Sl*SnRK1.1 and *Sl*SnRK1.2 sequence alignment, with required Arg/Lys highlighted in red. Acidic residues are favored in the center of the linker region and are highlighted blue; Proline as well as basic and hydrophobic residues are favored in the terminal regions of the linker and are highlighted green.

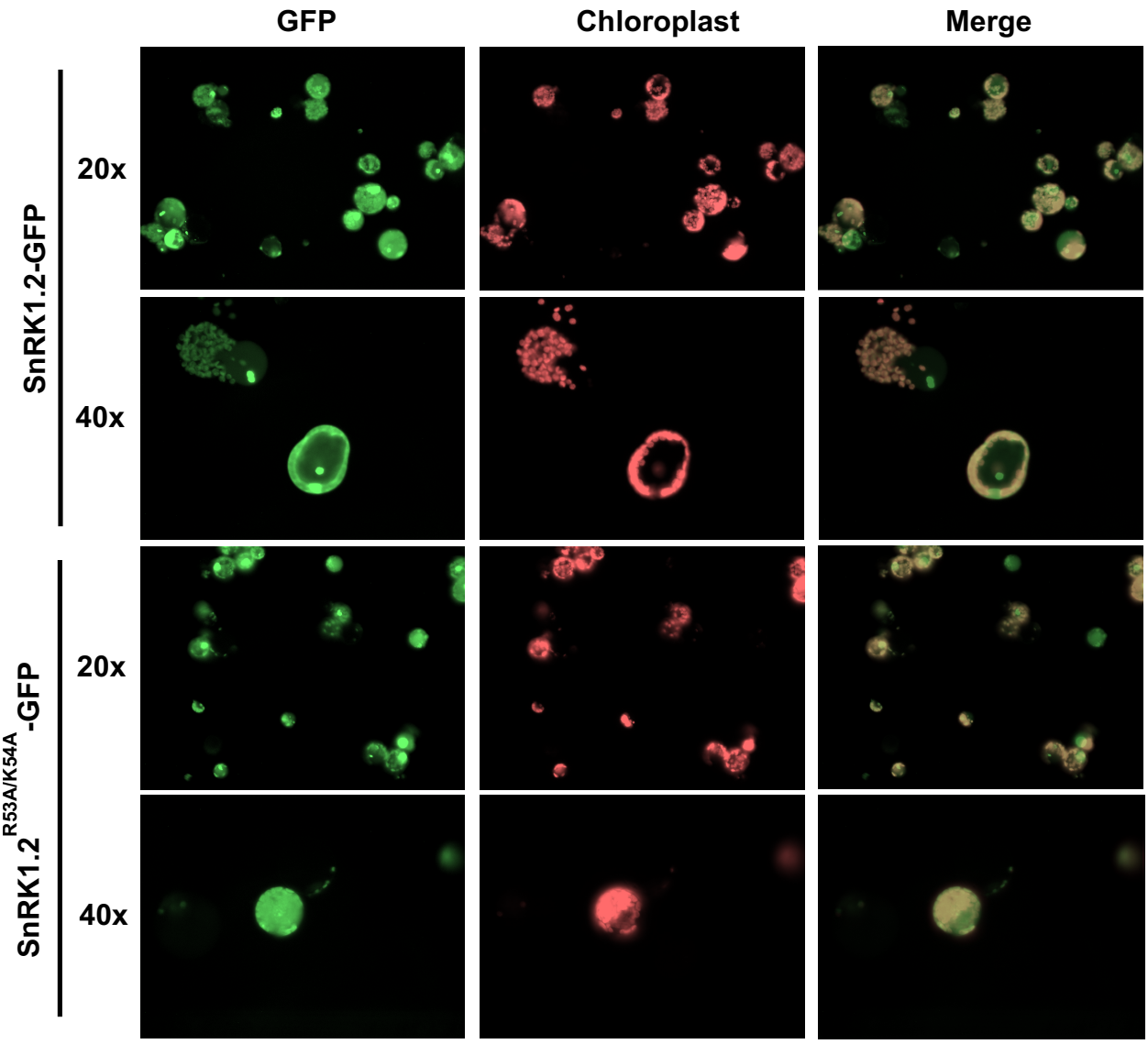

Figure 37. Mutation in NLS changed *Sl*SnRK1.2 nucleus localization. GFP tagged wild type *Sl*SnRK1.2 and *Sl*SnRK1.2 with the first part of the NLS mutated to Ala was transiently expressed in tomato protoplasts. After expression at 20 °C for 16 hrs, the protoplasts were visualized under florescent microscope. Wild type *Sl*SnRK1.2 showed localization close to chloroplasts and in a small defined area inside the nucleus. *Sl*SnRK1.2 NLS mutants showed either defused localization or localized to an area surrounding the nucleus.

5.4.2. Mutation of the putative NLS motif changes SlSnRK1.2 localization

Both parts of the bipartite NLS are required for nuclear localization [147]. As a test of this concept, we mutated both Arg53 and Lys54 in the first part of the bipartite NLS to Ala in a N-terminal GFP fusion of *Sl*SnRK1.2. We then compared the subcellular localization of wild type *Sl*SnRK1.2 and mutated *Sl*SnRK1.2$^{R53A/K54A}$ by expression in protoplast and visualizing the GFP signal by fluorescent microscopy. Wild type *Sl*SnRK1.2 located to areas surrounding chloroplasts and inside the nucleus (Figure 37, top two tows). On the other hand, *Sl*SnRK1.2$^{R53A/K54A}$ either had a completely defused localization or was localized to areas surrounding the nucleus (Figure 37, bottom two tows).

5.5. Discussion

Previous studies have shown that Adi3 regulates PCD induced by AvrPto containing *Pst* [50], and that *Sl*SnRK1.1 kinase activity could be inhibited by Adi3 [58]. However, a direct link between the regulation of the SnRK1 complex activity and *Pst* interaction is missing. In order to study SnRK1 complex regulation during *Pst* interacting, we utilized two different system for *in vivo* studies. One of the systems we used is *Agrobacterium* mediated AvrPto expression. This system offers a way to isolate the effect of AvrPto from the complex interactions *Pst* could have in tomato. However, this system also has its limitations that the expression of AvrPto is transient and could be much higher than the physiological level from *Pst*. Moreover, the spreading of *Agrobacterium* itself in tomato leaves could cause stress to the plants and add complexity to the interpretation of the data. In our studies, infiltration of *Agrobacterium* alone caused increase SnRK1 activity, suggesting certain components from the *Agrobacterium* alone could activate SnRK1. *Agrobacterium*-mediated transient expression of AvrPto showed lower SnRK1 kinase

activity than the empty vector control in PtoR plants, and stayed around pre-infiltration levels after an initial spike in activity. A possible explanation for these observations is that AvrPto inhibited SnRK1.1 activation caused by certain components from the *Agrobacterium*.

Though direct infection of leaves by *Pst* adds more components to the system, this approach has more physiological relevance. By using AvrPto and AvrPtoB single or double mutants, it is possible to separate the effect of AvrPto, AvrPtoB, and the rest of the components of the *Pst* interaction. Observation of cell death in the infiltrated area and measurement of ion leakage both indicate that AvrPto is a stronger inducer of the HR response in Pto plants than AvrPtoB. In agreement with *Agrobacterium*-mediated AvrPto transient expression assays, *Pst* containing AvrPto showed lower SnRK1 activity than AvrPto deleted *Pst*.

Adi3 suppress PCD when localized to the nucleus, and PCD occurs when Adi3 is sequestered to the endosome system [49]. However, when, where, and under what conditions Adi3 interacts with the SnRK1 complex is still unknown. To answer this question a good understanding of the regulation of SnRK1 localization is essential. In yeast, the SNF1 complex localization is determined by the β-subunit [149,150]. In tomato, localization regulation by β-subunit phosphorylation and myristoylation status has also been suggested. Besides regulation by β-subunits, the recent finding of a nuclear exporting signal (NES) in the AMPK α-subunit raised the possibility that the catalytic α-subunit could also determine its own cellular localization [151]. Using recently developed localization prediction tools, we were able to identify a non-classical bipartite NLS and mutation of this NLS in *Sl*SnRK1.2 shift its distribution to be more cytosolic. Having an NLS could potentially mean an active nuclear import process is important for SnRK1 complex localization regulation.

CHAPTER VI

CONCLUSIONS AND FUTURE DIRECTIONS

6.1. Chapter III Conclusions and Future Directions

6.1.1. The second SnRK1 complex α-subunit and its activity

We identified a second *Sl*SnRK1α-subunit, *Sl*SnRK1.2, in tomato and characterized its *in vitro* activity in comparison to *Sl*SnRK1.1. The results show that *Sl*SnRK1.2, although able to complement the yeast *Δsnf1* knockout, is a much weaker kinase than *Sl*SnRK1.2. This is demonstrated by overall weaker ability to *cis*-autophosphorylate, *trans*-autophosphorylate the β-subunits, and phosphorylate the artificial substrate AMARA peptide. A recent study of the *Arabidopsis* SnRK1.1 suggested the probability that its C-terminal region could inhibit kinase activity through interaction with the special βγ type γ-subunit in *Arabidopsis* [75]. It is not clear whether this inhibition quires the specific ADP binding pattern found in βγ type γ-subunit. To our knowledge, there is so far no βγ type γ-subunit characterized in tomato and it is still unclear whether the tomato SnRK1.2 contains a C-terminal inhibitory region. To test for the possible C-terminal inhibition hypothesis, we could compare the kinase activity of full length and C-terminal truncated *Sl*SnRK1.1 and *Sl*SnRK1.2.

6.1.2. Phosphorylation of Sl*SnRK1 complex β-subunits*

*Sl*SnRK1 complex β-subunits are phosphorylated by the α-subunit in yeast and this phosphorylation was suggested to play a role in substrate binding and complex cellular localization regulation [58]. Our studies showed that *Sl*SnRK1.1 and *Sl*SnRK1.2 can phosphorylate all four β-subunits. Sip1 and Tau2 are highly phosphorylated by *Sl*SnRK1.1,

while Gal83 and Tau2 are highly phosphorylated by *Sl*SnRK1.2. Considering that *Sl*SnRK1.1 and *Sl*SnRK1.2 could be differentially regulated during development and stress [120,141], the differential β-subunit phosphorylation by *Sl*SnRK1.1 and *Sl*SnRK1.2 could potentially be part of the mechanism of substrate regulation at different development stages or in response to stress. To test this hypothesis, we first need to have a better understanding of β-subunit phosphorylation, including the phosphorylation site(s) on each β-subunit. Since Tau2 shows the highest phosphorylation level among all β-subunits, it was chosen to be the candidate for β-subunit phosphorylation site analysis. Computational analysis of the Tau2 sequence identified Ser245 and Ser247 as candidate phosphorylation sites, and their phosphorylation were confirmed by MS analysis. However, a Ser245/Ser246 to Ala double mutant did not abolish Tau2 phosphorylation by *Sl*SnRK1.1. Instead, additional phosphorylation sites may arise after mutation due to major conformational changes induced by the mutations. Due to the potential of this conformational change, the Ser245/Ser246 to Ala double mutation may not be suitable for further *in vitro* or *in vivo* studies. However, based on our observation that Tau2 is highly phosphorylated, it is reasonable to hypothesize that the phosphomimetic Ser245/Ser246 to Asp double mutation could have physiologically relevant functions. Thus, future studies could compare the Ser245D/Ser246D double mutation with wild type Tau2 to analyze the role of these phosphorylation evetns in cellular SnRK1 localization or substrate binding.

6.1.3. Tomato SnRK1 activation kinase (SnAK)

In an attempt to better understand *Sl*SnRK1.2 kinase activity, we isolated and expressed the upstream kinase for tomato SnRK1. *Sl*SnAK greatly increased *Sl*SnRK1.1 activity while slightly increasing *Sl*SnRK1.2 activity. *Sl*SnAK could be an essential component for further

SnRK1 studies in addition to the phosphomimetic SnRK1s we have previously used. Previous studies show that SnRK1.1 in *Arabidopsis* could be phosphorylated on additional sites by SnAK besides the conserved Thr175 [63], suggesting SnAK activation could be a better alternative than using Thr175 phosphomimetic mutation in SnRK activity studies. The down side of using SnAK in *in vitro* studies is that the relatively high level of SnAK autophosphorylation can obscure the analysis of weak kinases like tomato *Sl*SnRK1.2. One possible way to mitigate this problem is co-expression of SnRK1s with SnAK. Studies using *Arabidopsis* proteins demonstrated that SnAK can phosphorylate and activate SnRK1s when co-expressed in *E. coli*. Co-expression also helped to solubilize SnRK1s, which tend to have solubility issues when expressed in *E. coli*.

6.2. Chapter IV Conclusions and Future Directions

6.2.1. Tomato NR phosphorylation by SlSnRK1.1

In this chapter, we confirmed that tomato NR is phosphorylated by *Sl*SnRK1.1 using *E. coli* expressed and partially purified NR. We show that constitutively active Adi3$^{S539D/S212D}$ increased NR phosphorylate in a process that is only partially dependent on the presence of the Gal83 β-subunit. Unexpectedly, NR phosphorylation by *Sl*SnRK1.1 did not result in inactivation of NR in our cell free assay. A possible cause is insufficient binding of regulating 14-3-3 proteins under the cell free assay conditions. However, this could not be tested without identifying the 14-3-3 proteins responsible for NR regulation in tomato. The first step for further study of NR regulation will require the identification of 14-3-3 proteins required for NR inactivation. A good starting point will be identifying the tomato 14-3-3 protein homologs of *Arabidopsis* isoforms ω, κ, and λ, which showed strong inhibition activity on *Arabidopsis* NR2 [111]. Then next step would be finding assay conditions that the responsible 14-3-3 protein could

bind and inactivate phosphorylated NR. Then, using these assay conditions we can study the effect of Adi3 and Gal83 on NR activity. Alternatively, we can overexpress Adi3$^{S539D/S212D}$ in tomato leaves and then analyze any potential changes in NR activity.

6.2.2. Could NR play a regulatory role in pathogen responses?

NR's main enzymatic activity is the reduction of nitrate to nitrite as part of nitrogen assimilation[152]. However, NR can also convert nitrite to nitric oxide (NO), which accounts for about 1% of NR activity *in vitro* [153,154]. Despite the low NO production activity of NR, NO has been shown to decrease when NR is inactivated by 14-3-3 protein binding [101]. NO has been shown to play a role in plant pathogen responses by being involved in HR responses, and promoting defense related protein and hormone production [154,155]. Thus, NR could also play an active role as a regulator of pathogen response through the regulation of NO production. Although NR is proposed to be the main producer of NO in plants by some studies, strong direct evidence is still lacking and the mechanism of NO synthesis remained elusive. Further studies on NO production by NR will be required to confirm any role NR might have in regulating pathogen response.

6.3. Chapter V Conclusions and Future Directions

Based on the previous finding that AvrPto and Pto interaction prevents Adi3 phosphorylation and activation by PDK1 [48], and that active Adi3 inhibits *Sl*SnRK1.1 [58], a model in which AvrPto inhibits Adi3 activity and thus increase SnRK1 activity was proposed [58]. To test this model, we analyze the changes of *Sl*SnRK1 kinase activity in response to AvrPto. Contrary to the expected increase in *Sl*SnRK1 activity based on the model,

Agrobacterium mediated transient expression of AvrPto resulted in lower *Sl*SnRK1 kinase activity than the empty vector control. Similarly, plants infiltrated by *Pst* containing AvrPto showed lower *Sl*SnRK1 activity than plants infiltrated by *Pst* that has an AvrPto knockout. Careful examination of the evidence for the previous model revealed several missing pieces of the puzzle in determining *Sl*SnRK1 response to AvrPto. First, Adi3 inhibition of *Sl*SnRK1 activity was only tested using tomato Gal83, which is the only β-subunit that has been shown to be phosphorylated by Adi3. Thus, the effect of AvrPto on *Sl*SnRK1 complexes formed with other β-subunits may not be regulated by Adi3.

Second, the study of the effect of Adi3 on *Sl*SnRK1 was done *in vitro* using purified protein and phosphomimetic *Sl*SnRK1. So, it is unclear how other components in the cell would affect *Sl*SnRK1 activity in the presence of AvrPto.

Third, previous studies showed kinase inactive Adi3 could also inhibit *Sl*SnRK1 activity, probably directly through binding [58]. Since *Sl*SnRK1 can localize to both cytosol and nucleus and the timing and location of the Adi3-*Sl*SnRK1 interaction is still unknown, it is possible there is a base level inhibition of *Sl*SnRK1 through binding by Adi3 regardless of Adi3 activity or the presence of AvrPto.

Lastly, the previous studies demonstrated the ability of Adi3 to inhibit the ability of the phosphomimetic *Sl*SnRK1 to phosphorylate substrate [58]. However, in the cell, if the upstream kinase SnAK is inhibited in response to AvrPto or some other signal, releasing the inhibition of Adi3 will not result in increased *Sl*SnRK1 activity because *Sl*SnRK1 is not phosphorylated and activated by SnAK.

Thus, more study is needed on the regulation of *Sl*SnRK1 activity in response to AvrPto. Several questions need to be answered to better understand the components in this model. Does

*Sl*SnRK1 interaction with Adi3 *in vivo* depend on Adi3 phosphorylation status or AvrPto? Is SnAK activation of *Sl*SnRK1 regulated by any mechanism in the presence of AvrPto? Is there any physiological significance of *Sl*SnRK1 complexes formed with different β-subunits in the context of AvrPto mediate resistance?

REFERENCES

[1] J.D.G. Jones, J.L. Dangl, The plant immune system, Nature, 444 (2006) 323–329.

[2] J. Monaghan, C. Zipfel, Plant pattern recognition receptor complexes at the plasma membrane, Curr. Opin. Plant Biol., 15 (2012) 349–357.

[3] L. Gomerz-Gomerz, T. Boller, FLS2: An LRR Receptor-like kinase involved in the preception of the bacterial elicitor flagellin in *Arabidopsis*, Mol. Cell, 5 (2000) 1003–1011.

[4] D. Chinchilla, C. Zipfel, S. Robatzek, B. Kemmerling, T. Nurnberger, J.D.G. Jones, G. Felix, T. Boller, A Flagellin-induced complex of the receptor FLS2 and BAK1 initiates plant defense, Nature, 448 (2007) 497–500.

[5] S. Chisholm, G. Coaker, B. Day, B.J. Staskawicz, Host-microbe interactions: shaping the evolution of the plant immune response, Cell, 124 (2006) 803–814.

[6] E. Jeworutzki, M.R.G. Roelfsema, U. Anschu, E. Krol, J.T.M. Elzenga, G. Felix, T. Boller, R. Hedrich, D. Becker, Early signaling through the *Arabidopsis* pattern recognition receptors FLS2 and EFR involves Ca 2 + -associated opening of plasma membrane anion channels, Plant J., 62 (2010) 367–378.

[7] M. Melotto, W. Underwood, J. Koczan, K. Nomura, S.Y. He, Plant stomata function in innate immunity against bacterial invasion, Cell, 126 (2006) 969–980.

[8] J.H. Chang, J.M. Urbach, T.F. Law, L.W. Arnold, A. Hu, S. Gombar, S.R. Grant, F.M. Ausubel, J.L. Dangl, A high-throughput, near-saturating screen for type III effector genes from *Pseudomonas syringae*, PNAS, 102 (2005) 2549–2554.

[9] J.L. Badel, A.O. Charkowski, W. Deng, A. Collmer, P. Pathology, U.S.A. Ny, A gene in the *Pseudomonas syringae* pv. *tomato* Hrp pathogenicity island conserved effector locus, hopPtoA1, contributes to efficient formation of bacterial colonies in planta and is duplicated elsewhere in the genome, Mol Plant Microbe Interact., 15 (2002) 1014–1024.

[10] S.R. Grant, E.J. Fisher, J.H. Chang, B.M. Mole, J.L. Dangl, Subterfuge and manipulation: type III effector proteins of phytopathogenic bacteria, Annu. Rev. Microbiol., 60 (2006) 425–49.

[11] K. Nomura, C. Mecey, Y.-N. Lee, L.A. Imboden, J.H. Chang, S.Y. He, L. Alice, J.H. Chang, S. Yang, Effector-triggered immunity blocks pathogen degradation of an immunity-associated vesicle traffic regulator in *Arabidopsis*, PNAS, 108 (2011) 10774–10779.

[12] A. Block, J.R. Alfano, Plant targets for *Pseudomonas syringae* type III effectors: virulence targets or guarded decoys?, Curr. Opin. Microbiol., 14 (n.d.) 39–46.

[13] J.L. Dangl, J.M. Mcdowell, Two modes of pathogen recognition by plants, PNAS, 103 (2006) 8575–8576.

[14] T.E. Mishina, J. Zeier, Pathogen-associated molecular pattern recognition rather than development of tissue necrosis contributes to bacterial induction of systemic acquired resistance in *Arabidopsis*, Plant J., 50 (2007) 500–513.

[15] E. Lam, Controlled cell death, plant survival and development, Nat. Rev., 5 (2004) 305–315.

[16] S. Elmore, Apoptosis: a review of programmed cell death, Toxicol. Pathol., 35 (2007) 495–516.

[17] N. Hatsugai, M. Kuroyanagi, M. Nishimura, A cellular suicide strategy of plants: vacuole-mediated cell death, Apoptosis, 11 (2006) 905–911.

[18] P.O. Lim, H.J. Kim, H.G. Nam, Leaf senescence, Annu. Rev. Plant Biol., 58 (2007) 115–36.

[19] N.S. Coll, P. Epple, J.L. Dangl, Programmed cell death in the plant immune system, Cell Death Differ., 18 (2011) 1247–1256.

[20] L.A.J. Mur, P. Kenton, A.J. Lloyd, H. Ougham, E. Prats, The hypersensitive response; the centenary is upon us but how much do we know?, J. Exp. Bot., 59 (2008) 501–520.

[21] C.R. Buell, V. Joardar, M. Lindeberg, J. Selengut, I.T. Paulsen, M.L. Gwinn, R.J. Dodson, R.T. Deboy, A.S. Durkin, J.F. Kolonay, R. Madupu, S. Daugherty, L. Brinkac, M.J. Beanan, D.H. Haft, W.C. Nelson, T. Davidsen, N. Zafar, L. Zhou, J. Liu, et al., The complete genome sequence of the *Arabidopsis* and tomato pathogen *Pseudomonas syringae* pv. *tomato* DC3000, PNAS, 100 (2003) 10181–10186.

[22] G.M. Preston, *Pseudomonas syringae* pv. *tomato*: the right pathogen, of the right plant, at the right time, Mol. Plant Pathol., 1 (2000) 263–275.

[23] G.B. Martin, Suppression and activation of the plant immune system by *Pst* effectors AvrPto and AvrPtoB, in: Eff. Plant-Microb Interact., 2012: pp. 123–154.

[24] A. Block, G. Li, Z.Q. Fu, J.R. Alfano, Phytopathogen type III effector weaponry and their plant targets, Curr. Opin. Plant Biol., 11 (2008) 396–403.

[25] S. Cunnac, M. Lindeberg, A. Collmer, *Pseudomonas syringae* type III secretion system effectors: repertoires in search of functions, Curr. Opin. Microbiol., 12 (2009) 53–60.

[26] R.E. Pitblado, B.H. Macneill, Genetic basis of resistance to *Pseudomonas syringae* pv *tomato* in field tomatoes, Can. J. Plant Pathol., 5 (1983) 251–255.

[27] G. Sessa, M.D. Ascenzo, Y. Loh, G.B. Martin, Biochemical properties of two protein kinases involved in disease resistance signaling in tomato, J. Biol. Chem., 273 (1998)

15860–15865.

[28] L. Shan, V.K. Thara, G.B. Martin, J. Zhou, X. Tang, The *Pseudomonas* AvrPto protein is differentially recognized by tomato and tobacco and is localized to the plant plasma membrane, Plant Cell, 12 (2000) 2323–2337.

[29] Y.J. Kim, N. Lin, G.B. Martin, Two distinct *Pseudomonas* effector proteins interact with the Pto kinase and activate plant immunity, Cell, 109 (2002) 589–598.

[30] T. Xiang, N. Zong, Y. Zou, Y. Wu, Report *Pseudomonas syringae* effector AvrPto blocks innate immunity by targeting receptor kinases, Curr Bio, 18 (2008) 74–80.

[31] L. Shan, P. He, J. Li, A. Heese, S.C. Peck, T. Nu, G.B. Martin, Bacterial effectors target the common signaling partner BAK1 to disrupt multiple MAMP receptor-signaling complexes and impede plant immunity, Cell Host Microbe,4 (2008) 17–27.

[32] D.K. Singh, M. Calviño, E.K. Brauer, N. Fernandez-pozo, S. Strickler, R. Yalamanchili, H. Suzuki, K. Aoki, D. Shibata, J.W. Stratmann, G. V Popescu, L.A. Mueller, S.C. Popescu, The tomato kinome and the tomato kinase library ORFeome: novel resources for the study of kinases and signal transduction in tomato and solanaceae species, Mol Plant Microbe Interact, 27 (2014) 7–17.

[33] V. Gohre, T. Spallek, H. Haweker, S. Mersmann, T. Mentzel, T. Boller, M. De Torres, J.W. Mansfield, S. Robatzek, Plant pattern-recognition receptor FLS2 is directed for degradation by the bacterial ubiquitin ligase AvrPtoB, Curr. Biol., 18 (2008) 1824–1832.

[34] O. Navarro, Lionel; Jay, Florence; Nomura, Kinya; He, Sheng Yang; Voinnet, Suppression of the MicroRNA pathway by bacterial effector proteins, Science, 321 (2014), 964-7.

[35] J.R. Cohn, G.B. Martin, T. Rd, *Pseudomonas syringae* pv. *tomato* type III effectors AvrPto and AvrPtoB promote ethylene-dependent cell death in tomato, The Plant J., 44 (2005) 139–154.

[36] M. De Torres-zabala, M.H. Bennett, J.W. Mansfield, R. Egea, L. Bo, M. Grant, *Pseudomonas syringae* pv. *tomato* hijacks the *Arabidopsis* abscisic acid signalling pathway to cause disease, The EMBO, 26 (2007) 1434–1443.

[37] R.R. Pitblado, E.A. Kerr, Resistance to bacterial spec (*pseudomonas tomato*) in tomato, Acta Hortic., 100 (1980) 379–382.

[38] K.F. Pedley, G.B. Martin, Molecular basis of Pto-mediated resistance to bacterial speck disease in tomato, Annu. Rev. Phytopathol., 41 (2003) 215–243.

[39] J.M. Salmeron, G.E.D. Oldroyd, C.M.T. Rommens, S.R. Scofield, H. Kim, D.T. Lavelle, D. Dahlbeck, B.J. Staskawicz, N. Carolina, Tomato Prf is a member of the leucine-rich repeat class of plant disease resistance genes and lies embedded within the Pto kinase gene cluster, Cell, 86 (1996) 123–133.

[40] T.S. Mucyn, A. Clemente, V.M.E. Andriotis, A.L. Balmuth, G.E.D. Oldroyd, B.J. Staskawicz, J.P. Rathjen, The tomato NBARC-LRR protein Prf interacts with Pto kinase *in vivo* to regulate specific plant immunity, Plant Cell, 18 (2006) 2792–2806.

[41] G. Sessa, M.D. Ascenzo, G.B. Martin, Thr38 and Ser198 are Pto autophosphorylation sites required for the AvrPto-Pto-mediated hypersensitive response, EMBO J., 19 (2000) 2257–2269.

[42] W. Xing, Y. Zou, Q. Liu, J. Liu, X. Luo, Q. Huang, S. Chen, L. Zhu, R. Bi, Q. Hao, J.-W. Wu, J.-M. Zhou, J. Chai, The structural basis for activation of plant immunity by bacterial effector protein AvrPto, Nature, 449 (2007) 243–247.

[43] V. Ntoukakis, A.L. Balmuth, T.S. Mucyn, J.R. Gutierrez, A.M.E. Jones, J.P. Rathjen, The tomato Prf complex is a molecular trap for bacterial effectors based on Pto transphosphorylation, PLOS, 9 (2013) e1003123.

[44] F. Xiao, P. He, R.B. Abramovitch, J.E. Dawson, L.K. Nicholson, J. Sheen, G.B. Martin, The N-terminal region of *Pseudomonas* type III effector AvrPtoB elicits Pto-dependent immunity and has two distinct virulence determinants, Plant J., 52 (2007) 595–614.

[45] J. Dong, F. Xiao, F. Fan, L. Gu, H. Cang, G.B. Martin, J. Chai, Crystal structure of the complex between Pseudomonas effector AvrPtoB and the tomato Pto kinase reveals both a shared and a unique interface compared with AvrPto-Pto, Plant Cell, 21 (2009) 1846–1859.

[46] A.J. Bogdanove, G.B. Martin, AvrPto-dependent Pto-interacting proteins and AvrPto-interacting proteins in tomato, PNAS, 97(2000) 8836-40.

[47] T.P. Devarenne, S.K. Ekengren, K.F. Pedley, G.B. Martin, Adi3 is a Pdk1-interacting AGC kinase that negatively regulates plant cell death, EMBO J., 25 (2006) 255–265.

[48] M.J. Ek-Ramos, J. Avila, C. Cheng, G.B. Martin, T.P. Devarenne, The T-loop extension of the tomato protein kinase AvrPto-dependent Pto-interacting protein 3 (Adi3) directs nuclear localization for suppression of plant cell death, J. Biol. Chem., 285 (2010) 17584–17594.

[49] J. Ek-ramos, J. Avila, A.C. Nelson, D. Su, J.W. Gray, T.P. Devarenne, The tomato cell death suppressor Adi3 is restricted to the endosomal system in response to the *Pseudomonas syringae* effector protein AvrPto, PLoS One, 9 (2014) e110807.

[50] T.P. Devarenne, G.B. Martin, Manipulation of plant programmed cell death pathways during plant-pathogen interactions, Plant Signal. Behav., 2 (2007) 188–189.

[51] M. Carlson, B.C. Osmond, D. Botstein, Mutants of yeast defective in sucrose utilization, genetics, 98 (1981) 25–40.

[52] J.L. Celenza, M. Carlson, A yeast gene that is essential for release from glucose repression encodes a protein kinase, Science, 233 (1986) 1175–1180.

[53] N.G. Halford, J.P. Bouly, M. Thomas, SNF1-related protein kinases (SnRKs) — regulators at the heart of the control of carbon metabolism and partitioning, Adv. Bot. Res., 32 (2000) 405–434.

[54] D.G. Hardie, AMP-activated / SNF1 protein kinases: conserved guardians of cellular energy, Nat. Rev., 8 (2007) 774–785.

[55] D.G. Hardie, F.A. Ross, S.A. Hawley, AMPK : a nutrient and energy sensor that maintains energy homeostasis, Nat. Rev. Mol. Cell Bio., 13 (2012) 251–262.

[56] E. Baena-gonzalez, F. Rolland, J.M. Thevelein, J. Sheen, A central integrator of transcription networks in plant stress and energy signaling, Nature, 448 (2007) 938–943.

[57] M. Ramon, P. Ruelens, Y. Li, J. Sheen, K. Geuten, F. Rolland, The hybrid Four-CBS-Domain KINβγ subunit functions as the canonical γ subunit of the plant energy sensor SnRK1, Plant J., 75 (2013) 11–25.

[58] J. Avila, O.G. Gregory, D. Su, T. a. Deeter, S. Chen, C. Silva-Sanchez, S. Xu, G.B. Martin, T.P. Devarenne, The β-subunit of the SnRK1 complex is phosphorylated by the plant cell death suppressor Adi3, Plant Physiol., 159 (2012) 1277–1290.

[59] R. Ghillebert, E. Swinnen, J. Wen, L. Vandesteene, M. Ramon, K. Norga, F. Rolland, J. Winderickx, The AMPK/SNF1/SnRK1 fuel gauge and energy regulator: structure, function and regulation, FEBS J., 278 (2011) 3978–3990.

[60] R. Farras, A. Ferrando, J. Jasik, T. Kleinow, K. Salchert, C. del Pozo, J. Schell, C. Koncz, SKP1-SnRK protein kinase interactions mediate proteasomal binding of a plant SCF ubiquitin ligase, EMBO J., 20 (2001) 2742–2756.

[61] L. Chen, F. Xin, J. Wang, J. Hu, Y. Zhang, S. Wan, L. Cao, C. Lu, P. Li, S.F. Yan, D. Neumann, U. Schlattner, B. Xia, Z. Wang, J. Wu, Conserved regulatory elements in AMPK, Nature, 498 (2013) E8–E10.

[62] S. Hong, F.C. Leiper, A. Woods, D. Carling, M. Carlson, Activation of yeast Snf1 and mammalian AMP-activated protein kinase by upstream kinases, PNAS, 100 (2003) 8839–8843.

[63] P. Crozet, F. Jammes, B. Valot, F. Ambard-Bretteville, S. Nessler, M. Hodges, J. Vidal, M. Thomas, Cross-phosphorylation between *Arabidopsis thaliana* sucrose nonfermenting 1-related protein kinase 1 (AtSnRK1) and its activating kinase (AtSnAK) determines their catalytic activities, J. Biol. Chem., 285 (2010) 12071–12077.

[64] P. Crozet, L. Margalha, A. Confraria, A. Rodrigues, C. Martinho, M. Adamo, C. Elias, E. Baena-Gonzalez, Mechanisms of regulation of SNF1/AMPK/SnRK1 protein kinases, Front. Plant Sci., 5 (2014) 190.

[65] K. Hedbacker, M. Carlson, SNF1/AMPK pathways in yeast, Front. Biosci., 13 (2008) 2408–2420.

[66] H.A. Wiatrowski, B.J.W. Van Denderen, C.D. Berkey, B.E. Kemp, D. Stapleton, M. Carlson, Mutations in the Gal83 glycogen-binding domain activate the Snf1/Gal83 kinase pathway by a glycogen-independent mechanism, Mol. Cell. Biol., 24 (2004) 352–361.

[67] A. McBride, S. Ghilagaber, A. Nikolaev, D.G. Hardie, The glycogen-binding domain on the AMPK β-subunit allows the kinase to act as a glycogen sensor, Cell Metab., 9 (2009) 23–34.

[68] A. Avila-Castañeda, N. Gutiérrez-Granados, A. Ruiz-Gayosso, A. Sosa-Peinado, E. Martínez-Barajas, P. Coello, Structural and functional basis for starch binding in the SnRK1 subunits AKINβ2 and AKINβγ, Front. Plant Sci., 5 (2014) 199.

[69] S.M. Warden, C. Richardson, J.O.D. Jr, D. Stapleton, B.E. Kemp, L.A. Witters, Post-translational modifications of the β-1 subunit of AMP-activated protein kinase affect enzyme activity and cellular localization, Biochem. J., 354 (2001) 275–283.

[70] K.I. Mitchelhill, B.J. Michell, C.M. House, D. Stapleton, J. Dyck, J. Gamble, C. Ullrich, L. Witters, B.E. Kemp, Posttranslational modifications of the 5 -AMP-activated protein kinase β1 subunit, J. Biol. Chem., 272 (1997) 24475–9.

[71] S. Mangat, C. Dakshayini, R.R. McCartney, K. Elbing, M.C. Schmidt, D. Chandrashekarappa, R.R. McCartney, K. Elbing, M.C. Schmidt, Differential roles of the glycogen-binding domains of β-subunits in regulation of the Snf1 kinase complex, Eukaryot. Cell, 9 (2010) 173–183.

[72] B. Xiao, M.J. Sanders, E. Underwood, R. Heath, F. V Mayer, D. Carmena, C. Jing, P. Walker, J.F. Eccleston, L.F. Haire, P. Saiu, S. Howell, R. Aasland, S.R. Martin, D. Carling, S.J. Gamblin, Structure of mammalian AMPK and its regulation by ADP, Nature, 472 (2011) 230–233.

[73] G.J. Gowans, S.A. Hawley, F.A. Ross, D.G. Hardie, Article AMP is a true physiological regulator of AMP-activated protein kinase by both allosteric activation and enhancing net phosphorylation, Cell Metab., 18 (2013) 556–566.

[74] R. Townley, L. Shapiro, Crystal structures of the adenylate, Science, 315 (2007) 1726–1730.

[75] J.L. Maya-bernal, A. Ávila, A. Ruiz-gayosso, R. Trejo-fregoso, N. Pulido, A. Sosa-peinado, E. Zúñiga-sánchez, E. Martínez-barajas, R. Rodríguez-Sotresa, P. Coello, Expression of recombinant SnRK1 in *E coli*. Characterization of adenine nucleotide binding to the SnRK11/AKIN βγ-β3 complex, Plant Sci., 263 (2017) 116–125.

[76] C. Sugden, R.M. Crawford, N.G. Halford, D.G. Hardie, Regulation of spinach SNF1-related (SnRK1) kinases by protein kinases and phosphatases is associated with phosphorylation of the T loop and is regulated by 5'-AMP, Plant J., 19 (1999) 433–439.

[77] F. V. Mayer, R. Heath, E. Underwood, M.J. Sanders, D. Carmena, R.R. Mccart- ney, ADP regulates SNF1, the *Saccharomyces cerevisiae* homolog of AMP-activated protein kinase,

Cell Metab., 14 (2011) 707–714.

[78] J.S. Oakhill, R. Steel, Z.P. Chen, J.W. Scott, N. Ling, S. Tam, AMPK is a direct adenylate charge-regulated protein kinase, Science, 332 (2011) 1433–1435.

[79] J.S. Oakhill, Z. Chen, J.W. Scott, R. Steel, L.A. Castelli, N. Ling, S.L. Macaulay, B.E. Kemp, β-Subunit myristoylation is the gatekeeper for initiating metabolic stress sensing by AMP-activated protein kinase (AMPK), PNAS, 107 (2010) 19237–19241.

[80] D.G. Chandrashekarappa, R.R. Mccartney, M.C. Schmidt, Ligand binding to the AMP-activated protein kinase active site mediates protection of the activation loop from dephosphorylation, J. Biol. Chem., 288 (2013) 89–98.

[81] L. Morphogenesis, Y. Minokoshi, T. Alquier, N. Furukawa, M.J. Birnbaum, B.J. Stuck, AMP-kinase regulates food intake by responding to hormonal and nutrient signals in the hypothalamus, Nature, 428 (2004) 569–574.

[82] C.E. Gleason, D. Lu, L.A. Witters, C.B. Newgard, M.J. Birnbaum, The role of AMPK and mTOR in nutrient sensing in pancreatic β-cells, J. Biol. Chem., 282 (2007) 10341–10351.

[83] M. Cesquini, G.R. Stoppa, P.O. Prada, A.S. Torsoni, T. Romanatto, A. Souza, M.J. Saad, L.A. Velloso, M.A. Torsoni, Citrate diminishes hypothalamic acetyl-CoA carboxylase phosphorylation and modulates satiety signals and hepatic mechanisms involved in glucose homeostasis in rats, Life Sci., 82 (2008) 1262–1271.

[84] J.E. Lunn, R. Feil, J.H.M. Hendriks, Y. Gibon, R. Morcuende, D. Osuna, Sugar-induced increases in trehalose 6-phosphate are correlated with redox activation of ADPglucose pyrophosphorylase and higher rates of starch synthesis in *Arabidopsis thaliana*, Biochem. J., 397 (2006) 139–148.

[85] Y. Zhang, L.F. Primavesi, D. Jhurreea, P.J. Andralojc, R.A.C. Mitchell, S.J. Powers, H. Schluepmann, T. Delatte, A. Wingler, M.J. Paul, Inhibition of SNF1-related protein kinase1 activity and regulation of metabolic pathways by trehalose-6-phosphate, Plant P, 149 (2009) 1860–1871.

[86] E. Martínez-Barajas, T. Delatte, H. Schluepmann, G.J. de Jong, G.W. Somsen, C. Nunes, L.F. Primavesi, P. Coello, R. a C. Mitchell, M.J. Paul, G.J. De Jong, R. a C. Mitchell, M.J. Paul, Wheat grain development is characterized by remarkable trehalose 6-phosphate accumulation pregrain filling: tissue distribution and relationship to SNF1-related protein kinase1 activity, Plant Physiol., 156 (2011) 373–381.

[87] S.P. Davies, A.T.R. Sim, D.G. Hardie, Location and function of three sites phosphorylated on rat acetyl-CoA carboxylase by the AMP-activated protein kinase, Eur. J. Biochem, 187 (1990) 183–190.

[88] A. Woods, M.R. Mundays, J. Scott, X. Yango, M. Carlson, Yeast SNF1 is functionally related to mammalian AMP-activated protein kinase and regulates acetyl-coA carboxylase *in vivo*, J. Biol. Chem., 269 (1994) 19509–19515.

[89] P.R. Clarke, D.G. Hardie, Regulation of HMG-CoA reductase: identification of the site phosphorylated by the AMP-activated protein kinase in vitro and in intact rat liver, EMBO J., 9 (1990) 2439–2446.

[90] K.L. Ball, J. Barker, N.G. Halford, D.G. Hardie, Immunological evidence that HMG-CoA reductase kinase-A is the cauliflower homologue of the RKIN1 subfamily of plant protein kinases, FEBS Lett., 377 (1995) 189–192.

[91] A. Kulma, D. Villadsen, D.G. Campbell, S.E.M. Meek, J.E. Harthill, T.H. Nielsen, C. Mackintosh, Phosphorylation and 14-3-3 binding of *Arabidopsis* 6-phosphofructo-2-kinase/fructose-2, 6-bisphosphatase, Plant J., 37 (2004) 654–667.

[92] J.E. Harthill, S.E.M. Meek, N. Morrice, M.W. Peggie, J. Borch, B.H.C. Wong, C. Mackintosh, Phosphorylation and 14-3-3 binding of *Arabidopsis* trehalose-phosphate synthase 5 in response to 2-deoxyglucose, Plant J., 47 (2006) 211–223.

[93] C. Sugden, P.G. Donaghy, N.G. Halford, D.G. Hardie, Two SNF1-related protein kinases from spinach leaf phosphorylate and inactivate 3-hydroxy-3-methylglutaryl-coenzyme A reductase, nitrate reductase, and sucrose phosphate synthase *in vitro*, Plant Physiol., 120 (1999) 257–274.

[94] M.A. Treitel, M. Carlson, Repression by SSN6-TUP1 is directed by MIG1, a repressor / activator protein, PNAS, 92 (1995) 3132–3136.

[95] M.A. Treitel, S. Kuchin, M. Carlson, Snf1 protein kinase regulates phosphorylation of the Mig1 repressor in *Saccharomyces cerevisiae*, Mol. Cell. Biol., 18 (1998) 6273–6280.

[96] J. Hanson, M. Hanssen, A. Wiese, M.M.W.B. Hendriks, S. Smeekens, The sucrose regulated transcription factor bZIP11 affects amino acid metabolism by regulating the expression of ASPARAGINE SYNTHETASE1 and PROLINE DEHYDROGENASE2, Plant J., 53 (2008) 935–949.

[97] M.D. Bolton, Primary metabolism and plant defense—fuel for the fire, Mol. Plant. Microbe. Interact., 22 (2009) 487–497.

[98] J. Schwachtje, P.E.H. Minchin, S. Jahnke, J.T. Van Dongen, U. Schittko, I.T. Baldwin, SNF1-related kinases allow plants to tolerate herbivory by allocating carbon to roots, PNAS, 103 (2006) 12935–12940.

[99] C. Polge, M. Thomas, SNF1/AMPK/SnRK1 kinases, global regulators at the heart of energy control?, Trends Plant Sci., 12 (2006) 20–28.

[100] N.G. Halford, S.J. Hey, Snf1-related protein kinases (SnRKs) act within an intricate network that links metabolic and stress signalling in plants, Biochem. J., 419 (2009) 247–259.

[101] W.H. Campbell, Structure and function of eukaryotic NAD(P)H:nitrate reductase, Cell. Mol. Life Sci., 58 (2001) 194–204.

[102] W.H. Campbell, J.R. Kinghorn, Functional domains of assimilatory nitrate reductases and nitrite reductases, Trends Biochem. Sci., 15 (1990) 315–319.

[103] K. Fischer, G.G. Barbier, H. Hecht, R.R. Mendel, W.H. Campbell, Structural basis of eukaryotic nitrate reduction: crystal structures of the nitrate reductase active site, Plant Cell, 17 (2005) 1167–1179.

[104] L. Skipper, W.H. Campbell, J.A. Mertens, D.J. Lowe, Pre-steady-state kinetic analysis of recombinant *Arabidopsis* NADH:nitrate reductase, J. Biol. Chem., 276 (2001) 26995–27002.

[105] W.M. Kaiser, S.C. Huber, Posttranslational regulation of nitrate reductase in higher-plants, Plant Physiol., 106 (1994) 817–821.

[106] J. Sinclair, Changes in spinach thylakoid activity due to nitrite ions, Photosynth. Res., 12 (1987) 255–263.

[107] W.M. Kaiser, E. Brendle-behnisch, Rapid modulation of spinach leaf nitrate reductase activity by photosynthesis, Plant Physiol., 96 (1991) 363–367.

[108] P. Douglas, E. Pigaglio, A. Ferrer, N.G. Halford, C. MacKintosh, Three spinach leaf nitrate reductase–3-hydroxy-3-methylglutaryl-CoA reductase kinases that are regulated by reversible phosphorylation and/or Ca^{2+} ions, Biochem. J., 325 (1997) 101–109.

[109] M. Bachmann, N. Shiraishi, W.H. Campbell, B.-C. Yoo, A.C. Harmomc, S.C. Huber, ldentification of Ser-543 as the major regulatory phosphorylation site in spinach leaf nitrate reductase, Plant Cell, 8 (1996) 505–517.

[110] W. Su, S.C. Huber, N.M. Crawford, ldentification *in vitro* of a post-translational regulatory site in the hinge 1 region of *Arabidopsis* nitrate reductase, New Phytol., 8 (1996) 519–527.

[111] I. Lambeck, J.C. Chi, S. Krizowski, S. Mueller, N. Mehlmer, M. Teige, K. Fischer, G. Schwarz, Kinetic analysis of 14-3-3-inhibited *Arabidopsis thaliana* nitrate reductase, Biochemistry, 49 (2010) 8177–8186.

[112] J.-C.C. Chi, J. Roeper, G. Schwarz, K. Fischer-Schrader, Dual binding of 14-3-3 protein regulates *Arabidopsis* nitrate reductase activity, J. Biol. Inorg. Chem., 20 (2015) 277–286.

[113] C. Polge, M. Jossier, P. Crozet, L. Gissot, M. Thomas, Beta-subunits of the SnRK1 complexes share a common ancestral function together with expression and function specificities; physical interaction with nitrate reductase specifically occurs via AKINbeta1-subunit, Plant Physiol., 148 (2008) 1570–82.

[114] X.-F. Li, Y.-J. Li, Y.-H. An, L.-J. Xiong, X.-H. Shao, Y. Wang, Y. Sun, AKINbeta1 is involved in the regulation of nitrogen metabolism and sugar signaling in *Arabidopsis*, J. Integr. Plant Biol., 51 (2009) 513–520.

[115] K. Aoki, K. Yano, A. Suzuki, S. Kawamura, N. Sakurai, K. Suda, A. Kurabayashi, T. Suzuki, T. Tsugane, M. Watanabe, K. Ooga, M. Torii, T. Narita, T. Shin-i, Y. Kohara, N. Yamamoto, H. Takahashi, Y. Watanabe, M. Egusa, M. Kodama, et al., Large-scale analysis of full-length cDNAs from the tomato (*Solanum lycopersicum*) cultivar Micro-Tom, a reference system for the Solanaceae genomics, BMC Genomics, 11 (2010) 2–6.

[116] S. Hey, H. Mayerhofer, N.G. Halford, J.R. Dickinson, DNA sequences from *Arabidopsis*, which encode protein kinases and function as upstream regulators of Snf1 in yeast, J. Biol. Chem., 282 (2007) 10472–10479.

[117] F. Daniel-Vedele, M.-F. Dorbe, M. Caboche, P. Rouzé, Cloning and analysis of the tomato nitrate reductase-encoding gene: protein domain structure and amino acid homologies in higher plants, Gene, 85 (1989) 371–380.

[118] S. a. Hawley, M. Davison, A. Woods, S.P. Davies, R.K. Beri, D. Carling, D.G. Hardie, Characterization of the AMP-activated protein kinase kinase from rat liver and identification of threonine 172 as the major site at which it phosphorylates AMP-activated protein kinase, J. Biol. Chem., 271 (1996) 27879–27887.

[119] C.J. Hastie, H.J. McLauchlan, P. Cohen, Assay of protein kinases using radiolabeled ATP: A protocol, Nat. Protoc., 1 (2006) 968–971.

[120] S. Fragoso, L. Espindola, J. Paez-Valencia, A. Gamboa, Y. Camacho, E. Martinez-Barajas, P. Coello, L. Espíndola, J. Páez-Valencia, A. Gamboa, Y. Camacho, E. Martínez-Barajas, P. Coello, SnRK1 isoforms AKIN10 and AKIN11 are differentially regulated in *Arabidopsis* plants under phosphate starvation, Plant Physiol., 149 (2009) 1906–1916.

[121] N.C. Lin, G.B. Martin, An *avrPto / avrPtoB* mutant of *Pseudomonas syringae* pv *tomato* DC3000 does not elicit pto-mediated resistance and is less virulent on tomato, MPMI, 18 (2005) 43–51.

[122] J.S. Heilig, K.L. Elbing, R. Brent, Large-scale preparation of plasmid DNA, Curr. Protoc. Mol. Biol., (1998) 1.7.1-1.7.16.

[123] A. Alderson, P.A. Sabellit, J.R. Dickinsont, D. Coleo, M. Richardson, M. Kreis, P.R. Shewryt, N.G.H. Ii, Complementation of *snf1*, a mutation affecting global regulation of carbon metabolism in yeast, by a plant protein kinase cDNA, 88 (1991) 8602–8605.

[124] S. Emanuelle, M.S. Doblin, D.I. Stapleton, A. Bacic, P.R. Gooley, Molecular insights into the enigmatic metabolic regulator, SnRK1, Trends Plant Sci., 21 (2016) 341–353.

[125] M. Takano, H. Kajiya-Kanegae, H. Funatsuki, S. Kikuchi, Rice has two distinct classes of protein kinase genes related to SNF1 of *Saccharomyces cerevisiae*, which are differently regulated in early seed development, Mol. Gen. Genet., 260 (1998) 388–394.

[126] Á. Lovas, A. Sós-Hegedus, A. Bimbó, Z. Bánfalvi, Functional diversity of potato SNF1-related kinases tested in *Saccharomyces cerevisiae*, Gene, 321 (2003) 123–129.

[127] S.W. Bledsoe, C. Henry, C.A. Griffiths, M.J. Paul, R. Feil, J.E. Lunn, M. Stitt, L.M. Lagrimini, The role of Tre6P and SnRK1 in maize early kernel development and events leading to stress-induced kernel abortion, BMC Bioinformatics, 17 (2017) 1–17.

[128] T. Muranaka, H. Banno, Y. Machida, Characterization of tobacco protein kinase NPK5, a homolog of *Saccharomyces cerevisiae* SNF1 that constitutively activates expression of the glucose-repressible SUC2 gene for a secreted invertase of *S. cerevisiae*, Mol. Cell. Biol., 14 (1994) 2958–2965.

[129] N. Tochio, S. Koshiba, N. Kobayashi, M. Inoue, T. Yabuki, M. Aoki, E. Seki, T. Matsuda, Y. Tomo, Y. Motoda, A. Kobayashi, A. Tanaka, Y. Hayashizaki, T. Terada, M. Shirouzu, T. Kigawa, S. Yokoyama, Solution structure of the kinase-associated domain 1 of mouse microtubule-associated protein / microtubule affinity-regulating kinase 3, (2006) 2534–2543.

[130] A. Rodrigues, M. Adamo, P. Crozet, L. Margaha, A. Confraria, C. Martinho, A. Elias, A. Rabissi, V. Lumbreras, M. González-guzmán, R. Antoni, P.L. Rodriguez, E. Baena-González, ABI1 and PP2CA phosphatases are negative regulators of Snf1-related protein kinase1 signaling in *Arabidopsis*, 25 (2013) 3871–3884.

[131] K. Moravcevic, J.M. Mendrola, K.R. Schmitz, Y. Wang, D. Slochower, P.A. Janmey, M.A. Lemmon, Kinase associated-1 domains drive MARK / PAR1 kinases to membrane targets by binding acidic phospholipids, Cell, 143 (2010) 966–977.

[132] M. Schmid, T.S. Davison, S.R. Henz, U.J. Pape, M. Demar, M. Vingron, B. Schölkopf, D. Weigel, J.U. Lohmann, A gene expression map of *Arabidopsis thaliana* development, Nat. Genet., 37 (2005) 501–506.

[133] N. Glab, C. Oury, T. Guerinier, S. Domenichini, P. Crozet, M. Thomas, J. Vidal, M. Hodges, The impact of *Arabidopsis thaliana* SNF1-related-kinase 1 (SnKR1)-activating kinase 1 (SnAK1) and SnAK2 on SnRK1 phosphorylation status: characterization of a SnAK double mutant, Plant J., 89 (2017) 1031–1041.

[134] K.J. Bradford, A.B. Downie, O.H. Gee, V. Alvarado, H. Yang, P. Dahal, Abscisic acid and gibberellin differentially regulate expression of genes of the SNF1-related kinase complex in tomato seeds, Plant Physiol., 132 (2003) 1560–1576.

[135] Q. Shen, Z. Liu, F. Song, Q. Xie, L. Hanley-Bowdoin, X. Zhou, Tomato *Sl*SnRK1 protein interacts with and phosphorylates βC1, a pathogenesis protein encoded by a geminivirus β-satellite, Plant Physiol., 157 (2011) 1394–1406.

[136] A.L. Man, P.C. Purcell, U. Hannappel, N.G. Halford, Potato SNF1-related protein kinase: molecular cloning, expression analysis and peptide kinase activity measurements, Plant Mol. Biol., 34 (1997) 31–43.

[137] E.M. Hrabak, C.W.M. Chan, M. Gribskov, J.F. Harper, J.H. Choi, N. Halford, J. Kudla, S. Luan, H.G. Nimmo, M.R. Sussman, M. Thomas, K. Walker-Simmons, J.-K. Zhu, A.C. Harmon, The *Arabidopsis* CDPK-SnRK superfamily of protein kinases, Plant Physiol.,

132 (2003) 666–680.

[138] R.P. Bhalerao, K. Salchert, L. Bakó, L. Okrész, L. Szabados, T. Muranaka, Y. Machida, J. Schell, C. Koncz, Regulatory interaction of PRL1 WD protein with *Arabidopsis* SNF1-like protein kinases, Proc. Natl. Acad. Sci. U. S. A., 96 (1999) 5322–5327.

[139] J. Beenstock, N. Mooshayef, D. Engelberg, How do protein kinases take a selfie (autophosphorylate)?, Trends Biochem. Sci., 41 (2016) 938–953.

[140] W. Shen, M.I. Reyes, L. Hanley-Bowdoin, *Arabidopsis* protein kinases GRIK1 and GRIK2 specifically activate SnRK1 by phosphorylating its activation loop, Plant Physiol., 150 (2009) 996–1005.

[141] Tomato functional genomics database, http://ted.bti.cornell.edu.

[142] W.H. Campbell, J. Smarrelli, Purification and kinetics of higher plant NADH:nitrate reductase, Plant Physiol., 61 (1978) 611–6.

[143] W.H. Campbell, P. Song, G.G. Barbier, Nitrate reductase for nitrate analysis in water, Environ. Chem. Lett., 4 (2006) 69–73.

[144] M. Bitrián, F. Roodbarkelari, M. Horváth, C. Koncz, BAC-recombineering for studying plant gene regulation: developmental control and cellular localization of SnRK1 kinase subunits, Plant J., 65 (2011) 829–842.

[145] K. Hedbacker, S.-P. Hong, M. Carlson, Pak1 protein kinase regulates activation and nuclear localization of Snf1-Gal83 protein kinase, Mol. Cell. Biol., 24 (2004) 8255–8263.

[146] J. Sperschneider, A.M. Catanzariti, K. Deboer, B. Petre, D.M. Gardiner, K.B. Singh, P.N. Dodds, J.M. Taylor, LOCALIZER: subcellular localization prediction of both plant and effector proteins in the plant cell, Sci. Rep., 7 (2017) 1–14.

[147] L. Cherezova, K.L. Burnside, T.M. Rose, Conservation of complex nuclear localization signals utilizing classical and non-classical nuclear import pathways in LANA homologs of KSHV and RFHV, PLoS One, 6 (2011).

[148] S. Kosugi, M. Hasebe, N. Matsumura, H. Takashima, E. Miyamoto-Sato, M. Tomita, H. Yanagawa, Six classes of nuclear localization signals specific to different binding grooves of importinα, J. Biol. Chem., 284 (2009) 478–485.

[149] K. Hedbacker, M. Carlson, Regulation of the nucleocytoplasmic distribution of Snf1-Gal83 protein kinase, Eukaryot. Cell, 5 (2006) 1950–6.

[150] Y. Zhang, R.R. McCartney, D.G. Chandrashekarappa, S. Mangat, M.C. Schmidt, Reg1 protein regulates phosphorylation of all three Snf1 isoforms but preferentially associates with the Gal83 isoform, Eukaryot. Cell, 10 (2011) 1628–1636.

[151] N. Kazgan, T. Williams, L.J. Forsberg, J.E. Brenman, Identification of a nuclear export

signal in the catalytic subunit of AMP-activated protein kinase, Mol. Bio. Cell, 21 (2010) 3433–3442.

[152] A. Krapp, Plant nitrogen assimilation and its regulation: a complex puzzle with missing pieces, Curr. Opin. Plant Biol., 25 (2015) 115–122.

[153] Y. Sakihama, S. Nakamura, H. Yamasaki, Nitric oxide production mediated by nitrate reductase in the green alga *Chlamydomonas reinhardtii* : an alternative NO production pathway in photosynthetic organisms, Plant Cell Physiol., 43 (2002) 290–297.

[154] P. Rockel, F. Strube, A. Rockel, J. Wildt, W.M. Kaiser, Regulation of nitric oxide (NO) production by plant nitrate reductase *in vivo* and *in vitro*, J. Exp. Bot., 53 (2002) 103–110.

[155] A. Chamizo-Ampudia, E. Sanz-Luque, A. Llamas, A. Galvan, E. Fernandez, Nitrate reductase regulates plant nitric oxide homeostasis, Trends Plant Sci., 22 (2017) 163–174.